2012-6

An Analysis of Drug Dissolution in Vivo

David McDonnell

Technological University Dublin

An Analysis of Drug Dissolution in Vivo

by

David McDonnell

A Thesis to be submitted to the Dublin Institute of Technology

for the degree of Doctor of Philosophy(Ph.D.)

June 7, 2012

Supervisor: Dr. Brendan Redmond, School of Mathematical Sciences,

Dublin Institute of Technology

Advisory Supervisor: Professor L.J. Crane

Abstract

The testing of drug dissolution rates from solid dosage forms is a very important area of research within the pharmaceutical industry. The ability to produce drugs with a given dissolution rate will lead to improved performance in the treatment of patients and will be of economic benefit to the pharmaceutical industry. However, dissolution testing in laboratories, aimed at reflecting in-vivo conditions, can be both time consuming and costly. Currently, most simulations of drug dissolution take place in standardized USP (United States Pharmaceutical) apparatuses. A number of these apparatuses exist, and it is the aim of this thesis to analyse drug dissolution in both the USP Paddle Apparatus and the USP Flow Through Apparatus.

The first part of this thesis examines drug dissolution from a solid dosage form (compact) in the USP Paddle Apparatus. The process is set up as a boundary layer problem for which there exists both a momentum boundary layer and a concentration boundary layer. The dominant mass transfer mechanism is that of forced convection. A semi-analytical technique is used to solve the boundary layer equations for which velocity data has been provided from computational fluid dynamic simulations. Wherever possible the results from this semi-analytical approach have been compared with that of an exact solution.

The second part of the thesis concentrates on the USP Flow Through Apparatus. As the process of drug dissolution in the Flow Through Apparatus is dependent on a vertical flow, the analysis is complicated by the introduction of buoyancy effects. Chapters five to nine analyse a number of general cases for buoyancy driven flows on both flat and curved surfaces. Later, in chapter ten,

these general cases are then applied to the process of drug dissolution from the surface of a compact in the USP Flow Through Apparatus. Throughout the thesis, the predicted dissolution rates from the theoretical approach are compared with those of experiment.

Declaration

I certify that this thesis which I now submit for examination for the award of Ph.D., is entirely my own work and has not been taken from the work of others save and to the extent that such work has been cited and acknowledged within the text of my work.

This thesis was prepared according to the regulations for postgraduate study by research of the Dublin Institute of Technology and has not been submitted in whole or in part for an award in any other Institute or University. The work reported on in this thesis conforms to the principles and requirements of the Institute's guidelines for ethics in research.

The Institute has permission to keep, to lend or to copy this thesis in whole or in part, on condition that any such use of the material of the thesis be duly acknowledged.

Signature _____ Date _____

David McDonnell

Acknowledgements

I would like to thank my supervisor, Dr. Brendan Redmond, for his assistance and supervision throughout the course of this work. Also, I would like to thank my advisory supervisor, Professor L.J. Crane, for his guidance and time. His expertise in the field of fluid mechanics was invaluable.

I would also like to thank Dr. Deirdre D'Arcy, School of Pharmacy and Pharmaceutical Sciences, Trinity College Dublin, for her assistance and sharing of information throughout the course of this work.

Finally to Ciara, for her love, support and encouragement during the last four years and beyond.

Nomenclature

a	radius of cylinder
c	concentration of dissolved particles
C	non-dimensional concentration
C_s	concentration saturation
D	coefficient of diffusion
$f(\eta)$	dimensionless distance variable
$F(\xi)$	dimensionless distance variable
F_r	Froude number
g	acceleration due to gravity
g_0	effect of gravity
$h(\eta)$	dimensionless concentration variable
j, k	arbitrary constants in stream function
p	pressure
p_0	stagnation point pressure
p_D	weight of dissolved particles
P_n	Padé coefficients
Q_n	Padé coefficients
r	radial distance
R	non-dimensional radial distance
R_L	Reynolds number
S_c	Schmidt number
T	non-dimensional shear stress
u	component of velocity in x direction
U_∞	outer stream velocity
U_0	velocity of counterflow
v	component of velocity in y direction
W_i	width of strips
x	distance from leading edge
x_{sep}	point of boundary layer separation
X	non-dimensional distance
y	distance normal to surface

Greek letters

α	velocity gradient
β	constant
δ	momentum boundary layer thickness
δ_c	concentration boundary layer thickness
ϵ	perturbation parameter
η	similarity variable
ψ	stream function
ν	kinematic viscosity
ρ	density
μ	dynamic viscosity
τ_0	surface shear stress
ξ	similarity variable
$\Gamma(n)$	gamma function
γ	constant
λ, λ_1	constant
θ	angular measurement
ζ	constant

Contents

List of Figures

List of Tables

Chapter 1

Introduction

Dissolution testing is a very important area of research within the pharmaceutical industry. The ability to produce drugs with a given dissolution rate will lead to improved performance in the treatment of patients and will be of economic benefit to the pharmaceutical industry. However, dissolution testing in laboratories, aimed at reflecting in-vivo conditions, can be both time consuming and costly. A mathematical model of the process would serve to alleviate some of these costs.

Currently, most simulations of drug dissolution take place in standardized USP (United States Pharmaceutical) apparatuses. A number of these apparatuses exist, and it is the aim of this thesis to analyse drug dissolution in both the USP Paddle Apparatus and the USP Flow Through Apparatus.

1.1 The USP Paddle Apparatus

The USP Paddle Apparatus, as shown in figure (1.1), consists of a rotating paddle that sits a few centimetres above the bottom of a hemispherically based vessel. A cylindrically shaped compressed mass of drug, called a compact, is positioned on the bottom surface of the vessel with the paddle rotating at 50rpm. The positioning of the compact on the bottom surface is very important as the velocity of the solution increases with distance from the centre of the vessel. Also, the curvilinear nature of these velocities becomes less important as the compact is moved away from the central position.

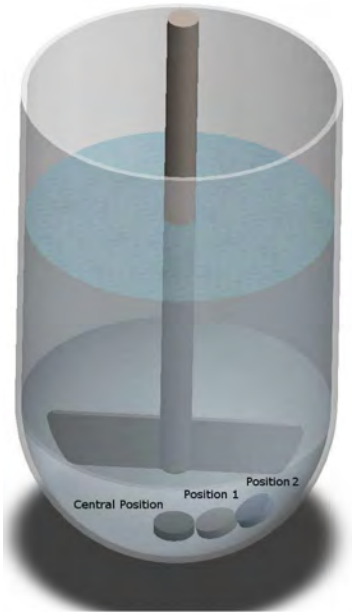

Figure 1.1: USP Paddle Apparatus

Experimental Work

The USP Paddle Apparatus is one of the most widely used dissolution apparatuses within the pharmaceutical industry. The apparatus is designed to mimic gastric conditions and is mainly used to assess batch consistency. As reported by Bai et al[10], a typical test begins with a compact being dropped into the Paddle Apparatus, at which point it is supposed to sink and settle at the base of the vessel in a central position. Bai et al[10] report that this is not always the case and that the compact has a tendency to adhere to the surface at off-centre positions, or indeed move along the bottom surface throughout the duration of an experiment.

To investigate the effects that an off-centre position has on the dissolution rate from the surface of the compact, experiments have been conducted by D'Arcy[6] in which the compact is fixed to a number of positions along the bottom surface

of the vessel. The results of these experiments have shown that an off-centre compact can have dissolution rates of up to 30% greater than a compact which sits directly below the paddle. D'Arcy[6] has also conducted Computational Fluid Dynamic (CFD) simulations in order to predict the dissolution rate from a compact surface, the results of which have been compared with those of experiment. The comparison between experimental and CFD results are somewhat mixed. The CFD results for the curved side surface of a compact correlate well with those of experiment; however D'Arcy[6] reports a significant underestimation when predicting the dissolution rates for the top planar surface. An example of the CFD simulation output is shown in figure (1.2). The generated velocity data files have been kindly provided by Dr. Deirdre D'Arcy of the School of Pharmacy and Pharmaceutical Sciences, Trinity College Dublin(TCD), for use in this thesis.

Compacts and Compact Position

The compacts used by D'Arcy[6] throughout the experimental work are composed of benzoic acid and are 13mm in diameter with a height of 3mm. The compacts are positioned in three different locations. The first position, called the central position, is at the centre of the bottom surface. Position 1 is directly adjacent to the central position with position 2 adjacent to position 1. Chapters three and four of this work look at the dissolution rates from both the top planar surface and the curved side surface of the compacts in all three positions respectively. For the central position, a compact of 8.5mm in height is also analysed.

The positioning of the compact has a significant impact on the rate of drug dissolution. A compact in position 2 is subject to larger velocities than a compact

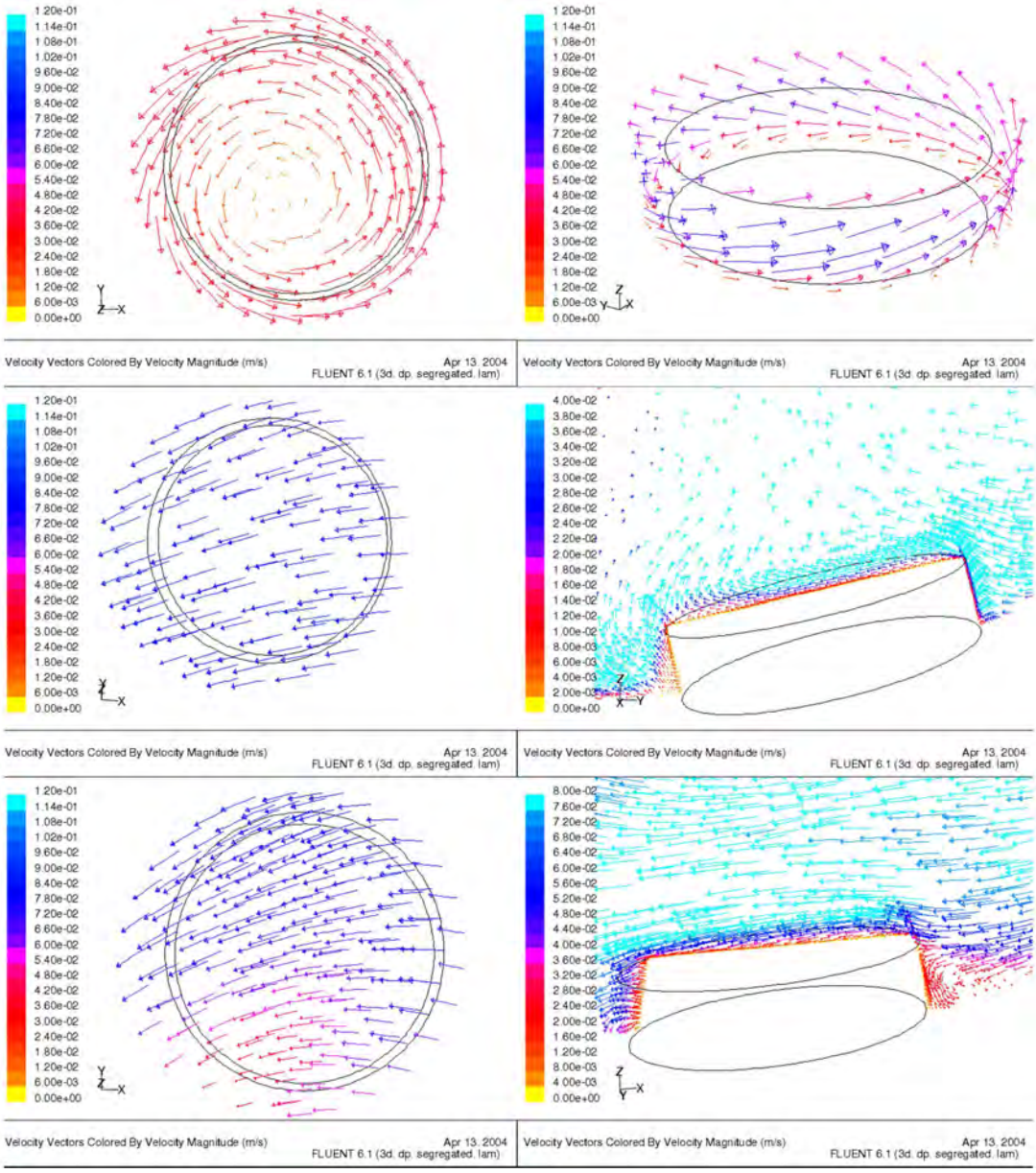

Figure 1.2: Fluent Simulations

in position 1. It can also be seen that the compact in position 2 is tilted more towards the vertical, due to the shape of the bottom surface of the vessel. This tilt leads to less variation in velocities from one side of the compact to the other

Image kindly provided by Dr. Deirdre D'Arcy[25]

and will lead to more accurate results. Another thing to note when analysing the top planar surface is that the curvilinear nature of the flow becomes less important as the compact is moved further away from the central position.

Initial Observations

The process of drug dissolution in the USP Paddle Apparatus can be set up as a boundary layer problem. The mathematical model consists of both a concentration boundary layer and a momentum boundary layer. The dissolution medium is water. Jeans[23] states that in a liquid, molecules diffuse much more slowly than does momentum. Consequently, the concentration boundary layer is an order of magnitude thinner than the momentum boundary layer.

The concentration boundary layer only occupies the region of the momentum boundary layer close to the compact surface in which the velocity gradient is linear, leading to significant simplifications in the analysis. The model of the process is therefore analogous to that of heat transfer for large Prandtl numbers, for which an exact solution for flat plate flow exists, due to Lévêque[1]. The existence of this exact solution serves as a standard from which the accuracy of the approximate methods used in the analysis may be judged.

1.2 The USP Flow Through Apparatus

The USP Flow Through Apparatus, as shown in figure (1.3), consists of four main elements; a reservoir, a pump, the flow through cell and a bath. The reservoir holds the dissolution medium which is then forced through the flow through cell by the pump. The pump typically delivers a flow rate of between 4 and 16 mL per

Figure 1.3: The USP Flow Through Apparatus

minute, although larger flow rates are achievable. The flow profile is sinusoidal with 120 pulses per minute. The bath is for the flow through cell to sit in and is used to maintain a temperature of 37°C.

The flow through cell is where the compact is housed. The cell is a cylindrical vessel with a conical base. The cone part of the vessel is usually filled with small glass beads to promote laminar flow. The compact sits about half-way up the cell and is held in place using a special holder. Two cell sizes are available; a large cell of diameter 22.6mm and a small cell with a diameter of 12mm.

Experimental Work

In recent times much research in the pharmaceutical sector has focused on the Flow Through Apparatus. Many commentators, including Stevens[13], Singh[12] and Beyssac[11], believe that the apparatus holds a number of advantages over the USP Paddle Apparatus. As reported by Stevens[13], the flow through cell controls the placement of the compact better than the Paddle Apparatus and, also, the hydrodynamics of the system are more clearly defined. The flow through cell can also be used in an open configuration, which according to Singh[12], makes it possible to maintain sink conditions. This better mimics the gastrointestinal tract. He notes that this is of particular importance for poorly soluble drugs.

Finally, the Flow Through Apparatus allows for the dissolution media to be changed over the course of an experiment. This creates a more realistic recreation of in-vivo conditions as a compact passes through different regions of the gastrointestinal tract (Stevens[13]).

Figure 1.4: An Image of a Compact in the USP Flow Through Apparatus

Image kindly provided by Dr. Deirdre D'Arcy[25]

Experiments have been conducted by D'Arcy and Liu[7] using the large flow through cell. Compacts composed of benzoic acid, and with a diameter of 13mm, were used. The experiments where conducted for different flow rates and also for when the pump is idle. The results of these experiments have shown that, in some cases, an increase in the flow rate has resulted in a decrease in the dissolution rate from the surface of the compact. Similar results have also been reported by Beyssac[11], who states that in certain cases an increase in flow rate resulted in no increase in the dissolution rate.

Initial Observations

As with the Paddle Apparatus, the process of drug dissolution in the USP Flow Through Apparatus can be set up as a boundary layer problem. The obvious approach is to first look at the case in which the pump is idle (i.e. no upward flow). This case is one of natural convection only in which the flow, and hence the dissolution process, will be driven purely by buoyancy effects.

Secondly, using the natural convection case as our base, the effect of the pump will be introduced. It seems likely that this case will need to be analysed for three distinct situations: small , intermediate and large upward velocities.

1.3 Introduction to Boundary Layer Flows

The idea of a boundary layer was first introduced in 1904 by Ludwig Prandtl. A boundary layer can be classified as a relatively thin fluid layer close to the surface of a body in which strong viscous effects exist. The formation of a boundary layer is a direct consequence of the no-slip condition. The no-slip condition states that

at the interface between a fluid and solid boundary the fluid has zero velocity relative to the solid. As such, the boundary layer is a region of large velocity gradients over which the velocity of the fluid changes from zero velocity relative to the solid boundary to the velocity of the main outer flow. The edge of the boundary layer is usually taken as the point at which the fluid velocity is 0.99 times that of the outer stream. The boundary layer discussed so far is known as the momentum boundary layer and is illustrated in figure (1.5) for flow across a flat plate. The equations that govern this type of flow, called the momentum boundary layer equations, are derived from the Navier Stokes equations. As well as momentum boundary layers, similar layers exist for processes such as heat and mass transfer, known as the thermal and concentration boundary layers. This work will primarily involve looking for solutions to the momentum and concentration boundary layer equations.

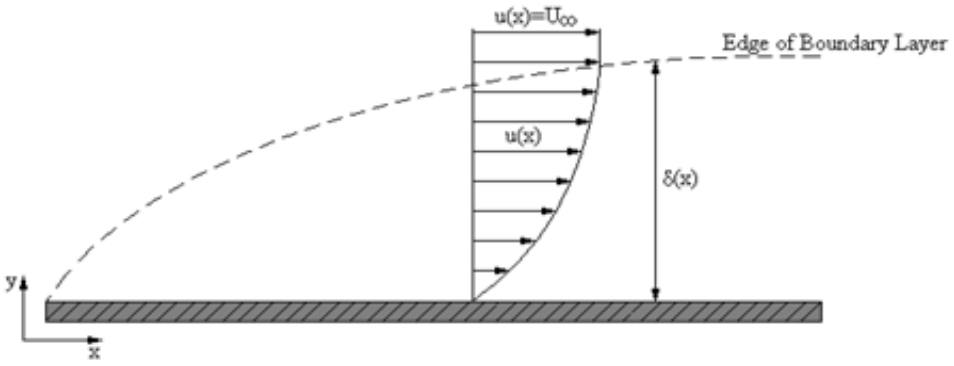

Figure 1.5: Boundary Layer across a Flat Surface

Navier-Stokes Equations

The Navier Stokes equations, named after Claude Louis Navier and George Gabriel Stokes, are a set of equations that describe the motion of Newtonian fluids. The equations are a set of partial differential equations, which establish relations between acceleration and internal pressure of a fluid.

The Navier Stokes equations are derived from the basic principles of conservation of mass, momentum and energy. This thesis will not look at the derivation of the Navier Stokes equations themselves but will use these equations as a starting point to derive the boundary layer equations necessary to model drug dissolution. These simplified equations are valid for incompressible flows with high Reynolds number or very small viscosity, where the Reynolds number is the ratio of internal forces to viscous forces. The two-dimensional Navier Stokes equations for steady flow are

$$u\frac{\partial u}{\partial x} + v\frac{\partial u}{\partial y} = -\frac{1}{\rho}\frac{\partial p}{\partial x} + \nu\left[\frac{\partial^2 u}{\partial x^2} + \frac{\partial^2 u}{\partial y^2}\right] \tag{1.1}$$

$$u\frac{\partial v}{\partial x} + v\frac{\partial v}{\partial y} = -\frac{1}{\rho}\frac{\partial p}{\partial y} + \nu\left[\frac{\partial^2 v}{\partial x^2} + \frac{\partial^2 v}{\partial y^2}\right] \tag{1.2}$$

$$\frac{\partial u}{\partial x} + \frac{\partial v}{\partial y} = 0, \tag{1.3}$$

where x is the distance from the leading edge, y is the distance from the wall, u and v are the components of velocity in the x and y directions respectively, ν is the kinematic viscosity of the dissolution medium, ρ is the density and p is the pressure.

Boundary Layer Equations

The boundary layer equations are a simplified version of the Navier Stokes equations. In boundary layer theory it is assumed that outside the boundary layer viscous effects are not important and that the thickness of the boundary layer itself is small compared to the length of the body on which it forms. The theory is also dependent on the no-slip condition, which states that, the fluid in contact with the solid boundary has zero velocity with respect to the boundary.

To derive the boundary layer equations we will start by taking the full Navier Stokes equations and reduce them by neglecting relatively small terms. The terms to be neglected will be found using an order of magnitude analysis. Now, as the boundary layer is thin, we can say that for all points in the boundary layer $\delta << x$ or $\frac{\delta}{x} << 1$, where δ is the momentum boundary layer thickness. The mainstream velocity is denoted by U_∞. u is of order U_∞, so the partial derivative $\frac{\partial u}{\partial x}$ has order of magnitude $\frac{U_\infty}{x}$. y is of order of magnitude δ, so the partial derivative $\frac{\partial v}{\partial y}$ has order of magnitude $\frac{v}{\delta}$. Putting these approximate values for $\frac{\partial u}{\partial x}$ and $\frac{\partial v}{\partial y}$ into the continuity equation (1.3) we obtain $v \sim \frac{U_\infty \delta}{x}$. Also, u and v vary much more rapidly in the y-direction than the x-direction, so we can say $\frac{\partial}{\partial x} << \frac{\partial}{\partial y}$. Inserting these order of magnitudes into equations (1.1) and (1.2) gives

$$\frac{U_\infty^2}{x} + \frac{U_\infty^2}{x} = -\frac{1}{\rho}\frac{\partial p}{\partial x} + \frac{\nu U_\infty}{x^2} + \frac{\nu U_\infty}{\delta^2} \tag{1.4}$$

$$\frac{U_\infty^2 \delta}{x^2} + \frac{U_\infty^2 \delta}{x^2} = -\frac{1}{\rho}\frac{\partial p}{\partial y} + \frac{\nu U_\infty \delta}{x^3} + \frac{\nu U_\infty}{\delta x}. \tag{1.5}$$

The second viscous term in equation (1.4), $\left[\frac{\nu U_\infty}{\delta^2}\right]$, is much larger than the first, namely $\left[\frac{\nu U_\infty}{x^2}\right]$, so the first viscous term can be neglected with an error $0\left[\frac{\delta^2}{x^2}\right]$. Assuming the larger viscous term has the same order of magnitude as the inertial

terms we can say: $\frac{\nu U_\infty}{\delta^2} \sim \frac{U_\infty^2}{x}$. This gives the order of magnitude for the boundary layer thickness as: $\delta \sim \sqrt{\frac{\nu x}{U_\infty}}$. From the condition $\frac{\delta}{x} << 1$, we get $\frac{x^2}{\delta^2} \sim \frac{U_\infty x}{\nu} >> 1$. i.e. $R_L >> 1$, where R_L is the Reynolds number. Therefore the term $\left[\frac{\nu U_\infty}{x^2}\right]$ in equation (1.4) can be neglected with error $0\left[\frac{1}{R_L}\right]$ because

$$\frac{\nu\frac{\partial^2 u}{\partial x^2}}{\nu\frac{\partial^2 u}{\partial y^2}} \sim \frac{\delta^2}{x^2} \sim \frac{1}{R_L}. \tag{1.6}$$

So equation (1.1) becomes

$$u\frac{\partial u}{\partial x} + v\frac{\partial u}{\partial y} = -\frac{1}{\rho}\frac{\partial p}{\partial x} + \nu\frac{\partial^2 u}{\partial y^2}. \tag{1.7}$$

Now, comparing equations (1.4) and (1.5), we can see that the inertial and viscous terms in (1.2) are of order $\frac{\delta}{x}$ smaller than the corresponding terms in (1.1), so they can be neglected with error $0\left[\frac{1}{\sqrt{R_L}}\right]$. Therefore equation (1.2) may be written:

$$0 = -\frac{1}{\rho}\frac{\partial p}{\partial y}. \tag{1.8}$$

This suggests that p is a function of x only, so the partial derivative $\frac{\partial p}{\partial x}$ in equation (1.7) can be written as an ordinary derivative, so equation (1.7) becomes

$$u\frac{\partial u}{\partial x} + v\frac{\partial u}{\partial y} = -\frac{1}{\rho}\frac{dp}{dx} + \nu\frac{\partial^2 u}{\partial y^2} \tag{1.9}$$

Since the pressure, p, is independent of y, the pressure distribution along the boundary layer is the same as that outside the boundary layer. This suggests that Bernoulli's equation is valid, i.e;

$$\frac{p}{\rho} + U_\infty^2 = C_1 \tag{1.10}$$

where C_1 is constant. Differentiating with respect to x gives

$$-\frac{1}{\rho}\frac{dp}{dx} = U_\infty\frac{dU_\infty}{dx}. \tag{1.11}$$

Substituting this into equation (1.9) gives

$$u\frac{\partial u}{\partial x} + v\frac{\partial u}{\partial y} = U_\infty \frac{dU_\infty}{dx} + \nu\frac{\partial^2 u}{\partial y^2}. \tag{1.12}$$

Now, in most cases of interest to us, the mainstream velocity U_∞ is constant so the term $\frac{dU_\infty}{dx}$ is zero. Therefore, the two-dimensional boundary layer equations for steady flow are

$$u\frac{\partial u}{\partial x} + v\frac{\partial u}{\partial y} = \nu\frac{\partial^2 u}{\partial y^2} \tag{1.13}$$

$$\frac{\partial u}{\partial x} + \frac{\partial v}{\partial y} = 0. \tag{1.14}$$

In the case of mass transfer, a similar equation to the momentum equation can be derived, called the concentration boundary layer equation. This is given as

$$u\frac{\partial c}{\partial x} + v\frac{\partial c}{\partial y} = D\frac{\partial^2 c}{\partial y^2}. \tag{1.15}$$

where c is the concentration of dissolved particles and D is the coefficient of diffusion of the soluble material.

1.4 Solution Methods

The boundary layer equations may be solved using several methods. The methods used in this thesis consist of both exact and approximate methods. The advantage of an exact solution is that an investigator can obtain a more complete view of the properties within the boundary layer. The disadvantage is the difficulty in solving the equations that arise from seeking an exact solution, an exercise that very often proves to be futile. Where an exact solution is not possible, an approximate method may be used to solve the boundary layer equations. These methods often sacrifice a more comprehensive view of the boundary layer to focus

instead on predicting certain characteristics such as shear stress, which in many cases can be very useful.

Similarity Solutions

In order to seek a similarity solution to the boundary layer equations, a function $\psi = kx^m f(\eta)$, where $\eta = j\frac{y}{x^n}$, is introduced such that ψ satisfies the continuity equation identically. That is to say: $u = \frac{\partial \psi}{\partial y}$ and $v = -\frac{\partial \psi}{\partial x}$. The function ψ is called the stream function. It obtains it's name due to the fact that lines corresponding to $\psi =$ constant are also the streamlines of the flow.

The introduction of the stream function in essence eliminates the continuity equation and its substitution, along with the relevant derivatives, into the momentum equation results in an ordinary differential equation in terms of $f(\eta)$. The value of m is determined by the geometry of the flow and the value of k is chosen in order to render the stream function dimensionless.

The similarity variable, $\eta = j\frac{y}{x^n}$, has the property that when η is constant, u is constant. The existence of a similarity solution is dependent on the problem having no length scale. An example of this is flow across a flat plate which was investigated by Blasius[3], where a similarity solution was obtained. It is important to note that if the case involved another plate, say at a distance y_1 from the original, a similarity type of solution would be restricted by the introduction of the length scale y_1. The Blasius solution will be examined in detail in chapter two. Again, like the stream function, the value of n depends on the geometry of the problem and j is chosen in order to render η dimensionless.

Asymptotic Series Solutions

On obtaining a similarity solution it is sometimes advantageous to expand this solution further. This can be achieved by the method of asymptotic expansion. The method involves expressing the solution as a series of $f(\eta)$ in ascending powers of x. The series is substituted into the boundary layer equations at which point the coefficients of x^i are equated. This results in a set of ordinary differential equations which may be solved numerically.

Pohlhausen Method

The Pohlhausen method is an approximate method based on the momentum integral equation. This equation is derived by integrating the momentum boundary layer equation over a cross section of the layer. A suitable velocity profile can then be substituted into the momentum integral equation. This leads to an ordinary differential equation that may be solved either numerically, or occasionally analytically. To look at the derivation, we will take the case of flow across a flat plate. The momentum boundary layer equation is

$$u\frac{\partial u}{\partial x} + v\frac{\partial u}{\partial y} = \nu\frac{\partial^2 u}{\partial y^2}. \tag{1.16}$$

Equation (1.16) may be rewritten as

$$\frac{\partial}{\partial x}(u^2) + \frac{\partial}{\partial y}(uv) = \nu\frac{\partial^2 u}{\partial y^2}. \tag{1.17}$$

Now integrating with respect to y, across the boundary layer gives

$$\int_0^\delta \frac{\partial}{\partial x}u^2 dy + \int_0^\delta \frac{\partial}{\partial y}(uv)dy = \nu\int_0^\delta \frac{\partial^2 u}{\partial y^2}dy. \tag{1.18}$$

Now, Leibniz's rule states:

$$\frac{d}{dx}\int_{y_0}^{y_1} f(x,y)dy = f(x,y_1)\frac{\partial y_1}{\partial x} - f(x,y_0)\frac{\partial y_0}{\partial x} + \int_{y_0}^{y_1}\frac{\partial}{\partial x}f(x,y)dy. \tag{1.19}$$

Using Leibniz's rule equation (1.18) can be written as

$$\frac{d}{dx}\int_0^\delta u^2 dy - \frac{\partial \delta}{\partial x}\left[u^2\right]_{y=\delta} + [uv]_0^\delta = \nu\left[\frac{\partial u}{\partial y}\right]_0^\delta. \tag{1.20}$$

Applying the boundary conditions

$$\begin{cases} y = 0, & u = 0, \quad v = 0 \\ y = \delta, & u = U_\infty \end{cases}$$

gives

$$\frac{d}{dx}\int_0^\delta u^2 dy - U_\infty^2\frac{\partial \delta}{\partial x} + U_\infty v(\delta) = -\nu\left[\frac{\partial u}{\partial y}\right]_{y=0}. \tag{1.21}$$

Now, taking the continuity equation (1.14) and integrating we get

$$v(\delta) = -\int_0^\delta \frac{\partial u}{\partial x} dy. \tag{1.22}$$

From Leibniz's rule, this becomes

$$v(\delta) = -\frac{d}{dx}\int_0^\delta dy + U_\infty\frac{\partial \delta}{\partial x}. \tag{1.23}$$

Substituting (1.23) into (1.21) gives

$$\frac{d}{dx}\int_0^\delta u^2 dy - U_\infty^2\frac{\partial \delta}{\partial x} + U_\infty^2\frac{\partial \delta}{\partial x} - U_\infty\frac{d}{dx}\int_0^\delta u dy = -\nu\left[\frac{\partial u}{\partial y}\right]_{y=0}. \tag{1.24}$$

This can be rearranged to give the momentum integral equation for flow across a flat plate:

$$\frac{d}{dx}\int_0^\delta u(U_\infty - u)dy = \nu\left[\frac{\partial u}{\partial y}\right]_{y=0} \tag{1.25}$$

In the case of mass transfer a similar equation may be derived yielding the concentration integral equation to be

$$\frac{d}{dx}\int_0^\delta u c dy = -D\left[\frac{\partial c}{\partial y}\right]_{y=0}. \tag{1.26}$$

Upon substitution of suitable velocity and concentration profiles, the concentration integral equation may be used to estimate the total flux along the surface.

Padé Approximation Technique

In some circumstances, where a series solution to the boundary layer equations has been sought, the resulting series can be found to be poorly convergent. One way to improve on such results is by means of a Padé approximant. The Padé technique involves rewriting the power series as a rational function. That is to say

$$\sum_{i=0}^{N} C_i x^i = \frac{P_0 + P_1 x + P_2 x^2 + ... + P_n x^n}{Q_0 + Q_1 x + Q_2 x^2 + ... + Q_m x^m} \tag{1.27}$$

It is most common to choose $Q_0 = 1$ and to make sure the degree of the numerator is greater than or equal to the degree of the denominator. The coefficients $P_0, P_1, P_2, ...$ and $Q_0, Q_1, Q_2, ...$ may be found by backward substitution. The resulting function usually shows better convergence than the original power series. The Padé approximant technique is therefore useful in extending the range of validity of a solution and is used in this thesis.

Chapter 2

Literature review

This thesis is concerned with evaluating drug dissolution rates from the surface of solid dosage forms in several standard apparatuses. Much of the analysis involves flat surfaces. In order to investigate mass transfer from a flat surface we must first examine flow across a flat plate. An exact solution to the boundary layer equations was obtained by Blasius[3], for such a flow. The similarity solution obtained by Blasius[3] is looked at in detail within this chapter.

Following on from Blasius, a French engineer by the name of André Lévêque[1] observed that in the case of heat transfer for large Prandtl numbers, the thermal boundary layer was an order of magnitude thinner than the momentum boundary layer. For this reason, the thermal boundary layer only occupies a very thin region close to the surface of the body across which the velocity gradient is linear. In order to solve the problem of heat transfer from a flat plate Lévêque[1] uses the Blasius velocity profile. Although the work of Lévêque[1] describes heat transfer, it can be easily modified to model mass transfer. Now, a drug dissolving into a liquid will diffuse much more slowly than momentum due to the tightly packed nature of the molecules. This leads to a concentration boundary layer with thickness an order of magnitude less than the momentum boundary layer. The problem of drug dissolution is therefore analogous to the problem presented by Lévêque[1]. This modified Lévêque solution is also examined within this chapter.

Finally, the chapter will review the case of heat transfer from the surface of a vertical flat plate for large Prandtl numbers presented by Kuiken[2], in which natural convection is the dominant mass transfer mechanism. As with the work

of Lévêque[1], the case presented by Kuiken[2] can be easily adapted to model mass transfer from the vertical flat surface of a soluble material. The problem posed by Kuiken[2] involves two separate regions, one in which buoyancy effects dominate and another in which the flow is categorised as one of forced convection only.

The work of Blasius[3], Lévêque[1], and Kuiken[2] form much of the basic ideas used in this thesis. Indeed, much of the material presented in subsequent chapters may be directly attributed to these authors, or at least be seen as expansions of their work.

2.1 Flow across a Flat Plate: Blasius

The case of flow across a flat plate was studied by Blasius[3]. In the case presented by Blasius[3], the outer stream velocity, U_∞, is assumed to be constant. This means that the pressure term in the boundary layer equation (1.12), namely $\frac{dU_\infty}{dx}$, is identically zero and may be neglected. The two-dimensional boundary layer equations for uniform flow across a flat plate are therefore given by

$$u\frac{\partial u}{\partial x} + v\frac{\partial u}{\partial y} = \nu\frac{\partial^2 u}{\partial y^2} \tag{2.1}$$

$$\frac{\partial u}{\partial x} + \frac{\partial v}{\partial y} = 0. \tag{2.2}$$

In order to reduce this set of equations to a single equation, a stream function is introduced that satisfies the continuity equation identically. This stream function is defined by $u = \frac{\partial \psi}{\partial y}$ and $v = -\frac{\partial \psi}{\partial x}$ and takes the form

$$\psi = kx^m f(\eta) \tag{2.3}$$

where

$$\eta = j\frac{y}{x^n}. \tag{2.4}$$

The momentum equation is written in terms of the stream function as

$$\frac{\partial\psi}{\partial y}\frac{\partial^2\psi}{\partial x\partial y} - \frac{\partial\psi}{\partial x}\frac{\partial^2\psi}{\partial y^2} = \nu\frac{\partial^3\psi}{\partial y^3}. \tag{2.5}$$

The various derivatives of the stream function are found to be

$$\begin{aligned}
\tfrac{\partial\psi}{\partial y} &= kjx^{m-n}f'(\eta) \\
\tfrac{\partial^2\psi}{\partial y^2} &= kj^2x^{m-2n}f''(\eta) \\
\tfrac{\partial^3\psi}{\partial y^3} &= kj^3x^{m-3n}f'''(\eta) \\
\tfrac{\partial\psi}{\partial x} &= kmx^{m-1}f(\eta) - kn\eta x^{m-1}f'(\eta) \\
\tfrac{\partial^2\psi}{\partial x\partial y} &= kj(m-n)x^{m-n-1}f'(\eta) - kjn\eta x^{m-n-1}f''(\eta).
\end{aligned} \tag{2.6}$$

Substituting these into equation (2.5) gives

$$\begin{aligned}
&\left[kjx^{m-n}f'(\eta)\right]\left[kj(m-n)x^{m-n-1}f'(\eta) - kjn\eta x^{m-n-1}f''(\eta)\right] \\
&-\left[kmx^{m-1}f(\eta) - kn\eta x^{m-1}f'(\eta)\right]\left[kj^2x^{m-2n}f''(\eta)\right] = \nu\left[kj^3x^{m-3n}f'''(\eta)\right].
\end{aligned} \tag{2.7}$$

Simplifying equation (2.7) leads to

$$\left[k^2j^2x^{2m-2n-1}\right]\left[(m-n)f'(\eta)f'(\eta) - mf(\eta)f''(\eta)\right] = \nu kj^3x^{m-3n}f'''(\eta). \tag{2.8}$$

Now, in order for a similarity solution to exist, it must be possible to eliminate the variable x from equation (2.8). This suggests

$$\begin{aligned}
2m-2n-1 &= m-3n \\
m &= 1-n.
\end{aligned} \tag{2.9}$$

Taking an order of magnitude approach to the momentum equation (2.1) gives

$$\frac{U_\infty^2}{x} + \frac{U_\infty^2}{x} = \frac{\nu U_\infty}{\delta^2}. \tag{2.10}$$

To estimate the boundary layer thickness, δ, we equate terms on each side of equation (2.10) to get

$$\frac{U_\infty^2}{x} \sim \frac{\nu U_\infty}{\delta^2}. \tag{2.11}$$

This leads to

$$\delta \sim \sqrt{\frac{\nu x}{U_\infty}}. \tag{2.12}$$

Now, in order for a similarity solution to exist the velocity at a point in the boundary layer must depend only on it's relative position in the boundary layer. That is to say, the similarity variable, η, must have the property that when η is constant, u is constant. Mathematically, this is expressed

$$\begin{aligned} \frac{u}{U_\infty} &\approx \phi\left(\frac{y}{\delta}\right) \\ \frac{u}{U_\infty} &\approx \phi\left(y\sqrt{\frac{U_\infty}{\nu x}}\right). \end{aligned} \tag{2.13}$$

This implies that

$$u \propto x^{-\frac{1}{2}} \tag{2.14}$$

and hence

$$\psi \propto x^m \propto x^{\frac{1}{2}}. \tag{2.15}$$

From this we have established that $m = \frac{1}{2}$. Substituting this value for m into (2.9) gives $n = \frac{1}{2}$. Putting the values of m and n into equation (2.8) results in

$$\nu k j^3 f'''(\eta) + \frac{1}{2} k^2 j^2 f(\eta) f''(\eta) = 0. \tag{2.16}$$

Equation (2.16) can be simplified to give

$$f'''(\eta) + \frac{1}{2} f(\eta) f''(\eta) = 0, \tag{2.17}$$

where $k = j\nu$. The values of k and j are chosen to be

$$k = \sqrt{\nu U_\infty} \qquad \text{and} \qquad j = \sqrt{\frac{U_\infty}{\nu}} \tag{2.18}$$

in order to render both the stream function, ψ, and the similarity variable, η, dimensionless. The stream function is given as

$$\psi = \sqrt{\nu U_\infty x} f(\eta), \qquad \text{where} \qquad \eta = y\sqrt{\frac{U_\infty}{\nu x}}. \tag{2.19}$$

The ordinary differential equation

$$f'''(\eta) + \frac{1}{2} f(\eta) f''(\eta) = 0 \tag{2.20}$$

is solved subject to the boundary conditions

$$\begin{cases} f(0) = f'(0) = 0 \\ f'(\eta) \to 1 \quad \text{as} \quad \eta \to \infty \end{cases}$$

to obtain

$$f''(0) \approx 0.332 \quad . \tag{2.21}$$

On solving the differential equation the following characteristics of interest may be obtained

$$u = 0.332 U_\infty \sqrt{\frac{U_\infty}{\nu x}} y \tag{2.22}$$

$$\tau_0 = 0.332 \mu U_\infty \sqrt{\frac{U_\infty}{\nu x}}, \tag{2.23}$$

where u is the component of velocity in the x-direction, τ_0 is the wall shear stress, μ is the dynamic viscosity, ν is the kinematic viscosity, and U_∞ is the outer stream velocity.

2.2 Mass Transfer from a Horizontal Flat Plate: Based on work by Lévêque[1]

The case of heat transfer from the surface of a horizontal flat plate for large Prandtl numbers was studied by Lévêque[1]. In the case presented by Lévêque[1]

it is observed that the thermal boundary layer is an order of magnitude thinner than the momentum boundary layer. This means that the thermal boundary layer only occupies a very thin region in which the velocity gradient is linear. For this reason, it is not essential to solve the momentum boundary layer equation. Instead, the velocity profile of Blasius[3] is inserted directly into the concentration boundary layer equations, given as

$$u\frac{\partial c}{\partial x} + v\frac{\partial c}{\partial y} = D\frac{\partial^2 c}{\partial y^2} \tag{2.24}$$

$$\frac{\partial u}{\partial x} + \frac{\partial v}{\partial y} = 0. \tag{2.25}$$

The Blasius velocity profile for flow across a flat plate is

$$u = \beta U_\infty \sqrt{\frac{U_\infty}{\nu x}} y, \tag{2.26}$$

where $\beta \approx 0.332$. Differentiating equation (2.26) gives

$$\frac{\partial u}{\partial x} = \beta y U_\infty \sqrt{\frac{U_\infty}{\nu x}} \left(-\frac{1}{2x}\right). \tag{2.27}$$

Substituting (2.27) into the continuity equation gives

$$\frac{\partial v}{\partial y} = \beta y U_\infty \sqrt{\frac{U_\infty}{\nu x}} \left(\frac{1}{2x}\right). \tag{2.28}$$

Integrating equation (2.28) leads to

$$v = \frac{y^2}{2} \beta U_\infty \sqrt{\frac{U_\infty}{\nu x}} \left(\frac{1}{2x}\right). \tag{2.29}$$

Now, we introduce the non-dimensional concentration

$$C = \frac{c}{C_s}, \tag{2.30}$$

where C_s is the concentration saturation. Substituting (2.30), (2.26) and (2.29) into equation (2.24) we get

$$\left[y\beta U_\infty \sqrt{\frac{U_\infty}{\nu x}}\right] \frac{\partial c}{\partial x} + \left[\frac{y^2}{4x} \beta U_\infty \sqrt{\frac{U_\infty}{\nu x}}\right] \frac{\partial c}{\partial y} = D\frac{\partial^2 c}{\partial y^2}. \tag{2.31}$$

Seeking a similarity solution we assume

$$C = kx^m h(\eta), \tag{2.32}$$

where

$$\eta = j\frac{y}{x^n}. \tag{2.33}$$

The various derivatives of the concentration stream function, C, are found to be

$$\begin{aligned}
\tfrac{\partial C}{\partial y} &= kjx^{m-n}h'(\eta) \\
\tfrac{\partial^2 C}{\partial y^2} &= kj^2x^{m-2n}h''(\eta) \\
\tfrac{\partial C}{\partial x} &= kmx^{m-1}h(\eta) - kn\eta x^{m-1}h'(\eta).
\end{aligned} \tag{2.34}$$

Substituting (2.34) into equation (2.31) gives

$$\left[\beta U_\infty\sqrt{\frac{U_\infty}{\nu x}}\right]\left[ykmx^{m-1}h(\eta) - ykn\eta x^{m-1}h'(\eta) + \frac{y^2}{4x}kjx^{m-n}h'(\eta)\right] = D\left[kj^2x^{m-2n}h''(\eta)\right]. \tag{2.35}$$

From equation (2.33) we have

$$y = \frac{\eta x^n}{j}. \tag{2.36}$$

Using this in equation (2.35) and simplifying leads to

$$\left[\beta U_\infty\sqrt{\frac{U_\infty}{\nu}}\frac{k}{j}x^{n+m-\frac{3}{2}}\right]\left[m\eta h(\eta) - n\eta^2h'(\eta) + \frac{\eta^2}{4}h'(\eta)\right] = D\left[kj^2x^{m-2n}h''(\eta)\right]. \tag{2.37}$$

Now, in order for a similarity solution to exist it must be possible to eliminate the variable x from the above equation. This suggests

$$n + m - \frac{3}{2} = m - 2n. \tag{2.38}$$

From this we obtain $n = \frac{1}{2}$, which like in the case of Blasius[3] is standard for a flat plate. To obtain a value for m we must look at the concentration stream

function:

$$C = kx^m h(\eta). \tag{2.39}$$

Now at the surface, i.e. when $y = 0$, $C = 1$, that is to say a constant. For this reason there can be no dependency on x at the wall, suggesting $m = 0$. Also, as a dimensionless similarity variable will now automatically render the stream function dimensionless, k is taken to be unity. Taking all this information into account, equation (2.37) may be rewritten as

$$\left[\beta U_\infty \sqrt{\frac{U_\infty}{\nu}}\right]\left[-\frac{\eta^2}{4}h'(\eta)\right] = D\left[j^3 h''(\eta)\right]. \tag{2.40}$$

Now letting

$$j^3 = \frac{\beta U_\infty}{12D}\sqrt{\frac{U_\infty}{\nu}}, \tag{2.41}$$

equation (2.40) reduces to

$$h''(\eta) = -3\eta^2 h'(\eta). \tag{2.42}$$

Rearranging (2.42) gives

$$\frac{h''(\eta)}{h'(\eta)} = -3\eta^2. \tag{2.43}$$

Integrating (2.43) leads to

$$\ln\left[h'(\eta)\right] = -\eta^3 + C_1, \tag{2.44}$$

where C_1 is constant. Rearranging we obtain

$$h'(\eta) = Ae^{-\eta^3}. \tag{2.45}$$

The differential equation (2.45) is solved subject to the boundary conditions

$$\begin{cases} h(\infty) = 0 \\ h'(0) = 1. \end{cases}$$

Integrating equation (2.45) gives

$$h(\eta) = A \int_{\infty}^{\eta} e^{-\eta^3} d\eta. \tag{2.46}$$

Applying the boundary conditions we get

$$-A \int_{0}^{\infty} e^{-\eta^3} d\eta = 1. \tag{2.47}$$

Letting $z = \eta^3$ leads to

$$-A \left[\frac{1}{3}\right] \int_{0}^{\infty} e^{-z} z^{-\frac{2}{3}} dz = 1. \tag{2.48}$$

The Gamma function, $\Gamma(n)$ is defined by

$$\Gamma(n) \equiv \int_{0}^{\infty} e^{-z} z^{n-1} dz. \tag{2.49}$$

Therefore, we find

$$\Gamma\left(\frac{1}{3}\right) \equiv \int_{0}^{\infty} e^{-z} z^{-\frac{2}{3}} dz. \tag{2.50}$$

From the Gamma function tables $\Gamma\left(\frac{1}{3}\right) \approx 2.6789$. Substituting this into equation (2.48) we find

$$A \approx -1.1199. \tag{2.51}$$

From before we had

$$h'(\eta) = Ae^{-\eta^3}, \tag{2.52}$$

which leads to

$$h'(0) \approx -1.1199. \tag{2.53}$$

The flux from the surface is given by

$$\begin{aligned} \text{Total Flux} &= -D \left[\frac{\partial c}{\partial y}\right]_{y=0} \\ &= \frac{-jDC_s h'(0)}{\sqrt{x}}. \end{aligned} \tag{2.54}$$

The total flux per unit width is given as

$$\begin{aligned} \text{Flux / Unit Width} &= \int_0^x \frac{-jDC_s h'(0)}{\sqrt{x}} dx \\ &= -2jDC_s h'(0) x^{\frac{1}{2}}, \end{aligned} \tag{2.55}$$

where x is the length of the flat plate. Recalling that $j^3 = \frac{\beta U_\infty^{\frac{3}{2}}}{12D\nu^{\frac{1}{2}}}$ and $h'(0) = -1.1199$, the total flux per unit width may be expressed as

$$\text{Flux / Unit Width} = 0.677 \frac{U_\infty^{\frac{1}{2}} D^{\frac{2}{3}} C_s x^{\frac{1}{2}}}{\nu^{\frac{1}{6}}}, \tag{2.56}$$

where U_∞ is the outer stream velocity, x is the length of the flat plate, ν is the kinematic viscosity, D is the coefficient of diffusion and C_s is the concentration saturation.

2.3 Mass Transfer from a Vertical Flat Surface due to Natural Convection: Based on work by Kuiken[2]

The case of heat transfer from the surface of a vertical flat plate for large Prandtl numbers was studied by Kuiken[2], in which flow is induced by changes in density close to the surface due to a difference in temperature. The case presented by Kuiken[2] can be easily adapted to model mass transfer from the flat surface of a soluble material. The approach used is to split the problem into two regions: a thin inner layer in which all mass transfer takes place and buoyancy forces dominate, and an outer layer in which buoyancy forces may be neglected. The solution to the inner layer is sought first, at which point it is possible to match the outer layer to the inner solution.

The Inner Layer

The boundary layer equations are

$$\frac{\partial^2 u}{\partial y^2} + \frac{gc}{\rho\nu} = 0 \tag{2.57}$$

$$u\frac{\partial c}{\partial x} + v\frac{\partial c}{\partial y} = D\frac{\partial^2 c}{\partial y^2} \tag{2.58}$$

$$\frac{\partial u}{\partial x} + \frac{\partial v}{\partial y} = 0, \tag{2.59}$$

where x is the distance from the leading edge, y is the distance from the wall, u and v are the components of velocity in the x and y directions respectively, g is acceleration due to gravity, ν is the kinematic viscosity of the dissolution medium, ρ is the density, c is the concentration of dissolved particles and D is the coefficient of diffusion of the soluble material. Introducing $c = C_s C$, where C_s is the concentration saturation, and letting $\gamma = \frac{gC_s}{\rho\nu}$, equations (2.57) and (2.58) can be written:

$$\frac{\partial^2 u}{\partial y^2} + \gamma C = 0 \tag{2.60}$$

$$u\frac{\partial C}{\partial x} + v\frac{\partial C}{\partial y} = D\frac{\partial^2 C}{\partial y^2} \tag{2.61}$$

Introducing a stream function of the form $u = \frac{\partial \psi}{\partial y}$, from the continuity equation we obtain $v = -\frac{\partial \psi}{\partial x}$. Substituting in for u and v, equations (2.60) and (2.61) become

$$\frac{\partial^3 \psi}{\partial y^3} + \gamma C = 0 \tag{2.62}$$

$$\frac{\partial \psi}{\partial y}\frac{\partial C}{\partial x} - \frac{\partial \psi}{\partial x}\frac{\partial C}{\partial y} = D\frac{\partial^2 C}{\partial y^2} \tag{2.63}$$

where the stream function is of the form

$$\psi = kx^{\frac{3}{4}} f(\eta) \tag{2.64}$$

and

$$\eta = jyx^{-\frac{1}{4}}. \tag{2.65}$$

It is also assumed that the non-dimensional concentration, C, is a function of η and takes the form

$$C = h(\eta). \tag{2.66}$$

The various derivatives of both the stream function and the non-dimensional concentration are found to be

$$\begin{aligned}
\tfrac{\partial \psi}{\partial y} &= jkx^{\frac{2}{4}} f'(\eta) \\
\tfrac{\partial^2 \psi}{\partial y^2} &= j^2 kx^{\frac{1}{4}} f''(\eta) \\
\tfrac{\partial^3 \psi}{\partial y^3} &= j^3 k f'''(\eta) \\
\tfrac{\partial \psi}{\partial x} &= \tfrac{3}{4} kx^{-\frac{1}{4}} f(\eta) - \tfrac{1}{4} kx^{-\frac{1}{4}} \eta f'(\eta) \\
\tfrac{\partial C}{\partial x} &= -\tfrac{1}{4} x^{-1} \eta h'(\eta) \\
\tfrac{\partial C}{\partial y} &= jx^{-\frac{1}{4}} h'(\eta) \\
\tfrac{\partial C^2}{\partial y^2} &= j^2 x^{-\frac{2}{4}} h''(\eta).
\end{aligned} \tag{2.67}$$

Substituting these into equations (2.62) and (2.63) leads to

$$f'''(\eta) + \frac{\gamma}{kj^3} h(\eta) = 0 \tag{2.68}$$

$$h''(\eta) + \frac{3k}{4Dj} f(\eta) h'(\eta) = 0. \tag{2.69}$$

Equations (2.68) and (2.69) may be simplified by taking $kj^3 = \gamma$ and $\frac{k}{Dj} = 4$, where $j = \left[\frac{gC_s}{4D\rho\nu}\right]^{\frac{1}{4}}$ and $k = 4D\left[\frac{gC_s}{4D\rho\nu}\right]^{\frac{1}{4}}$. This leads to the stream function

$$\psi = 4D\left[\frac{gC_s x^3}{4D\rho\nu}\right]^{\frac{1}{4}} f(\eta), \tag{2.70}$$

where

$$\eta = y\left[\frac{gC_s}{4D\rho\nu x}\right]^{\frac{1}{4}}. \tag{2.71}$$

The differential equations to be solved are

$$f'''(\eta) + h(\eta) = 0 \tag{2.72}$$

$$h''(\eta) + 3f(\eta)h'(\eta) = 0. \tag{2.73}$$

Equations (2.72) and (2.73) were solved by Kuiken[2] subject to the boundary conditions

$$\begin{cases} \eta = 0, h_0(\eta) = 1, f_0(\eta) = f_0'(\eta) = 0 \\ \eta \to \infty, h_0(\eta) \to 0. \end{cases}$$

The results obtained by Kuiken[2] are given as

$$\begin{aligned} f_0''(0) &\approx 0.825 \\ h_0'(0) &\approx -0.711 \\ f_0'(\infty) &\approx 0.511. \end{aligned}$$

The resulting flux per unit area is given by

$$\begin{aligned} \text{Flux / Unit Area} &= -D\left[\frac{\partial c}{\partial y}\right]_{y=0} \\ &= -DC_s\left[jh'(0)x^{-\frac{1}{4}}\right]. \end{aligned} \tag{2.74}$$

From equation (2.74), the total flux per unit width is given by

$$\begin{aligned} \text{Flux / Unit Width} &= -DC_s\left[jh'(0)\right]\int_0^x x^{-\frac{1}{4}}dx \\ &= -\frac{4}{3}h'(0)DC_s\left[\frac{gC_s}{4D\rho\nu}\right]^{\frac{1}{4}}x^{\frac{3}{4}}. \end{aligned} \tag{2.75}$$

The Outer Layer

The boundary layer equations are

$$u\frac{\partial u}{\partial x}+v\frac{\partial u}{\partial y}=\nu\frac{\partial^2 u}{\partial y^2} \tag{2.76}$$

$$\frac{\partial u}{\partial x}+\frac{\partial v}{\partial y}=0. \tag{2.77}$$

Introducing a stream function of the form $\psi = k_1 x^{\frac{3}{4}}F(\xi)$ where $\xi = j_1 y x^{-\frac{1}{4}}$, $k_1 = 4D\left[\frac{S_c^2}{4}\right]^{\frac{1}{4}}\left[\frac{gC_s}{4D\rho\nu}\right]^{\frac{1}{4}}$, $j_1 = \left[\frac{1}{4S_c^2}\right]^{\frac{1}{4}}\left[\frac{gC_s}{4D\rho\nu}\right]^{\frac{1}{4}}$ and $S_c = \frac{\nu}{D}$, leads to the following ordinary differential equation:

$$F_0'''(\xi)+3F_0''(\xi)F_0(\xi)-2F_0'(\xi)F_0'(\xi)=0. \tag{2.78}$$

In order to match the solution with that of the inner layer, equation (2.78) was solved for the following boundary conditions:

$$\begin{cases} \xi = 0, F_0(\xi)=0, F_0'(\xi)=f_0'(\infty)=0.511 \\ \xi\to\infty, F_0(\xi)\to\text{constant}, F_0'(\xi)\to 0, F_0''(\xi)\to 0. \end{cases}$$

The results obtained are given as

$$\begin{aligned} F_0''(0) &\approx -0.5628 \\ f_0(\infty) &\approx 0.43. \end{aligned}$$

Velocity and Concentration Profiles

In order to plot an overall velocity profile it should be noted that $\eta = S_c^{\frac{1}{2}}\xi$. Figure (2.1) shows the velocity profile for both the inner and outer layer for $S_c = 100$. Figure (2.2) shows the concentration profile that exists within the inner layer.

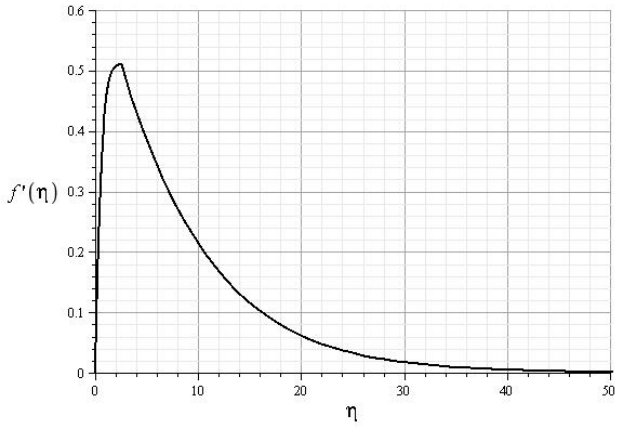

Figure 2.1: Velocity Profile: Pure Natural Convection ($S_c = 100$)

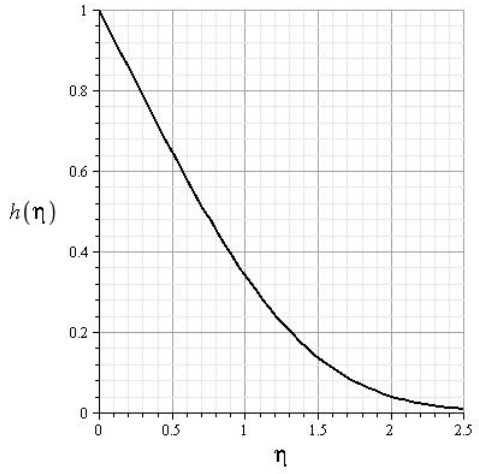

Figure 2.2: Concentration Profile: Pure Natural Convection

Chapter 3

Dissolution Rates from the Top Planar Surface of a Compact in the USP Paddle Apparatus

This chapter examines the rate of drug dissolution from the top planar surface of a compact in all three positions (see figure 1.1). The flow in position 1 and position 2 is treated as flow over a flat plate. The chapter first looks at the Pohlhausen method for flow over a flat plate using the Blasius velocity profile with various concentration profiles. The Pohlhausen solutions are then compared with the exact solution of Lévêque[1] to choose the most suitable concentration profile. The approximate solution is then applied to the surface of the compact by dividing the surface into strips.

For the compact in the central position a converging radial flow exists. Using CFD velocity data an appropriate velocity profile is constructed and used in conjunction with the previously constructed concentration profile. To apply the method to the compact in the central position the compact surface is divided into an outer annular area and an inner circular area. For the central position an exact solution is also sought using the method of asymptotic expansions to verify the results of the approximate method. All results obtained are then compared with those of experiment, as conducted by D'Arcy[6].

3.1 Determination of Suitable Concentration Profile

As mentioned in chapter two, an exact solution to mass transfer from the surface of a flat plate exists based on the work of Lévêque[1]. Later, in section (3.2), it will be shown that this solution may be applied directly to the case of drug dissolution from the top planar surface of a compact in positions 1 and 2. However, in the case of a centrally placed compact this exact solution is not valid. For this reason it is advantageous to derive an approximate solution, the accuracy of which will be measured against that of the Lévêque[1] solution in the case of off-centre compacts, that may be used in instances where an exact solution is not possible. The approximate solution will be obtained by means of the Pohlhausen method as discussed in chapter one. The concentration boundary layer equation is

$$u\frac{\partial c}{\partial x} + v\frac{\partial c}{\partial y} = D\frac{\partial^2 c}{\partial y^2}, \tag{3.1}$$

where (u, v) are the velocity components in the (x, y) directions, D is the coefficient of diffusion and c is the concentration of dissolved particles.

The Pohlhausen method involves integrating the boundary layer equation with respect to y across the boundary layer. Performing this integration and applying the boundary conditions for flow across a flat plate leads to the concentration integral equation:

$$\frac{d}{dx}\int_0^{\delta_C} ucdy = -D\left[\frac{\partial c}{\partial y}\right]_{y=0}, \tag{3.2}$$

where δ_C is the concentration boundary layer thickness. In order to solve this equation appropriate velocity and concentration profiles must be substituted in for u and c respectively. In the case presented by Lévêque[1], the Blasius velocity

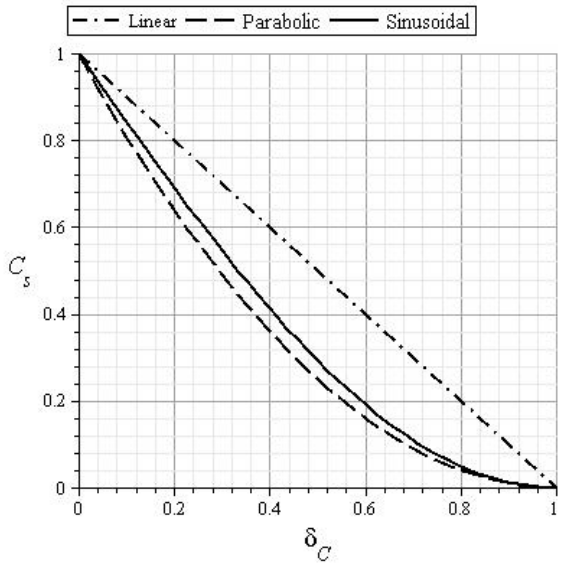

Figure 3.1: Illustration of Concentration Profiles

profile for flow across a flat plate is applied. It is therefore appropriate that this velocity profile is also applied to the approximate methods used in this section. The Blasius profile is given as

$$u = 0.332 y U_\infty \sqrt{\frac{U_\infty}{\nu x}}, \tag{3.3}$$

where U_∞ is the outer stream velocity and ν is the kinematic viscosity.

Having chosen a suitable velocity profile it is now required that a suitable concentration profile be chosen. Now, in the case of drug dissolution the concentration at the surface must be equal to that of the concentration saturation, C_s. The concentration level must also diminish to zero as the edge of the concentration boundary layer is approached. Three separate concentration profiles, as illustrated in figure (3.1), are applied to the integral equation (3.2). The results are then compared with that of the exact solution to obtain the concentration profile that best fits the model.

Linear Concentration Profile

The linear concentration profile is chosen to be

$$c = C_s \left[1 - \frac{y}{\delta_c}\right], \tag{3.4}$$

where C_s is the concentration saturation and δ_c is the concentration boundary layer thickness. Substituting (3.4), along with the Blasius velocity profile (3.3) into the concentration integral equation (3.2) gives

$$\frac{d}{dx}\left[x^{-\frac{1}{2}}\delta_c^2\right] = \frac{6D}{0.332\delta_c}\sqrt{\frac{\nu}{U_\infty^3}}. \tag{3.5}$$

Performing the differentiation on the left hand side of equation (3.5) and simplifying leads to the ordinary differential equation

$$2\delta_c^2\frac{d\delta_c}{dx} - \frac{\delta_c^3}{2x} = \frac{6D}{0.332}\sqrt{\frac{\nu x}{U_\infty^3}}. \tag{3.6}$$

The ordinary differential equation (3.6) is solved by means of an integrating factor to obtain an expression for the concentration boundary layer thickness, δ_c. This is found to be

$$\delta_c = \left[\frac{12D}{0.332}\sqrt{\frac{\nu}{U_\infty^3}}\right]^{\frac{1}{3}}\left[x^{\frac{1}{2}}\right]. \tag{3.7}$$

The total flux per unit area is given by

$$\begin{aligned} \text{Flux / Unit Area} &= -D\left[\frac{\partial c}{\partial y}\right]_{y=0} \\ &= \frac{DC_s}{\delta_c}. \end{aligned} \tag{3.8}$$

Substituting in for δ_c, equation (3.8) becomes

$$\text{Flux / Unit Area} = \left[\frac{0.332}{12}\right]^{\frac{1}{3}}\left[\frac{U_\infty^{\frac{1}{2}}D^{\frac{2}{3}}C_s}{\nu^{\frac{1}{6}}x^{\frac{1}{2}}}\right]. \tag{3.9}$$

From equation (3.9), the flux per unit width is given as

$$\begin{aligned} \text{Flux / Unit Width} &= \left[\frac{0.332}{12}\right]^{\frac{1}{3}} \left[\frac{U_\infty^{\frac{1}{2}} D^{\frac{2}{3}} C_s}{\nu^{\frac{1}{6}}}\right] \int_0^x x^{-\frac{1}{2}} dx \\ &= 0.605 \frac{U_\infty^{\frac{1}{2}} D^{\frac{2}{3}} C_s x^{\frac{1}{2}}}{\nu^{\frac{1}{6}}}. \end{aligned} \tag{3.10}$$

Parabolic Concentration Profile

The parabolic concentration profile is chosen to be

$$c = C_s \left[1 - \frac{y}{\delta_c}\right]^2. \tag{3.11}$$

Substituting equation (3.11) into the concentration integral equation (3.2), along with the Blasius velocity profile gives

$$\frac{d}{dx}\left[x^{-\frac{1}{2}} \delta_c^2\right] = \frac{24D}{0.332\delta_c} \sqrt{\frac{\nu}{U_\infty^3}}, \tag{3.12}$$

which leads to the ordinary differential equation

$$3\delta_c^2 \frac{d\delta_c}{dx} - \frac{\delta_c^3}{2x} = \frac{24D}{0.332} \sqrt{\frac{\nu x}{U_\infty^3}}. \tag{3.13}$$

As in the case of the linear concentration profile, equation (3.13) is solved by means of an integrating factor to obtain

$$\delta_c = \left[\frac{48D}{0.332} \sqrt{\frac{\nu}{U_\infty^3}}\right]^{\frac{1}{3}} \left[x^{\frac{1}{2}}\right]. \tag{3.14}$$

The total flux per unit area is given by

$$\begin{aligned} \text{Flux / Unit Area} &= -D \left[\frac{\partial c}{\partial y}\right]_{y=0} \\ &= \frac{2DC_s}{\delta_c}. \end{aligned} \tag{3.15}$$

Substituting in for δ_c, equation (3.15) becomes

$$\text{Flux / Unit Area} = \left[\frac{0.332}{6}\right]^{\frac{1}{3}} \left[\frac{U_\infty^{\frac{1}{2}} D^{\frac{2}{3}} C_s}{\nu^{\frac{1}{6}} x^{\frac{1}{2}}}\right]. \tag{3.16}$$

From equation (3.16), the flux per unit width is found to be

$$\begin{aligned} \text{Flux / Unit Width} &= \left[\frac{0.332}{6}\right]^{\frac{1}{3}} \left[\frac{U_\infty^{\frac{1}{2}} D^{\frac{2}{3}} C_s}{\nu^{\frac{1}{6}}}\right] \int_0^x x^{-\frac{1}{2}} dx \\ &= 0.762 \frac{U_\infty^{\frac{1}{2}} D^{\frac{2}{3}} C_s x^{\frac{1}{2}}}{\nu^{\frac{1}{6}}}. \end{aligned} \tag{3.17}$$

Sinusoidal Concentration Profile

The sinusoidal concentration profile is chosen to be

$$c = C_s \left[1 - \sin\left(\frac{y\pi}{2\delta_c}\right)\right]. \tag{3.18}$$

Substituting equations (3.18) and (3.3) into the concentration integral equation (3.2) gives

$$\frac{d}{dx}\left[x^{-\frac{1}{2}}\delta_c^2\right] = \frac{D\pi^3}{0.332\delta_c\left(\pi^2 - 8\right)}\sqrt{\frac{\nu}{U_\infty^3}}. \tag{3.19}$$

Equation (3.19) is simplified to give the ordinary differential equation

$$3\delta_c^2 \frac{d\delta_c}{dx} - \frac{3\delta_c^3}{4x} = \frac{3D\pi^3}{2\left(0.332\right)\left(\pi^2 - 8\right)}\sqrt{\frac{\nu x}{U_\infty^3}}. \tag{3.20}$$

Again equation (3.20) is solved by means of an integrating factor to give

$$\delta_c = \left[\frac{2D\pi^3}{0.332\left(\pi^2 - 8\right)}\sqrt{\frac{\nu}{U_\infty^3}}\right]^{\frac{1}{3}} \left[x^{\frac{1}{2}}\right]. \tag{3.21}$$

The total flux per unit area is given by

$$\begin{aligned} \text{Flux / Unit Area} &= -D\left[\frac{\partial c}{\partial y}\right]_{y=0} \\ &= \frac{\pi D C_s}{2\delta_c}. \end{aligned} \tag{3.22}$$

Substituting in for δ_c and integrating along the length gives the flux per unit width as

$$\text{Flux / Unit Width} \quad = \quad 0.677\frac{U_\infty^{\frac{1}{2}} D^{\frac{2}{3}} C_s x^{\frac{1}{2}}}{\nu^{\frac{1}{6}}}. \tag{3.23}$$

Comparison of Concentration Profiles

Table (3.1) shows the comparison between the approximate method using several concentration profiles and the exact solution based on the work of Lévêque[1]. It is clear from table (3.1) that the linear and parabolic concentration profiles under-estimate and over-estimate the flux from the surface respectively. The flux determined using the sinusoidal concentration profile seems to match that of the exact solution well. Indeed, the flux obtained using the sinusoidal profile is equal to that of the exact solution to 0.1%. The sinusoidal concentration profile may therefore be used to calculate an approximate solution in cases where an exact solution may not be obtained.

Table 3.1: Comparison of Approximate Methods with Exact Solution

		Flux per Unit Width
Exact Solution		$0.677\frac{U_\infty^{\frac{1}{2}} D^{\frac{2}{3}} C_s x^{\frac{1}{2}}}{\nu^{\frac{1}{6}}}$
Pohlhausen Method	Sinusoidal Profile	$0.677\frac{U_\infty^{\frac{1}{2}} D^{\frac{2}{3}} C_s x^{\frac{1}{2}}}{\nu^{\frac{1}{6}}}$
	Linear Profile	$0.605\frac{U_\infty^{\frac{1}{2}} D^{\frac{2}{3}} C_s x^{\frac{1}{2}}}{\nu^{\frac{1}{6}}}$
	Parabolic Profile	$0.762\frac{U_\infty^{\frac{1}{2}} D^{\frac{2}{3}} C_s x^{\frac{1}{2}}}{\nu^{\frac{1}{6}}}$

3.2 Dissolution Rates from the Top Planar Surface of a Compact in Position1 and Position2

In this section the rate of drug dissolution from the top planar surface of a compact in position 1 and position 2 is calculated. To achieve this the surface is divided up into strips of width 1mm. The characteristic length of each strip is taken down the centre. Finding the area of the strips and using the characteristic length of each, rectangular strips of equal area and length are constructed. The outer stream velocity for each strip is determined from CFD simulations kindly provided by D'Arcy[25] for use in this thesis. Any required intermediate velocities are calculated by means of linear regression.

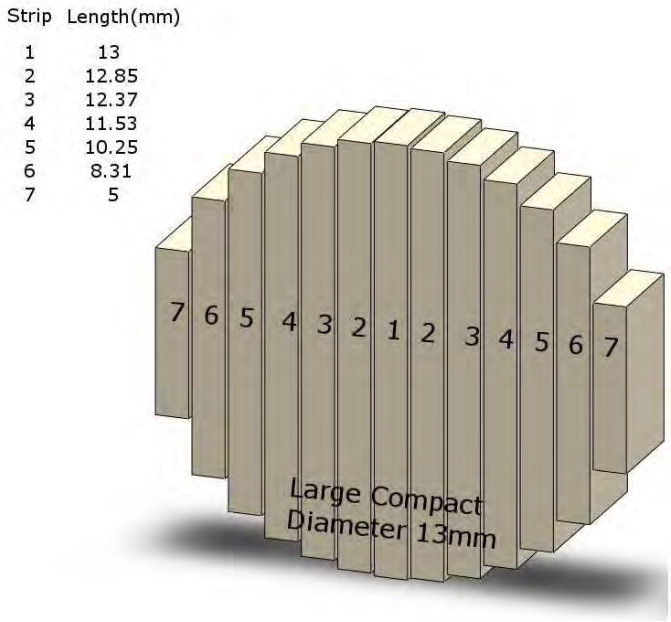

Figure 3.2: Illustration of Surface Strips

Experimental work

In the experimental work conducted by D'Arcy[6] the compacts used are composed of benzoic acid and are 13mm in diameter. Values for the coefficient of diffusion and the concentration saturation of benzoic acid are given as $D = 1.236 \times 10^{-5}\text{cm}^2/\text{s}$ and $C_s = 4.564 \times 10^{-3}\text{g/cm}^3$ respectively. These values are used throughout this chapter in determining the rate of drug dissolution from the surface of a compact.

Outer Stream Velocities

The velocity data for each strip is obtained from CFD simulations performed by D'Arcy[6].

Table 3.2: Outer Stream Velocity Data

				Velocity (cm/s)
Strip	Length (cm)	Width (cm)	Position 1	Position 2
7_L	0.5	0.094	5	8.7
6_L	0.831	0.099	5.234	8.667
5_L	1.025	0.099	5.667	8.633
4_L	1.153	0.099	6	8.6
3_L	1.237	0.099	6.334	8.567
2_L	1.285	0.099	6.667	8.533
1	1.3	0.1	7	8.5
2_R	1.285	0.099	7.334	8.467
3_R	1.237	0.099	7.667	8.433
4_R	1.153	0.099	8	8.4
5_R	1.025	0.099	8.334	8.367
6_R	0.831	0.099	8.667	8.334
7_R	0.5	0.094	8.998	8.3

Any intermediate velocities required are obtained by means of linear regression. Table (3.2) shows the outer stream velocity, U_∞, for each strip in both

position 1 and position 2. Also contained in table (3.2) are the length and width of each strip.

Calculation of the Dissolution Rate from the Surface

For the top planar surface of a compact in positions 1 and 2, the process of drug dissolution from the surface can be treated as mass transfer from a horizontal flat plate. The solution of Lévêque[1] is therefore valid and from equation (2.56) the flux per unit width is given as

$$\text{Flux / Unit Width} = 0.677\frac{U_{\infty}^{\frac{1}{2}} D^{\frac{2}{3}} C_s x^{\frac{1}{2}}}{\nu^{\frac{1}{6}}}. \tag{3.24}$$

Applying equation (3.24) to each strip, the total flux from the surface is given by

$$\text{Total Flux} = 0.677 \left[\frac{D^{\frac{2}{3}} C_s}{\nu^{\frac{1}{6}}}\right] \left[\sum_{i=-6}^{6} U_i^{\frac{1}{2}} x_i^{\frac{1}{2}} W_i\right], \tag{3.25}$$

where U_i represents the velocity , x_i the length and W_i the width of each strip. Taking the values presented in table (3.2), the flux from the surface of a compact in position 1 and 2 are calculated and shown in table (3.3) along with the experimental results of D'Arcy[6].

Table 3.3: Dissolution Rates from Top Surface of a Compact in Position 1 and 2

Compact	Theoretical Results(g/s)	Experimental Results(g/s)
Position 1	1.22×10^{-5}	1.36×10^{-5}
Position 2	1.41×10^{-5}	1.40×10^{-5}

3.3 Dissolution Rates from the Top Planar Surface of a Compact in the Central Position

This section examines the drug dissolution rate from the top planar surface of a compact in the central position. For the case in the central position two types of compact are examined, the first of height 3mm and the second of height 8.5mm. The taller compact has been used in experimental work and it is examined here to determine the possible effect of the paddle when in close proximity to the top planar surface. It has been noted in CFD simulations that a region of low velocity exists directly beneath the paddle, which may lead to a decrease in mass transfer rates from the surface. Both compacts are composed of benzoic acid and are of diameter 13mm. Again, velocity data is obtained from CFD simulations. For the case presented in the previous section the flow was treated as that of flow across a flat plate. This means that the exact solution of Lévêque[1], which depends on the Blasius velocity profile, can be applied. However, for the compact in the central position the flow is that of a converging radial flow, for which the Blasius velocity profile is no longer valid. A relevant velocity profile is constructed using CFD simulation data. This velocity profile is then used in conjunction with the sinusoidal concentration profile constructed in section (3.2) to obtain an approximate solution based on the Pohlhausen method. In the case of the 3mm tall compact an exact solution is also obtained by means of an asymptotic series expansion in order to verify the approximate solution.

Dissolution Rates from the Surface of a 3mm Tall Compact

The velocity data obtained from CFD simulations is plotted for a 3mm tall compact in the central position and is shown in figure (3.3).

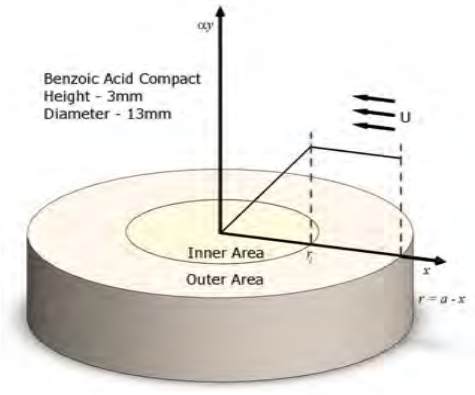

Figure 3.3: Velocity Profile along Top Surface:Central Position(3mm Compact)

Figure (3.3) shows a plot of αy versus r, where α is the velocity gradient and r is the radial distance along the compact surface. From this data a suitable velocity profile is constructed. This is given as

$$u = \begin{cases} -\alpha y & \text{for} \quad r_1 \leq r \leq a \\ -\frac{\alpha y r}{r_1} & \text{for} \quad 0 \leq r \leq r_1 \end{cases}$$

where $r = a - x$, a is the compact radius and r_1 is the distance from the centre at which the velocity gradient begins to diminish toward zero. This velocity profile, along with the previously constructed sinusoidal concentration profile are used to solve the concentration integral equation. To apply the method to the compact the surface is divided into an outer annular area and an inner circular area.

Outer Annular Area

The concentration integral equation in polar coordinates is

$$\frac{d}{dr}\int_0^{\delta_c} rucdy = -rD\left[\frac{\partial c}{\partial y}\right]_{y=0}. \tag{3.26}$$

The velocity and concentration profiles are given by

$$u = -\alpha y \tag{3.27}$$

$$c = C_s\left[1-\sin\left[\frac{\pi y}{2\delta_c}\right]\right]. \tag{3.28}$$

Substituting equations (3.27) and (3.28) into the concentration integral equation (3.26) gives

$$\frac{d}{dr}\left[\alpha r\int_0^{\delta_c}\left[y - y\sin\left[\frac{\pi y}{2\delta_c}\right]\right]dy\right] = \frac{-D\pi r}{2\delta_c}. \tag{3.29}$$

Now, noting that $\int_0^{\delta_c}\left[y - y\sin\left[\frac{\pi y}{2\delta_c}\right]\right]dy = \frac{\delta_c^2\left[\pi^2-8\right]}{2\pi^2}$ and performing the differentiation on the left hand side, equation (3.29) may be reduced to

$$3\delta_c^2\frac{d\delta_c^2}{dr} + \frac{3\delta_c^3}{2r} = -\frac{3D\pi}{4\alpha}\left[\frac{2\pi^2}{\pi^2-8}\right]. \tag{3.30}$$

Now letting $\Delta = \delta_c^3$, equation (3.30) is written

$$\frac{d\Delta}{dr} + \frac{3\Delta}{2r} = -\frac{3D\pi}{4\alpha}\left[\frac{2\pi^2}{\pi^2-8}\right]. \tag{3.31}$$

The ordinary differential equation (3.31) is solved by means of an integrating factor to yield

$$\Delta_{\text{outer}} = \frac{3\pi Da}{10\alpha}\left[\frac{2\pi^2}{\pi^2-8}\right]\left[\frac{1-R^{\frac{5}{2}}}{R^{\frac{3}{2}}}\right], \tag{3.32}$$

where $R = \frac{r}{a}$.

Inner Circular Area

From equation (3.26) the concentration integral equation is

$$\frac{d}{dr}\int_0^{\delta_c} rucdy = -rD\left[\frac{\partial c}{\partial y}\right]_{y=0}. \tag{3.33}$$

The velocity and concentration profiles are given as

$$u = -\frac{\alpha y r}{r_1} \tag{3.34}$$

$$c = C_s\left[1 - \sin\left[\frac{\pi y}{2\delta_c}\right]\right]. \tag{3.35}$$

Substituting equations (3.34) and (3.35) into the concentration integral equation (3.33) gives

$$\frac{d}{dr}\left[\frac{\alpha r^2}{r_1}\int_0^{\delta_c}\left[y - y\sin\left[\frac{\pi y}{2\delta_c}\right]\right]dy\right] = \frac{-D\pi r}{2\delta_c}. \tag{3.36}$$

Equation (3.36) may be simplified to give the ordinary differential equation

$$\frac{d\Delta}{dr} + \frac{3\Delta}{r} = -\frac{3D\pi r_1}{4\alpha r}\left[\frac{2\pi^2}{\pi^2 - 8}\right], \tag{3.37}$$

where $\Delta = \delta_c^3$. Solving equation (3.37) by means of an integrating factor leads to

$$\Delta_{\text{inner}} = \frac{\pi Da R_1}{4\alpha}\left[\frac{2\pi^2}{\pi^2 - 8}\right]\left[\frac{B}{R^3} - 1\right], \tag{3.38}$$

where $R = \frac{r}{a}$. Now, at $R = 0.46$, $\Delta_{\text{inner}} = \Delta_{\text{outer}}$. Equating (3.32) and (3.38), B is found to be 0.7945 and equation (3.38) becomes

$$\Delta_{\text{inner}} = \frac{\pi Da R_1}{4\alpha}\left[\frac{2\pi^2}{\pi^2 - 8}\right]\left[\frac{0.7945 - R^3}{R^3}\right]. \tag{3.39}$$

Flux from the Surface

The flux per unit area is given as

$$\begin{aligned} \text{Flux / Unit Area} &= -D\left[\frac{\partial c}{\partial y}\right]_{y=0} \\ &= \frac{\pi D C_s}{2\delta_c}. \end{aligned} \tag{3.40}$$

From equation (3.40) we obtain the total flux from the surface as

$$\text{Flux} = \int_a^0 2\pi r \left[\frac{\pi D C_s}{2\delta_c}\right] dr. \tag{3.41}$$

This leads to

$$\begin{aligned}\text{Flux} = &\left[\pi^5 D^2 C_s^3 a^5 \alpha \left[\frac{\pi^2 - 8}{2\pi^2}\right]\right]^{\frac{1}{3}} \\ &\times \left[\sqrt[3]{\frac{4}{R_1}} \int_0^{R_1} R \left[\frac{R}{[0.7945 - R^3]^{\frac{1}{3}}}\right] dR + \sqrt[3]{\frac{10}{3}} \int_{R_1}^1 R \left[\frac{R^{\frac{3}{2}}}{1 - R^{\frac{5}{2}}}\right]^{\frac{1}{3}} dR\right].\end{aligned} \tag{3.42}$$

Performing the integration in equation (3.42) and simplifying gives

$$\text{Total Flux} = \left[\frac{0.17442}{\sqrt[3]{R_1}} + 2.482\right] D^{\frac{2}{3}} C_s \alpha^{\frac{1}{3}} a^{\frac{5}{3}}, \tag{3.43}$$

where $R_1 = \frac{r_1}{a}$, a is the compact radius, C_s is the concentration saturation and D is the coefficient of diffusion.

Dissolution Rates from the Surface of an 8.5mm Tall Compact

The CFD velocity data for a 8.5mm tall compact in the central position is plotted and shown in figure (3.4). Figure (3.4) shows a plot of αy versus r, where α is the velocity gradient and r is the radial distance along the compact surface. From this a suitable velocity profile is constructed and is given as

$$u = \begin{cases} -\alpha y & \text{for} \quad r_1 \leq r \leq a \\ -\frac{\alpha y r}{r_1} & \text{for} \quad 0 \leq r \leq r_1. \end{cases}$$

The concentration profile is again taken to be

$$c = C_s \left[1 - \sin\left[\frac{\pi y}{2\delta_c}\right]\right]. \tag{3.44}$$

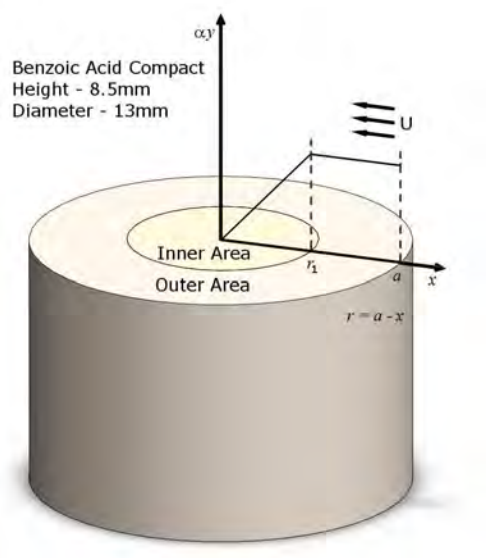

Figure 3.4: Velocity Profile along Top Surface:Central Position(8.5mm Compact)

The process is the same as that used for the 3mm tall compact. The only values to change are that of R_1 and α, which are given as $R_1 = 0.615$ and $\alpha = 130$. This leads to

$$\Delta_{\text{outer}} = \frac{3\pi Da}{10\alpha}\left[\frac{2\pi^2}{\pi^2 - 8}\right]\left[\frac{1 - R^{\frac{5}{2}}}{R^{\frac{3}{2}}}\right] \tag{3.45}$$

$$\Delta_{\text{inner}} = \frac{\pi Da R_1}{4\alpha}\left[\frac{2\pi^2}{\pi^2 - 8}\right]\left[\frac{0.89776 - R^3}{R^3}\right]. \tag{3.46}$$

Flux from the Surface

The flux from the surface is given by

$$\begin{aligned}\text{Flux} = &\left[\pi^5 D^2 C_s^3 a^5 \alpha \left[\frac{\pi^2 - 8}{2\pi^2}\right]\right]^{\frac{1}{3}} \\ &\times \left[\sqrt[3]{\frac{4}{R_1}}\int_0^{R_1} R\left[\frac{R}{[0.89776 - R^3]^{\frac{1}{3}}}\right]dR + \sqrt[3]{\frac{10}{3}}\int_{R_1}^{1} R\left[\frac{R^{\frac{3}{2}}}{1 - R^{\frac{5}{2}}}\right]^{\frac{1}{3}} dR\right]. \end{aligned} \tag{3.47}$$

Performing the integration in equation (3.47) and simplifying gives

$$\text{Total Flux} = \left[\frac{0.3495}{\sqrt[3]{R_1}} + 2.177\right] D^{\frac{2}{3}} C_s \alpha^{\frac{1}{3}} a^{\frac{5}{3}}, \tag{3.48}$$

where $R_1 = \frac{r_1}{a}$, a is the compact radius, α is the velocity gradient, C_s is the concentration saturation and D is the coefficient of diffusion.

Results

As before the values for the concentration saturation and the coefficient of diffusion are taken to be $C_s = 4.564 \times 10^{-3}\text{g/cm}^3$ and $D = 1.236 \times 10^{-5}\text{cm}^2/\text{s}$ respectively. The theoretical and experimental results for the dissolution rate from the top surface of a compact in the central position are shown in table (3.4).

Table 3.4: Dissolution Rates from Top Surface of Compacts in Central Position

Central Position	Theoretical Results(g/s)	Experimental Results(g/s)
8.5mm Compact	1.15×10^{-5}	0.92×10^{-5}
3mm Compact	0.998×10^{-5}	0.99×10^{-5}

3.4 Exact Solution for the Top Surface of a 3mm Tall Compact in the Central Position

In this section an exact solution is sought by means of an asymptotic series solution. The solution is only valid across the outer annular area of the compact surface. The boundary layer equations are

$$u\frac{\partial c}{\partial r} + v\frac{\partial c}{\partial y} = D\frac{\partial^2 c}{\partial y^2} \tag{3.49}$$

$$\frac{\partial}{\partial r}(ur) + \frac{\partial}{\partial y}(vr) = 0. \tag{3.50}$$

Taking the radial velocity component as $u = -\alpha y$ and substituting into the continuity equation (3.50), the axial velocity component is found to be $v = \frac{\alpha y^2}{2r}$. Substituting both of these into the concentration boundary layer equation (3.49) and simplifying we obtain

$$y\frac{\partial C}{\partial X} + \left[\frac{1}{2(1-X)}\right] y^2 \frac{\partial C}{\partial y} = \frac{aD}{\alpha}\frac{\partial^2 C}{\partial y^2}, \tag{3.51}$$

where $r = a - x$, $X = \frac{x}{a}$ and $C = \frac{c}{C_s}$. A concentration profile of the form

$$C = f_0(\eta) + xf_1(\eta) + x^2 f_2(\eta) + x^3 f_3(\eta) + ... \tag{3.52}$$

is assumed, where $\eta = \frac{jy}{\sqrt[3]{x}}$. Substituting (3.52) into equation (3.51) and equating coefficients of x results in the following set of differential equations.

$$\begin{aligned}
&f_0''(\eta) + 3\eta^2 f_0'(\eta) = 0 \\
&f_1''(\eta) + 3\eta^2 f_1'(\eta) - 9\eta f_1(\eta) = \tfrac{9}{2}\eta^2 f_0'(\eta) \\
&f_2''(\eta) + 3\eta^2 f_2'(\eta) - 18\eta f_2(\eta) = \tfrac{9}{2}\eta^2 \left[f_1'(\eta) + f_0'(\eta)\right] \\
&f_3''(\eta) + 3\eta^2 f_3'(\eta) - 27\eta f_3(\eta) = \tfrac{9}{2}\eta^2 \left[f_2'(\eta) + f_1'(\eta) + f_0'(\eta)\right] \\
&f_4''(\eta) + 3\eta^2 f_4'(\eta) - 36\eta f_4(\eta) = \tfrac{9}{2}\eta^2 \left[f_3'(\eta) + f_2'(\eta) + f_1'(\eta) + f_0'(\eta)\right],
\end{aligned}$$

where j is chosen to be $\sqrt[3]{\frac{\alpha}{9aD}}$. The first differential equation is solved analytically, with the rest solved numerically subject to the boundary conditions

$$f_i(0) = 0, f_i(\infty) = 0 \quad \text{for} \quad i \geq 1.$$

The results are found to be $f_0'(0) = -1.2$, $f_1'(0) = 0.3$, $f_2'(0) = 0.2$, $f_3'(0) = 0.13$ and $f_4'(0) = 0.087$. The dissolution rate from the surface is given by the expression

$$\begin{aligned}
\text{Total Flux} = &\left[6D\pi j C_s \sqrt[3]{ax^2}\right] \\
&\times \left[-\frac{af_0'(0)}{2} + \frac{x}{5}\left[f_0'(0) - f_1'(0))\right] + \frac{x^2}{8a}\left[f_1'(0) - f_2'(0)\right] + \frac{x^3}{11a^2}....\right].
\end{aligned} \tag{3.53}$$

This can be improved upon by means of a Padé approximation to give

$$\text{Total Flux} = 6D\pi jC_s\sqrt[3]{ax^2}\left[\frac{0.39 - 1.143x + 0.633x^2}{1 - 2.161x - 0.089x^2}\right]. \tag{3.54}$$

The results for the exact solution for the dissolution rate from the outer annular surface of the 3mm tall compact in the central position are shown in table (3.5) alongside the approximate results obtained in the previous section.

Table 3.5: Dissolution Rates From Outer Annular Section of Top Surface

Exact Solution(g/s)	Padé Solution(g/s)	Pohlhausen Method(g/s)
0.977×10^{-5}	0.983×10^{-5}	0.912×10^{-5}

3.5 Discussion

Off-Centre Compacts

The good agreement between the exact solution and the Pohlhausen solution in the analysis of the top planar surface of the compact in position 1 and 2, means that the Pohlhausen method can be used in cases where an exact solution is not available. Indeed this was the case for the compact in the central position. Comparing the results for position 1 and 2 with the experimental results of D'Arcy [6], we see that the result for position 2 is more accurate. The error is about 1%, compared with an error of 10% in position 1. This variation in error may arise due to the fact that the streamlines of the flow over the top surface are in fact curved. This would have more effect in position 1 as the curvilinear nature of the streamlines becomes less important as the compact is moved away from the central position. Another consideration is the tilt of the compact in position 2. The hemispherical shape of the container causes the compact in position 2 to be

tilted more to the vertical and this leads to less variation in the velocities from one side of the compact to the other.

Centrally Positioned Compacts

The calculated rate of drug dissolution from the top planar surface of the 3mm tall compact is in good agreement with the experimental data. However, for the 8.5mm tall compact the result is less accurate. The error with experimental data is about 1% and 25% respectively. In the case of the 8.5mm tall compact the reason for such a large error is unclear. However, it is known that the Pohlhausen method is largely dependent on the accuracy of the velocity profile used and this may be an area worth analysing in more detail.

Chapter 4

An Analysis of Dissolution Rates from the Curved Side Surface of a Compact in the USP Paddle Apparatus

This chapter examines the rate of drug dissolution from the curved side surface of a compact in the USP Paddle Apparatus. The chapter first looks at the curved side surface of a compact in the central position. An axial flow is dominant along the curved surface and velocity data obtained from D'Arcy[25] is used to construct appropriate velocity profiles which, along with the previously constructed concentration profile, is applied to the concentration integral equation.

For the off-centre positions the flow along the curved surface is more complex due to the tilted nature of the compacts. The CFD velocity data is analysed in greater detail and streamlines of the flow close to the surface are constructed. The streamlines give a clearer view as to the dominant direction of the flow around the surface. As position 2 is the extreme case, we have chosen to examine the compact in this position rather than position 1.

4.1 Dissolution Rates from the Curved Side Surface of a Compact in the Central Position

For the curved side surface of the compact in the central position we first analyse a compact of height 8.5mm. The CFD data in this case clearly shows boundary layer separation at a height of 5.6mm from the base of the compact, after which a second boundary layer forms. The surface is therefore divided into an upper and lower section, each with it's own velocity profile. The velocity profile is given by

$$u = \begin{cases} \alpha_1 y \sin^2\left(\frac{\pi x^{\frac{1}{2}}}{\beta_1^{\frac{1}{2}}}\right) & \text{for} \quad 0 \leq x \leq x_1 \\ \alpha_2 y e^{\beta_2 x} & \text{for} \quad x_1 \leq x \leq x_{max} \end{cases}$$

where α_1 and α_2 are the velocity gradients for each section, $\beta_1 = 0.56$, $\beta_2 = 10.76$ and x_1 is the distance from the base at which boundary layer separation occurs. These velocity profiles, along with the previously constructed concentration profile were used to solve the concentration integral equation, given as

$$\frac{d}{dx}\int_0^\delta ucdy = -D\left[\frac{\partial c}{\partial y}\right]_{y=0}. \tag{4.1}$$

The resulting dissolution rates from each section are given as

$$\text{Flux(lower)} = 3\sqrt{\beta_1}DC_s a\left[\frac{2\alpha_1\zeta\pi}{3D\sqrt{\beta_1}}\right]^{\frac{1}{3}}\left[\sqrt{\beta_1}sin\left(\frac{\pi\sqrt{x}}{\sqrt{\beta_1}}\right) - \sqrt{x}\pi cos\left(\frac{\pi\sqrt{y}}{\sqrt{\beta_1}}\right)\right]^{\frac{2}{3}} \tag{4.2}$$

$$\text{Flux(upper)} = \frac{3\pi^2 DC_s a}{\beta_2}\left[\frac{2\alpha\zeta\beta_2}{3D\pi}\right]^{\frac{1}{3}}\left[\left(e^{\frac{x\beta_2}{2}} - 1\right)^{\frac{2}{3}} - \left(e^{\frac{x_1\beta_2}{2}} - 1\right)^{\frac{2}{3}}\right], \tag{4.3}$$

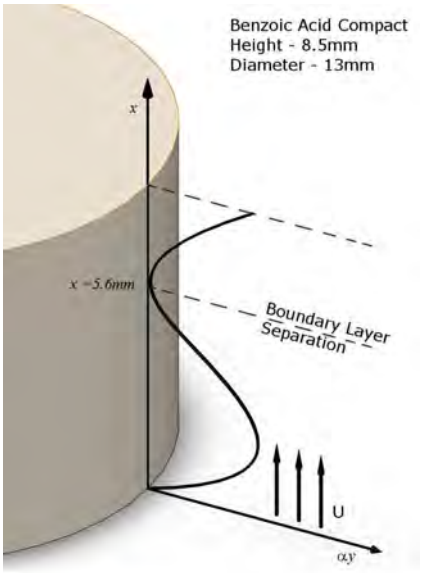

Figure 4.1: Velocity Profile along Curved Side Surface of an 8.5mm Tall Compact

where $\zeta = \frac{\pi^2-8}{2\pi^2}$.

For the 3mm tall compact in the central position, velocity data is only available at three points along the surface(base, mid-height and top). The surface has therefore been divided into a lower and upper section, each with a separate velocity profile which must be matched at the mid-point. The lack of substantial velocity data leads to a somewhat simpler velocity profile and it will be interesting to observe the effect that this has on the results. The velocity profiles for the curved side surface of the 3mm tall compact are given by

$$u = \begin{cases} \frac{\alpha x y}{x_{mid}} & \text{for} \quad 0 \leq x \leq x_{mid} \\ \alpha y & \text{for} \quad x_{mid} \leq x \leq x_{max}. \end{cases}$$

Substituting these profiles into the given concentration integral equation (4.1) results in the following expression for the dissolution rate from the surface.

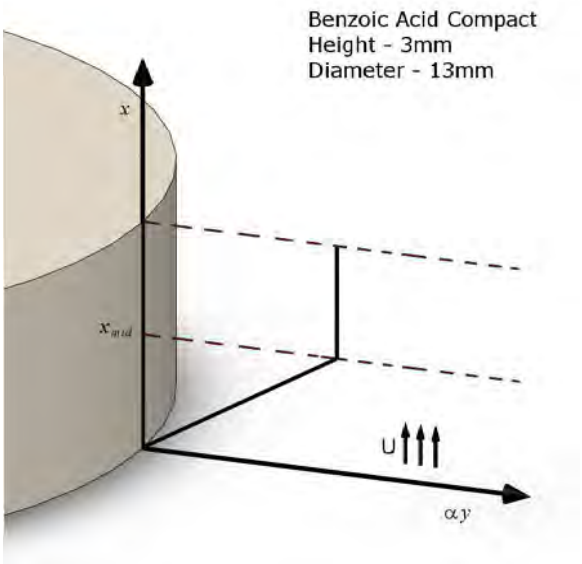

Figure 4.2: Velocity Profile along Curved Side Surface of a 3mm Tall Compact

$$\text{Total Flux} = aC_s \left[\frac{2D^2\pi^5\zeta\alpha}{x_{mid}}\right]^{\frac{1}{3}} \left[x_{mid} + \frac{(2x_{mid})^{\frac{1}{3}}}{3}\left[(3x - x_{mid})^{\frac{2}{3}} - (2x_{mid})^{\frac{2}{3}}\right]\right]. \tag{4.4}$$

The theoretical and experimental results for the dissolution rate from the curved side surface of a compact in the central position are shown below in Table (4.1).

Table 4.1: Dissolution Rates from Side Surface of Compacts in Central Position

Central Position	Theoretical Results(g/s)	Experimental Results(g/s)
8.5mm Compact	3.1989×10^{-5}	3.24×10^{-5}
3mm Compact	1.5152×10^{-5}	1.1245×10^{-5}

4.2 Dissolution Rates from the Curved Side Surface of a Compact in Position 2

For the curved side surface of a compact in position 2 the CFD velocity data is examined in greater detail. Due to the complex nature of the flow, the streamlines of the flow close to the surface have been plotted. The streamlines are shown below in figure (4.3).

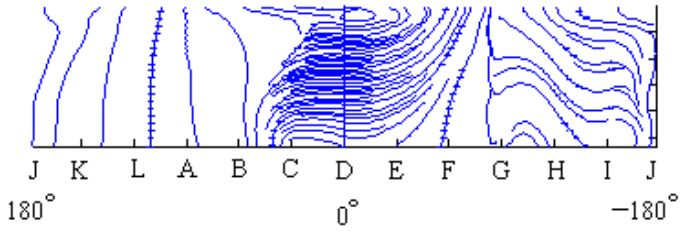

Figure 4.3: Streamlines about Curved Side Surface

We can see from the streamlines the complexity of the flow about the curved side surface of the compact in position 2. The flow as a whole cannot be described as either axially or tangentially dominant; there are instead different sections in which the flow is either axially or tangentially dominant. For this reason, the surface has been divided into a total of eighteen strips of varying length. A linear velocity profile is constructed for each strip and is given by

$$u = \begin{cases} \alpha xy & \text{for} \quad 0 \leq x \leq x_{max}, \end{cases}$$

where α is the velocity gradient for each section, x is the distance from the leading edge, y is the distance from the wall and x_{max} is the maximum length of each strip . This velocity profile, along with the previously constructed concentration profile are used to solve the concentration integral equation, namely;

$$\frac{d}{dx}\int_0^{\delta} ucdy = -D\left[\frac{\partial c}{\partial y}\right]_{y=0}. \tag{4.5}$$

The theoretical and experimental results for the dissolution rate from the curved side surface of a compact in position 2 are shown in table (4.2).

Table 4.2: Dissolution Rates from the side surface of a Compact in Position 2

3mm Compact	Theoretical Results(g/s)	Experimental Results(g/s)
Position 2	1.174×10^{-5}	1.431×10^{-5}

4.3 Discussion

Following the relative success of applying the Pohlhausen method to the top planar surface of the compact the same technique was used to analyse the curved side surface. The analysis of the compact in the central position has mixed results. The calculated dissolution rate from the side surface of the 8.5mm tall compact is extremely accurate when compared with that of experiment, however the result for the 3mm tall compact is less accurate. The respective errors are about 1.3% and 35%. The main factor in these varying results was the CFD data available for both compacts. For the 8.5mm compact, data was available for points along the surface at increments of 0.5mm which allowed for a very accurate velocity profile to be constructed. Also, the data clearly showed boundary layer separation occurring at a height of 5.6mm along the surface, after which a second boundary layer formed. In contrast, data was only available at three points (bottom, mid-height and top) along the surface of the smaller compact. This led to a somewhat estimated velocity profile and hence, a less accurate result.

For the compact in position 2, the complexity of the flow about the surface led to a more difficult analysis. On obtaining the streamlines about the surface the area was divided up into numerous sections, each with it's own linear velocity profile based on the dominant direction (axial or tangential) of the flow in that section. In reality, although the direction of the flow in a number of the sections was apparent, many sections did not exhibit clear flow regimes. The error between experimental and theoretical results was 18%.

Conclusion

In conclusion, the results for the 8.5mm compact were much more accurate then those of the 3mm tall compact. The variation in error appears to be due to the inaccurate velocity profile applied to the surface of the smaller compact, and serves to show just how dependent the Pohlhausen method is on the velocity profile. The result for the 3mm tall compact could be improved with more CFD data for that surface. As for the analysis of the compact in position 2, the results are relatively poor. The streamlines in figure (4.3) show the complexity of the flow and it is not certain whether or not the results can be improved upon using the Pohlhausen method and perhaps an alternative approach would be more suited to this problem.

Chapter 5

Mass Transfer from a Vertical Flat Plate due to Natural Convection with a Constant Counterflow

This chapter first examines both the concentration and momentum boundary layers formed on a vertical flat surface due to natural convection. The surface is composed of a soluble material placed in a liquid medium. In a liquid, molecules diffuse much more slowly than momentum. Consequently, the concentration boundary layer is an order of magnitude thinner than the momentum layer. This model is analogous to that of heat transfer due to natural convection for large Prandtl numbers, for which an exact solution exists due to Kuiken[2]. The approach taken by Kuiken[2] is to divide the problem into two regions: a thin region close to the wall in which buoyancy effects dominate and a much thicker outer region in which buoyancy effects may be neglected. In the case of mass transfer, the inner region is one of natural convection only in which the velocity is generated by the weight of dissolved particles. On obtaining a solution to this inner layer, the outer layer is treated as one of forced convection in which the velocity is generated solely by its contact with the inner layer. This case is taken as a first approximation.

Having examined this first approximation, a perturbation term is introduced to the stream function to model a constant counterflow. In a reversal of the case of Kuiken[2], the outer layer is treated first with its solution then matched into the inner layer. The main aim is to examine the effect that this counterflow has on the maximum downward velocity due to natural convection and consequently the effect that this has on the rate of mass transfer from the surface.

5.1 Mass Transfer from a Vertical Flat Plate due to Natural Convection: Kuiken[2]

The case of heat transfer from the surface of a vertical flat plate for large Prandtl numbers was studied by Kuiken[2], in which flow is induced by changes in density close to the surface due to a difference in temperature. In this section the case presented by Kuiken[2] is adapted to model mass transfer from the vertical flat surface of a soluble material. Kuiken[2] has divided the problem into an inner layer, in which buoyancy forces dominate, and an outer layer in which buoyancy forces may be neglected. The solution to the inner layer is sought first, at which point it is possible to match the outer layer to the inner solution.

The Inner Layer

The concentration boundary layer equation is

$$u\frac{\partial c}{\partial x} + v\frac{\partial c}{\partial y} = D\frac{\partial^2 c}{\partial y^2}, \tag{5.1}$$

where x measures distance from the leading edge, y measures distance from the wall, u and v are the components of velocity in the x and y directions respectively,

c is the concentration of dissolved particles and D is the coefficient of diffusion of the soluble material. The concentration layer thickness is δ_c and within this thin layer the velocity gradient is taken to be α, where

$$\alpha = \left(\frac{\partial u}{\partial y}\right)_{y=0}. \tag{5.2}$$

Examining orders of magnitude in equation (5.1) gives

$$u \sim \alpha\delta_c, \;\; v \sim u\frac{\delta_c}{x}, \;\; \frac{\partial}{\partial x} \sim \frac{1}{x}, \;\; \frac{\partial}{\partial y} \sim \frac{1}{\delta_c}. \tag{5.3}$$

Now, the convection terms on the left hand side of equation (5.1) must be of the same order of magnitude as the diffusion term, $D\frac{\partial^2 c}{\partial y^2}$. This gives

$$\frac{\alpha\delta_c}{x} \sim \frac{D}{\delta_c^2}, \tag{5.4}$$

which leads to

$$\frac{\alpha\delta_c^3}{x} \sim D. \tag{5.5}$$

The momentum boundary layer equation is

$$u\frac{\partial u}{\partial x} + v\frac{\partial u}{\partial y} = \nu\frac{\partial^2 u}{\partial y^2} + \frac{gc}{\rho}, \tag{5.6}$$

where g is acceleration due to gravity, ν is the kinematic viscosity of the dissolution medium and ρ is the density of the pure solvent. Performing a similar order of magnitude analysis as before gives

$$u\frac{\partial u}{\partial x} \sim v\frac{\partial u}{\partial y} \sim \frac{\alpha^2\delta_c^2}{x} \tag{5.7}$$

and

$$\nu\frac{\partial^2 u}{\partial y^2} \sim \frac{\nu\alpha}{\delta_c}. \tag{5.8}$$

This leads to

$$\frac{u\frac{\partial u}{\partial x}}{\nu\frac{\partial^2 u}{\partial y^2}} \sim \frac{\alpha\delta^3}{\nu x}. \tag{5.9}$$

Now, from equation (5.5) we have $\frac{\alpha\delta_c^3}{x} \sim D$, which gives

$$\frac{u\frac{\partial u}{\partial x}}{\nu\frac{\partial^2 u}{\partial y^2}} \sim \frac{D}{\nu} \sim \frac{1}{S_c}, \tag{5.10}$$

where S_c is the Schmidt number. Now for liquids, $S_c >> 1$, and therefore the inertia terms in equation (5.6) may be neglected with error of order $\frac{1}{S_c}$ inside the concentration layer where the momentum boundary layer equation (5.6) reduces to

$$\nu\frac{\partial^2 u}{\partial y^2} = -\frac{gc}{\rho}. \tag{5.11}$$

Therefore, the boundary layer equations are

$$\frac{\partial^2 u}{\partial y^2} + \frac{gc}{\rho\nu} = 0 \tag{5.12}$$

$$u\frac{\partial c}{\partial x} + v\frac{\partial c}{\partial y} = D\frac{\partial^2 c}{\partial y^2} \tag{5.13}$$

$$\frac{\partial u}{\partial x} + \frac{\partial v}{\partial y} = 0. \tag{5.14}$$

Introducing $c = C_s C$, where C_s is the concentration saturation, and letting $\gamma = \frac{gC_s}{\rho\nu}$, equations (5.12) and (5.13) can be written:

$$\frac{\partial^2 u}{\partial y^2} + \gamma C = 0 \tag{5.15}$$

$$u\frac{\partial C}{\partial x} + v\frac{\partial C}{\partial y} = D\frac{\partial^2 C}{\partial y^2}. \tag{5.16}$$

Introducing a stream function of the form $u = \frac{\partial\psi}{\partial y}$, from the continuity equation we obtain $v = -\frac{\partial\psi}{\partial x}$. Substituting in for u and v, equations (5.15) and (5.16) become

$$\frac{\partial^3\psi}{\partial y^3} + \gamma C = 0 \tag{5.17}$$

$$\frac{\partial \psi}{\partial y}\frac{\partial C}{\partial x} - \frac{\partial \psi}{\partial x}\frac{\partial C}{\partial y} = D\frac{\partial^2 C}{\partial y^2}, \tag{5.18}$$

where the stream function is of the form

$$\psi_{\text{inner}} = kx^{\frac{3}{4}} f_0(\eta) \tag{5.19}$$

and

$$\eta = jyx^{-\frac{1}{4}}. \tag{5.20}$$

It is also assumed that the non-dimensional concentration, C, is a function of η and takes the form

$$C = h_0(\eta). \tag{5.21}$$

The various derivatives of both the stream function and the non-dimensional concentration are found to be

$$\begin{aligned}
\tfrac{\partial \psi}{\partial y} &= jkx^{\frac{2}{4}} f_0'(\eta) \\
\tfrac{\partial^2 \psi}{\partial y^2} &= j^2 kx^{\frac{1}{4}} f_0''(\eta) \\
\tfrac{\partial^3 \psi}{\partial y^3} &= j^3 k f_0'''(\eta) \\
\tfrac{\partial \psi}{\partial x} &= \tfrac{3}{4} kx^{-\frac{1}{4}} f_0(\eta) - \tfrac{1}{4} kx^{-\frac{1}{4}} \eta f_0'(\eta) \\
\tfrac{\partial C}{\partial x} &= -\tfrac{1}{4} x^{-1} \eta h_0'(\eta) \\
\tfrac{\partial C}{\partial y} &= jx^{-\frac{1}{4}} h_0'(\eta) \\
\tfrac{\partial C^2}{\partial y^2} &= j^2 x^{-\frac{2}{4}} h_0''(\eta).
\end{aligned} \tag{5.22}$$

Substituting these into equations (5.17) and (5.18) leads to

$$f_0'''(\eta) + \frac{\gamma}{kj^3} h_0(\eta) = 0 \tag{5.23}$$

$$h_0''(\eta) + \frac{3k}{4Dj} f_0(\eta) h_0'(\eta) = 0. \tag{5.24}$$

Equations (5.23) and (5.24) may be simplified by taking $kj^3 = \gamma$ and $\frac{k}{Dj} = 4$, where $j = \left[\frac{gC_s}{4D\rho\nu}\right]^{\frac{1}{4}}$ and $k = 4D\left[\frac{gC_s}{4D\rho\nu}\right]^{\frac{1}{4}}$. This leads to the stream function

$$\psi_{\text{inner}} = 4D\left[\frac{gC_s x^3}{4D\rho\nu}\right]^{\frac{1}{4}} f_0(\eta), \tag{5.25}$$

where

$$\eta = y\left[\frac{gC_s}{4D\rho\nu x}\right]^{\frac{1}{4}}. \tag{5.26}$$

The differential equations to be solved are

$$f_0'''(\eta) + h_0(\eta) = 0 \tag{5.27}$$

$$h_0''(\eta) + 3f_0(\eta)h_0'(\eta) = 0. \tag{5.28}$$

Equations (5.27) and (5.28) are solved numerically subject to the boundary conditions

$$\begin{cases} \eta = 0, h_0(\eta) = 1, f_0(\eta) = f_0'(\eta) = 0 \\ \eta \to \infty, h_0(\eta) \to 0. \end{cases}$$

The results obtained are given as

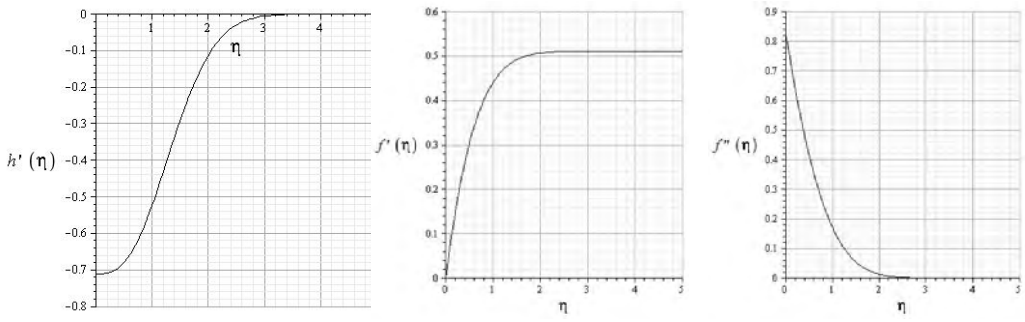

Figure 5.1: Graphical Results for $h'(\eta)$, $f'(\eta)$ and $f''(\eta)$

$$\begin{aligned} f_0''(0) &\approx 0.825 \\ h_0'(0) &\approx -0.711 \\ f_0'(\infty) &\approx 0.511. \end{aligned}$$

The resulting flux per unit area is given by

$$\begin{aligned} \text{Flux / Unit Area} &= -D\left[\frac{\partial c}{\partial y}\right]_{y=0} \\ &= -DC_s\left[jh_0'(0)x^{-\frac{1}{4}}\right]. \end{aligned} \tag{5.29}$$

From equation (5.29), the total flux per unit width is given by

$$\begin{aligned} \text{Flux / Unit Width} &= -DC_s\left[jh_0'(0)\right]\int_0^x x^{-\frac{1}{4}}dx \\ &= -\frac{4}{3}h_0'(0)DC_s\left[\frac{gC_s}{4D\rho\nu}\right]^{\frac{1}{4}}x^{\frac{3}{4}}. \end{aligned} \tag{5.30}$$

The Outer Layer

Since there is no dissolved substance in the outer layer, the boundary layer equations are

$$u\frac{\partial u}{\partial x}+v\frac{\partial u}{\partial y}=\nu\frac{\partial^2 u}{\partial y^2} \tag{5.31}$$

$$\frac{\partial u}{\partial x}+\frac{\partial v}{\partial y}=0. \tag{5.32}$$

Introducing a stream function of the form $u=\frac{\partial\psi}{\partial y}$, from the continuity equation we obtain $v=-\frac{\partial\psi}{\partial x}$. Substituting in for u and v, equation (5.31) becomes

$$\frac{\partial\psi}{\partial y}\frac{\partial^2\psi}{\partial x\partial y}-\frac{\partial\psi}{\partial x}\frac{\partial^2\psi}{\partial y^2}=\nu\frac{\partial^3\psi}{\partial y^3}, \tag{5.33}$$

where

$$\psi_{\text{outer}}=k_1x^{\frac{3}{4}}F_0(\xi) \tag{5.34}$$

and

$$\xi=j_1yx^{-\frac{1}{4}}. \tag{5.35}$$

The various derivatives of the stream function are found to be

$$\begin{aligned}
\frac{\partial\psi}{\partial y} &= j_1 k_1 x^{\frac{2}{4}} F_0'(\xi) \\
\frac{\partial^2\psi}{\partial y^2} &= j_1^2 k_1 x^{\frac{1}{4}} F_0''(\xi) \\
\frac{\partial^3\psi}{\partial y^3} &= j_1^3 k_1 F_0'''(\xi) \\
\frac{\partial\psi}{\partial x} &= \tfrac{3}{4} k_1 x^{-\frac{1}{4}} F_0(\xi) - \tfrac{1}{4} k_1 x^{-\frac{1}{4}} \xi F_0'(\xi). \qquad (5.36)
\end{aligned}$$

Substituting these into equation (5.33) leads to

$$F_0'''(\xi) + \frac{3k_1}{4j_1\nu} F_0''(\xi) F_0(\xi) - \frac{2k_1}{4j_1\nu} F_0'(\xi) F_0'(\xi) = 0. \qquad (5.37)$$

Equation (5.37) may be simplified by taking $\frac{k_1}{j_1\nu} = 4$, where $j_1 = \left[\frac{1}{4S_c^2}\right]^{\frac{1}{4}} \left[\frac{gC_s}{4D\rho\nu}\right]^{\frac{1}{4}}$, $k_1 = 4D\left[\frac{S_c^2}{4}\right]^{\frac{1}{4}} \left[\frac{gC_s}{4D\rho\nu}\right]^{\frac{1}{4}}$ and $S_c = \frac{\nu}{D}$. This leads to the stream function:

$$\psi_{\text{outer}} = 4D\left[\frac{S_c^2}{4}\right]^{\frac{1}{4}} \left[\frac{gC_s x^3}{4D\rho\nu}\right]^{\frac{1}{4}} F_0(\xi), \qquad (5.38)$$

where

$$\xi = y\left[\frac{1}{4S_c^2}\right]^{\frac{1}{4}} \left[\frac{gC_s}{4D\rho\nu x}\right]^{\frac{1}{4}}. \qquad (5.39)$$

The differential equation to be solved is

$$F_0'''(\xi) + 3F_0''(\xi) F_0(\xi) - 2F_0'(\xi) F_0'(\xi) = 0. \qquad (5.40)$$

In order to match the solution with that of the inner layer, equation (5.40) was solved for the following boundary conditions

$$\begin{cases} \xi = 0, F_0(\xi) = 0, F_0'(\xi) = f_0'(\infty) = 0.511 \\ \xi \to \infty, F_0(\xi) \to \text{constant}, F_0'(\xi) \to 0, F_0''(\xi) \to 0. \end{cases}$$

The results obtained are

$$\begin{aligned}
F_0''(0) &\approx -0.5628 \\
F_0'(0) &\approx 0.511 \\
F_0(\infty) &\approx 0.43.
\end{aligned}$$

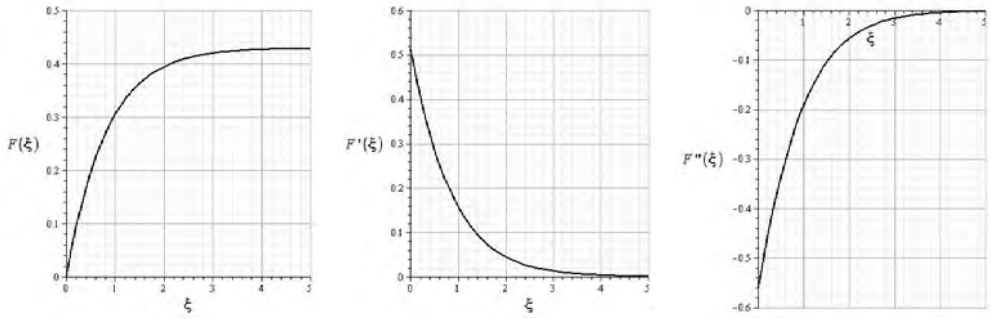

Figure 5.2: Graphical Results for $F(\xi)$, $F'(\xi)$ and $F''(\xi)$

Velocity and Concentration Profiles

In order to plot an overall velocity profile it should be noted that $\eta = S_c^{\frac{1}{2}}\xi$. Figure (5.3) shows the velocity profile for both the inner and outer layer for $S_c = 100$. Figure (5.4) shows the concentration profile that exists within the inner layer.

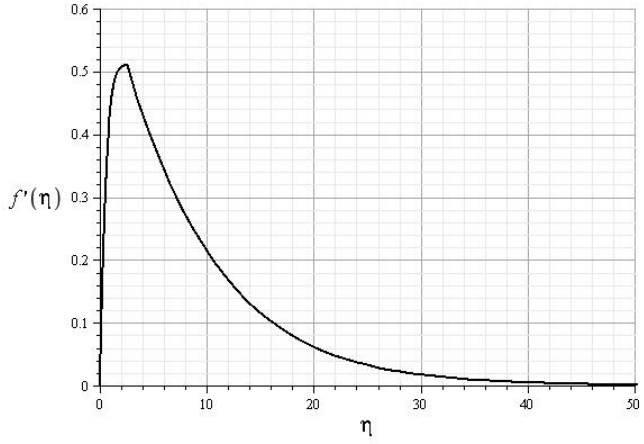

Figure 5.3: Velocity Profile: Pure Natural Convection ($S_c = 100$)

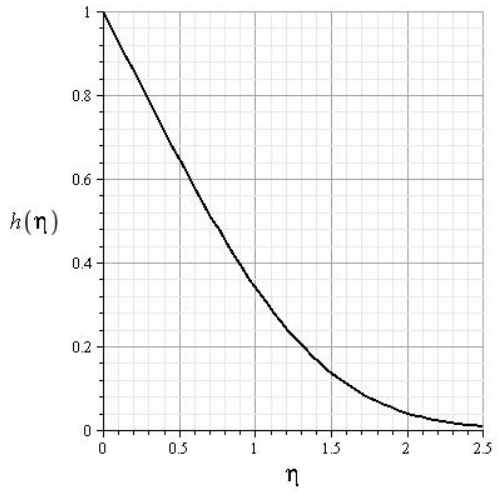

Figure 5.4: Concentration Profile: Pure Natural Convection

5.2 Mass Transfer for Natural Convection with a Constant Counterflow

In this section a perturbation term is introduced to the stream function in order to model a constant counterflow. The outer layer is treated first and then matched to the inner layer. The boundary layer equations for both layers are solved simultaneously by means of a shooting method. The velocity and concentration profiles are plotted for $S_c = 100$ and compared with those for the case of natural convection only. Finally an expression for the non-dimensional flux from the surface is derived.

The Outer Layer

From the outer layer solution of Kuiken[2] the stream function is given by

$$\psi_{\text{outer}} = k_1 x^{\frac{3}{4}} F_0(\xi), \tag{5.41}$$

where $j_1 = \left[\frac{1}{4S_c^2}\right]^{\frac{1}{4}} \left[\frac{gC_s}{4D\rho\nu}\right]^{\frac{1}{4}}$ and $k_1 = 4D \left[\frac{S_c^2}{4}\right]^{\frac{1}{4}} \left[\frac{gC_s}{4D\rho\nu}\right]^{\frac{1}{4}}$. A perturbation term is now introduced to account for a constant counterflow to give

$$\psi_{\text{outer}} = k_1 x^{\frac{3}{4}} \left[F_0(\xi) - \epsilon x^n F_1(\xi)\right], \tag{5.42}$$

where $\xi = j_1 y x^{-\frac{1}{4}}$. Equation (5.42) is differentiated to give

$$u = \frac{\partial \psi}{\partial y} = j_1 k_1 x^{\frac{1}{2}} F_0'(\xi) - \epsilon j_1 k_1 x^{\frac{1}{2}+n} F_1'(\xi). \tag{5.43}$$

On examination of equation (5.43) it is noted that $n = -\frac{1}{2}$, as the upward velocity is constant and can therefore have no dependency on x. Also, at large values of ξ, the perturbation term must approach U_0, where U_0 represents the velocity of the counterflow. This gives

$$\frac{\partial \psi}{\partial y} = j_1 k_1 x^{\frac{1}{2}} F_0'(\xi) - U_0 F_1'(\xi) \tag{5.44}$$

which in turn leads to

$$\psi_{\text{outer}} = k_1 x^{\frac{3}{4}} F_0(\xi) - \frac{U_0 x^{\frac{1}{4}}}{j_1} F_1(\xi), \tag{5.45}$$

where the perturbation parameter is $\epsilon = \frac{U_0 x^{-\frac{1}{2}}}{j_1 k_1}$. This may also be written as $\epsilon = F_r \left[\frac{\rho S_c}{C_s}\right]^{\frac{1}{2}}$, where F_r is the non-dimensional Froude number, given as $F_r = \frac{U_0}{\sqrt{gx}}$. The boundary layer equation for the outer layer in terms of the stream function is

$$\frac{\partial \psi}{\partial y}\frac{\partial^2 \psi}{\partial x \partial y} - \frac{\partial \psi}{\partial x}\frac{\partial^2 \psi}{\partial y^2} = \nu \frac{\partial^3 \psi}{\partial y^3}, \tag{5.46}$$

where the stream function is given by

$$\psi_{\text{outer}} = 4D \left[\frac{S_c^2}{4}\right]^{\frac{1}{4}} \left[\frac{gC_s x^3}{4D\rho\nu}\right]^{\frac{1}{4}} F_0(\xi) - U_0 \left[\frac{4S_c^2}{1}\right]^{\frac{1}{4}} \left[\frac{4D\rho\nu x}{gC_s}\right]^{\frac{1}{4}} F_1(\xi) \tag{5.47}$$

and

$$\xi = y \left[\frac{1}{4S_c^2}\right]^{\frac{1}{4}} \left[\frac{gC_s}{4D\rho\nu x}\right]^{\frac{1}{4}}. \tag{5.48}$$

Introducing equation (5.47), along with the relevant derivatives, the following differential equation is obtained for the first perturbation:

$$F_1'''(\xi) + 3F_1''(\xi)F_0(\xi) - 2F_1'(\xi)F_0'(\xi) + F_1(\xi)F_0''(\xi) = 0. \tag{5.49}$$

The Inner Layer

In order to match the outer and inner layer solutions, the stream function for the inner layer is taken to be

$$\psi_{\text{inner}} = kx^{\frac{3}{4}} f_0(\eta) - \frac{U_0 x^{\frac{1}{4}}}{j} f_1(\eta), \tag{5.50}$$

where $\eta = jyx^{-\frac{1}{4}}$ and the perturbation parameter is given as $\epsilon = \frac{U_0 x^{-\frac{1}{2}}}{jk}$. A similar perturbation is applied to the concentration profile to yield

$$C = h_0(\eta) - \epsilon h_1(\eta). \tag{5.51}$$

The boundary layer equations for the inner layer are

$$\frac{\partial^3 \psi}{\partial y^3} + \frac{gCC_s}{\rho\nu} = 0 \tag{5.52}$$

$$\frac{\partial \psi}{\partial y}\frac{\partial C}{\partial x} - \frac{\partial \psi}{\partial x}\frac{\partial C}{\partial y} = D\frac{\partial^2 C}{\partial y^2}. \tag{5.53}$$

Substituting equations (5.50) and (5.51), along with the relevant derivatives, into the boundary layer equations leads to the following differential equations for the first perturbation:

$$f_1'''(\eta) + h_1(\eta) = 0 \tag{5.54}$$

$$h_1''(\eta) + 2f_0'(\eta)h_1(\eta) + 3f_0(\eta)h_1'(\eta) + f_1(\eta)h_0'(\eta) = 0. \tag{5.55}$$

Velocity and Concentration Profiles

Equations (5.49), (5.54) and (5.55) are solved simultaneously using a shooting method for the boundary conditions:

$$\begin{array}{rlll}
\eta = 0: & f_1(\eta) = 0 & f_1'(\eta) = 0 & f_1''(\eta) = \text{constant} \\
 & h_1(\eta) = \text{constant} & h_1'(\eta) = \text{constant} & \\
\eta \to \infty: & f_1(\eta) \to \infty & f_1'(\eta) = F_1(0) & f_1''(\eta) = 0 \\
 & h_1(\eta) = 0 & h_1'(\eta) \to \text{constant} & \\
\xi = 0: & F_1(\xi) = 0 & F_1'(\xi) = f_1'(\infty) & F_1''(\xi) = 0 \\
\xi \to \infty: & F_1(\xi) \to \infty & F_1'(\xi) = 1 & F_1''(\xi) = 0
\end{array}$$

The boundary condition $F_1'(0) = f_1'(\infty)$ is of particular importance, as it is the condition that matches the outer layer and inner layer solutions. The results obtained are

$$\begin{aligned}
F_1'(0) &\approx 0.388 \\
f_1''(0) &\approx 0.62 \\
h_1'(0) &\approx -0.36 \\
h_1(0) &\approx 0.692 \quad .
\end{aligned}$$

The non-dimensional velocity for the inner and outer layers are

$$\begin{aligned}
f'(\eta) &= f_0'(\eta) - \frac{U_0 x^{-\frac{1}{2}}}{jk} f_1'(\eta) \\
F'(\xi) &= F_0'(\xi) - \frac{U_0 x^{-\frac{1}{2}}}{j_1 k_1} F_1'(\xi).
\end{aligned}$$

Taking U_0 to be equal to 10% of the maximum downward velocity due to natural convection, which is found to be $U_{max} = \left[\frac{gC_s x}{\rho S_c}\right]^{\frac{1}{2}}$, and taking $S_c = 100$, figure (5.5) compares the velocity profile obtained due to the counterflow with that of

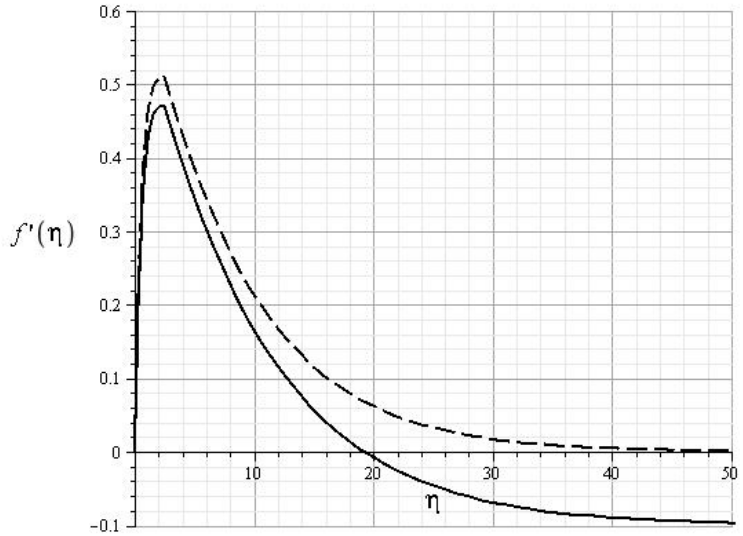

Figure 5.5: Velocity Profile: Natural Convection with Counterflow ($S_c = 100$)

the solution of Kuiken[2]. Similarly, figure (5.6) shows the concentration profiles for both the case of pure natural convection and that of natural convection with counterflow.

Flux from Surface

The flux per unit area is given by

$$\begin{aligned} \text{Flux / Unit Area} &= -D\left[\frac{\partial c}{\partial y}\right]_{y=0} \\ &= -DC_s\left[jx^{-\frac{1}{4}}h_0'(0) - \tfrac{U_0}{k}x^{-\frac{3}{4}}h_1'(0)\right]. \end{aligned} \tag{5.56}$$

Integrating equation (5.56) with respect to x, the flux per unit width is found to be

$$\text{Flux / Unit Width} = -DC_s\left[\frac{4}{3}jx^{\frac{3}{4}}h_0'(0) - \frac{4U_0}{k}x^{\frac{1}{4}}h_1'(0)\right]. \tag{5.57}$$

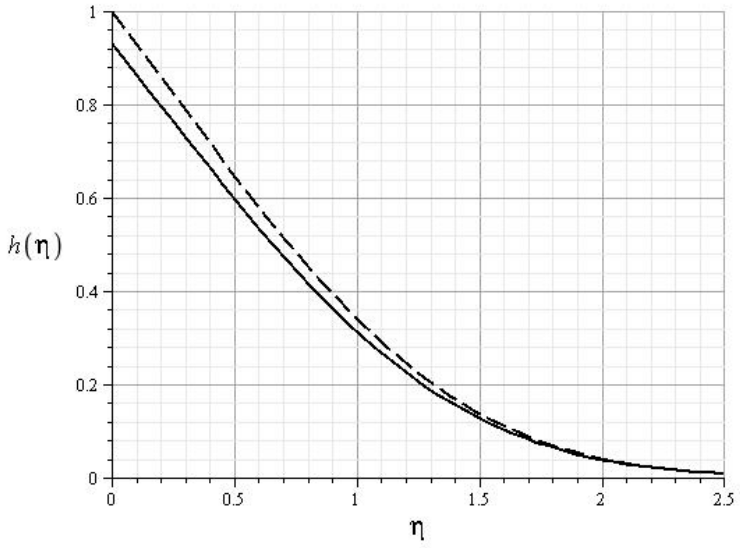

Figure 5.6: Concentration Profile: Natural Convection with Counterflow, 1st Approx.(dashed) vs 2nd Approx.(solid)

Equation (5.57) is divided across by the flux due to natural convection to obtain the non-dimensional flux from the surface, $\tilde{M}$. This is given as

$$\tilde{M} = 1 - 0.76 \left[\frac{U_0}{\sqrt{gx}} \right] \left[\frac{\rho S_c}{C_s} \right]^{\frac{1}{2}}. \tag{5.58}$$

5.3 Discussion

This work arose from problems in the pharmaceutical industry; more specifically in the area of drug dissolution testing of solid dosage forms. In the testing of dissolution rates the soluble material is often subject to a small vertical flow. In such cases the role of natural convection may not be overlooked. Indeed this chapter has taken natural convection to be the dominant mass transfer mechanism with the counterflow introduced as a perturbation term. Figure (5.5) shows that the outer vertical flow penetrates the inner layer leading to a significant decrease

in the maximum downward velocity due to buoyancy effects. This deceleration of the inner layer flow may only be attributed to a decrease in mass transfer from the surface. Figure (5.6) shows the effect that the counterflow has on the overall concentration of dissolved material. Also, from equation (5.58) it can be shown that a counterflow velocity equivalent to 10% of the maximum downward velocity due to natural convection leads to a 7.6% decrease in the mass transfer rate from the surface of the soluble material.

Chapter 6

Mass Transfer from a Vertical Flat Plate due to a Constant Upward Flow

This chapter examines the concentration boundary layer formed on a vertical flat surface due to a constant upward flow. The surface is composed of a soluble material placed in a liquid medium. The emphasis is on estimating the point of separation of the boundary layer. Mass transfer will occur due to the upward flow, leading to an increase in density of the dissolution medium close to the surface. At some level along the surface the weight of these dissolved particles will counteract the upward force causing boundary layer separation. For the case of sufficiently large upward velocities separation will not occur over the height of the plate, and as the velocity of the upward flow approaches infinity the effect of the dissolved particles will be negligent. In the case of lower velocities, separation will occur at some distance along the plate.

In a liquid, molecules diffuse much more slowly than momentum. Consequently, the concentration boundary layer is an order of magnitude thinner then the momentum layer. The concentration boundary layer therefore occupies the region of the momentum boundary layer close to the surface in which the velocity gradient is linear. This model is therefore analogous to that of heat transfer for large Prandtl numbers, for which an exact solution for horizontal flat plate flow

exists due to Lévêque[1]. A correction term which represents the shear stress due to the mass of particles dissolved is introduced to give an expression for the net shear stress. This expression is inserted into the Lévêque[1] solution and solved to give the overall shear stress as a function of the upward distance from the lower edge of the plate. The total mass transfer due to the upward flow is then calculated and compared with that of a corresponding horizontal flow.

6.1 Point of Boundary Layer Separation

The concentration boundary layer equation is

$$u\frac{\partial c}{\partial x} + v\frac{\partial c}{\partial y} = D\frac{\partial^2 c}{\partial y^2}, \tag{6.1}$$

where x measures height above the leading edge, y measures distance from the wall, u and v are the components of velocity in the x and y directions respectively, c is the concentration of dissolved particles and D is the coefficient of diffusion of the soluble material. The concentration layer thickness is δ_c and within this thin layer the velocity gradient is taken to be α, where

$$\alpha = \left(\frac{\partial u}{\partial y}\right)_{y=0}. \tag{6.2}$$

Examining order of magnitudes in equation (6.1) gives

$$u \sim \alpha\delta_c, \;\; v \sim u\frac{\delta_c}{x}, \;\; \frac{\partial}{\partial x} \sim \frac{1}{x}, \;\; \frac{\partial}{\partial y} \sim \frac{1}{\delta_c}. \tag{6.3}$$

Now, the convection terms on the left hand side of equation (6.1) must be of the same order of magnitude as the diffusion term, $D\frac{\partial^2 c}{\partial y^2}$. This gives

$$\frac{\alpha\delta_c}{x} \sim \frac{D}{\delta_c^2} \tag{6.4}$$

which leads to

$$\frac{\alpha\delta_c^3}{x} \sim D. \tag{6.5}$$

The momentum boundary layer equation is

$$u\frac{\partial u}{\partial x} + v\frac{\partial u}{\partial y} = \nu\frac{\partial^2 u}{\partial y^2} - \frac{gc}{\rho}, \tag{6.6}$$

where g is the acceleration due to gravity, ν is the kinematic viscosity of the dissolution medium and ρ is the density of the pure solvent. Performing a similar order of magnitude analysis as before gives

$$u\frac{\partial u}{\partial x} \sim v\frac{\partial u}{\partial y} \sim \frac{\alpha^2\delta_c^2}{x} \tag{6.7}$$

and

$$\nu\frac{\partial^2 u}{\partial y^2} \sim \frac{\nu\alpha}{\delta_c}. \tag{6.8}$$

This leads to

$$\frac{u\frac{\partial u}{\partial x}}{\nu\frac{\partial^2 u}{\partial y^2}} \sim \frac{\alpha\delta^3}{\nu x}. \tag{6.9}$$

Now, from equation (6.5) we have $\frac{\alpha\delta_c^3}{x} \sim D$, which gives

$$\frac{u\frac{\partial u}{\partial x}}{\nu\frac{\partial^2 u}{\partial y^2}} \sim \frac{D}{\nu} \sim \frac{1}{S_c}, \tag{6.10}$$

where S_c is the Schmidt number. Now for liquids, $S_c >> 1$, and therefore the inertia terms in equation (6.6) may be neglected with error of order $\frac{1}{S_c}$ inside the concentration layer where the momentum boundary layer equation (6.6) reduces to

$$\nu\frac{\partial^2 u}{\partial y^2} = \frac{gc}{\rho}. \tag{6.11}$$

Integrating across the concentration boundary layer gives

$$\nu\left[\frac{\partial u}{\partial y}\right]_0^{\delta_c} = \frac{g}{\rho}\int_0^{\delta_c} c dy \tag{6.12}$$

which in turn leads to

$$\left[\frac{\partial u}{\partial y}\right]_{Blas} - \alpha = \frac{g}{\nu\rho}\int_0^{\delta_c} c dy, \tag{6.13}$$

where $\left[\frac{\partial u}{\partial y}\right]_{Blas}$ is the velocity gradient of Blasius' flow at $y = 0$, taken from Schlichting[20]. Now, taking $C = \frac{c}{C_s}$ and rearranging (6.13) gives

$$\alpha = \frac{1}{3}U_\infty\sqrt{\frac{U_\infty}{\nu x}} - \frac{gC_s}{\nu\rho}\int_0^{\infty} C dy, \tag{6.14}$$

where C_s is the concentration saturation. Finally, dividing across by $\left[\frac{\partial u}{\partial y}\right]_{Blas}$ and letting $T = \alpha/\left[\frac{\partial u}{\partial y}\right]_{Blas}$ gives

$$T = 1 - \left[\frac{3gC_s}{\mu}\sqrt{\frac{\nu x}{U_\infty^3}}\right]\int_0^{\infty} C dy. \tag{6.15}$$

It is clear that α decreases with increasing x and so we may introduce the method of Lévêque[1], which gives the forced heat transfer from a horizontal plate at large Prandtl numbers as a function of variable wall shear stress. When the appropriate changes have been made to the Lévêque[1] solution, the following expression for the concentration of dissolved particles for flow over a flat plate may be deduced:

$$C = h(\eta) = \frac{3}{\Gamma\left(\frac{1}{3}\right)}\int_\eta^{\infty} exp\left(-\eta^3\right) d\eta, \tag{6.16}$$

where η is given by

$$\eta = \frac{y\sqrt{\alpha}}{\left[9D\int_0^x \sqrt{\alpha}dx\right]^{\frac{1}{3}}}. \tag{6.17}$$

Introducing (6.16) and (6.17) into (6.15) gives

$$T = 1 - \frac{3}{\Gamma\left(\frac{1}{3}\right)}\left[\frac{3gC_s}{\mu}\sqrt{\frac{\nu x}{U_\infty^3}}\right]\left[\frac{\left[9D\int_0^x \sqrt{\alpha}dx\right]^{\frac{1}{3}}}{\sqrt{\alpha}}\right]\int_0^{\infty} \eta exp\left(-\eta^3\right) d\eta. \tag{6.18}$$

Noting that $\int_0^\infty \eta exp\left(-\eta^3\right) d\eta = \frac{1}{3}\Gamma\left(\frac{2}{3}\right)$ and introducing a non-dimensional unit of length , $X = \frac{U_\infty x}{\nu}$, the above expression can be simplified to give

$$T = 1 - \lambda\left[\frac{\left[\int_0^X T^{\frac{1}{2}}X^{-\frac{1}{4}}dX\right]^{\frac{1}{3}}X^{\frac{3}{4}}}{T^{\frac{1}{2}}}\right], \tag{6.19}$$

where $\lambda = \frac{\Gamma\left(\frac{2}{3}\right)}{\Gamma\left(\frac{1}{3}\right)}\left[\frac{9gC_s\sqrt[3]{\nu^2 D}}{\rho U_\infty^3}\right]$. Finally to eliminate λ we introduce $\tilde{X} = \lambda X$ and rearrange (6.19) to obtain

$$(1-T)^3 T^{\frac{3}{2}} = \tilde{X}^{\frac{9}{4}} \int_0^{\tilde{X}} T^{\frac{1}{2}} \tilde{X}^{-\frac{1}{4}} d\tilde{X}. \tag{6.20}$$

The integral equation (6.20) is solved by expanding T in the power series $T = 1 + \sum_{n=1}^{\infty} a_n \tilde{X}^n$ and equating coefficients of $\tilde{X}$; this is extended to terms of order $\tilde{X}^5$. This leads to the following relationship between the non-dimensional shear stress, T, and $\tilde{X}$:

$$T \doteq 1 - 1.10\tilde{X} - 0.52\tilde{X}^2 - 0.69\tilde{X}^3 - 1.17\tilde{X}^4 - 2.24\tilde{X}^5, \tag{6.21}$$

neglecting terms of order $\tilde{X}^6$. Figure 6.1 shows successive polynomial approximations of equation (6.21). These results show convergence to the curve on the far left and indicate that separation occurs when $\tilde{X}$ is about one half, where

$$\tilde{X} = 9\left[\frac{\Gamma(\frac{2}{3})}{\Gamma(\frac{1}{3})}\right]\left[\frac{gx}{U_\infty^2}\right]\left[\frac{C_s}{\rho}\right]\left[\frac{1}{S_c}\right]^{\frac{1}{3}}. \tag{6.22}$$

Equation (6.22) may be rearranged to give

$$F_r = \left[\frac{9\Gamma\left(\frac{2}{3}\right)C_s}{\Gamma\left(\frac{1}{3}\right)\rho\tilde{X}}\right]^{\frac{1}{2}}\left[\frac{1}{S_c}\right]^{\frac{1}{6}}. \tag{6.23}$$

where F_r is the non-dimensional Froude number, defined by $F_r = \frac{U_\infty}{\sqrt{gx}}$. Noting that $\Gamma\left(\frac{2}{3}\right) \approx 1.3541$, $\Gamma\left(\frac{1}{3}\right) \approx 2.6789$ and that separation occurs at $\tilde{X} = 0.5$, the criterion for separation is given in terms of the Froude number as

$$F_r \doteq 3\left[\frac{C_s}{\rho}\right]^{\frac{1}{2}}\left[\frac{1}{S_c}\right]^{\frac{1}{6}}. \tag{6.24}$$

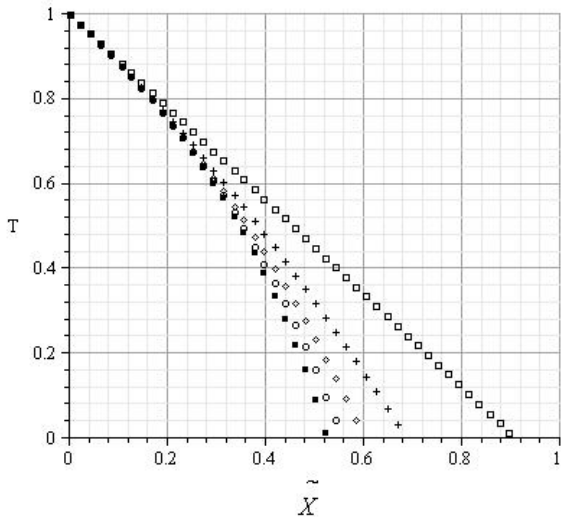

Figure 6.1: Graph of Polynomial Approximations to Equation (6.21)

6.2 Calculation of Flux from Surface due to Upward Flow below Separation Point

In this section the total flux due to the upward velocity is calculated. From equation (6.16) we have

$$C = \frac{3}{\Gamma\left(\frac{1}{3}\right)} \int_{\eta}^{\infty} exp\left(-\eta^3\right) d\eta. \tag{6.25}$$

Differentiating with respect to y gives

$$\frac{\partial C}{\partial y} = \frac{3}{\Gamma\left(\frac{1}{3}\right)} \frac{\partial \eta}{\partial y} \frac{d}{d\eta} \left[\int_{\eta}^{\infty} exp\left(-\eta^3\right) d\eta \right]. \tag{6.26}$$

Now the total flux from the surface is given as

$$\begin{aligned} \text{Flux / Unit Area} &= D \left[\frac{\partial c}{\partial y}\right]_{y=0} \\ &= \beta_3 \left[\frac{\sqrt{\alpha}}{\left[\int_0^x \sqrt{\alpha} dx\right]^{\frac{1}{3}}} \right], \end{aligned} \tag{6.27}$$

where $\beta_3 = D^{2/3} C_s \sqrt[3]{3} \frac{1}{\Gamma(\frac{1}{3})}$. The total flux per unit width is given by

$$\text{Flux / Unit Width} = \beta_3 \int_0^x \frac{\sqrt{\alpha}}{\left[\int_0^x \sqrt{\alpha} dx\right]^{\frac{1}{3}}} dx. \tag{6.28}$$

Equation (6.28) can be integrated by substituting $z = \int_0^x \sqrt{\alpha} dx$ to give

$$\text{Flux / Unit Width} = \frac{3}{2} \beta_3 \left[\int_0^x \sqrt{\alpha} dx\right]^{\frac{2}{3}}. \tag{6.29}$$

Now, $\alpha = T \left[\frac{\partial u}{\partial y}\right]_{Blas}$. This leads to

$$\sqrt{\alpha} = \sqrt{\frac{1}{3\nu}} U_\infty \lambda^{\frac{1}{4}} \tilde{X}^{-\frac{1}{4}} \left[1 - 1.10\tilde{X} - 0.52\tilde{X}^2 - 0.69\tilde{X}^3 - 1.17\tilde{X}^4 - 2.24\tilde{X}^5\right]^{\frac{1}{2}}. \tag{6.30}$$

By applying the binomial expansion equation (6.30) becomes

$$\sqrt{\alpha} = \sqrt{\frac{1}{3\nu}} U_\infty \lambda^{\frac{1}{4}} \left[\tilde{X}^{-\frac{1}{4}} - 0.55\tilde{X}^{\frac{3}{4}} - 0.26\tilde{X}^{\frac{7}{4}} - 0.345\tilde{X}^{\frac{11}{4}} - 0.585\tilde{X}^{\frac{15}{4}} - 1.12\tilde{X}^{\frac{19}{4}}\right]. \tag{6.31}$$

Substituting (6.31) into (6.29) gives

$$\text{Flux / Unit Width} = \beta_4 \left[\int_0^x \left[\tilde{X}^{-\frac{1}{4}} - 0.55\tilde{X}^{\frac{3}{4}} - 0.26\tilde{X}^{\frac{7}{4}} - 0.345\tilde{X}^{\frac{11}{4}} - ...\right] dx\right]^{\frac{2}{3}}, \tag{6.32}$$

where $\beta_4 = \frac{3}{2}\beta_3 \sqrt[3]{\frac{U_\infty^2}{3\nu}} \lambda^{\frac{1}{6}}$. Noting that $x = \frac{\nu \tilde{X}}{\lambda U_\infty}$, equation (6.32) becomes

$$\text{Flux / Unit Width} = \beta_4 \left[\frac{\nu}{\lambda U_\infty} \int_0^{\tilde{X}} \left[\tilde{X}^{-\frac{1}{4}} - 0.55\tilde{X}^{\frac{3}{4}} - 0.26\tilde{X}^{\frac{7}{4}} - 0.345\tilde{X}^{\frac{11}{4}} - ...\right] d\tilde{X}\right]^{\frac{2}{3}}. \tag{6.33}$$

Performing the integration in equation (6.33) and substituting in for β_4 gives the total flux per unit width as

$$\text{Flux / Unit Width} = 0.2625 \left[\frac{DC_s \rho U_\infty^3 \tilde{X}}{g}\right]^{\frac{1}{2}} \left[1.33 - 0.314\tilde{X} - 0.095\tilde{X}^2 - 0.092\tilde{X}^3 - ...\right]^{\frac{2}{3}}. \tag{6.34}$$

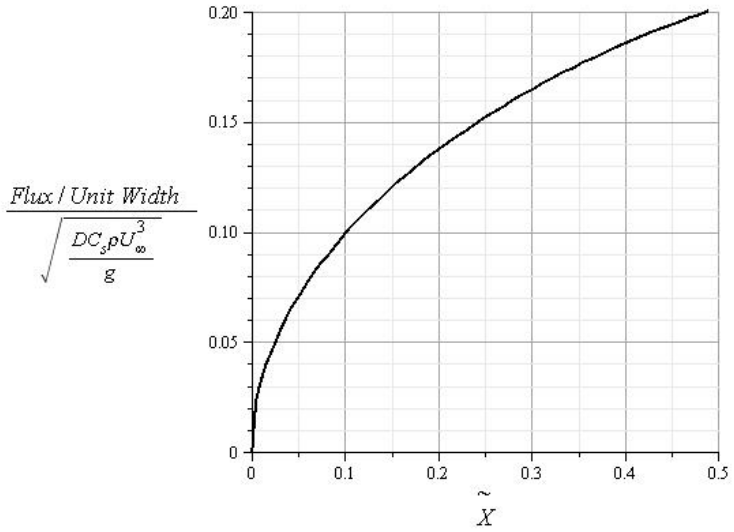

Figure 6.2: Dependency of Flux per Unit Width on the variable $\tilde{X}$

6.3 Discussion

Often in the testing of dissolution rates from solid dosage forms the soluble material is subject to a vertical flow. Typical values for a tablet composed of benzoic acid placed in water are $C_s = 4.564 \times 10^{-3}\text{g/cm}^3$, $D = 1.236 \times 10^{-5}\text{cm}^2/\text{s}$ and $\nu = 0.7 \times 10^{-2}\text{cm}^2/\text{s}$, as reported by D'Arcy[6]. Using these values table (6.1) gives the distance along the surface at which boundary layer separation occurs for several outer stream velocities in the range $0 \leq U_\infty \leq 10\text{cm/s}$. The typical diameter of a cylindrical tablet is about 1cm and table (6.1) shows that, for an upward flow along a vertical flat plate of this height where mass transfer occurs, the upward flow will only begin to have a significant effect on the surface when the outer stream velocity is greater then 1cm/s. That is to say, for velocities less then this value the boundary layer will separate, due to the weight of the dissolved particles, at relatively short distances from the leading edge.

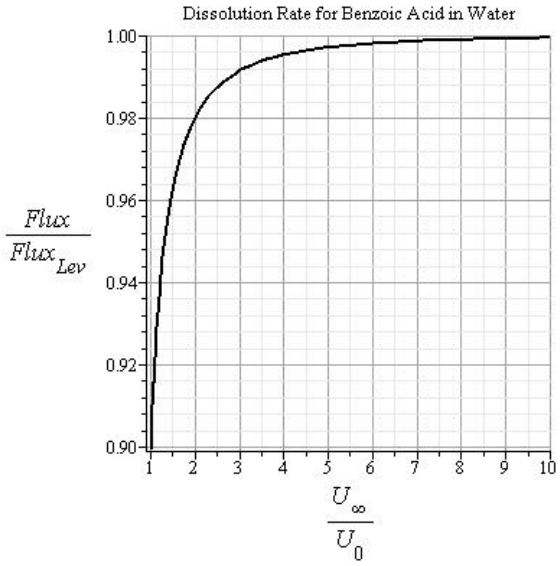

Figure 6.3: Proportional Flux vs Non-Dimensional Velocity ($U_\infty \geq U_0$)

For sufficiently large upward velocities separation of the boundary layer will not occur. For the case of a benzoic acid compact of diameter 1cm dissolving in water, the criterion to prevent separation occurring across the height of the compact can be calculated from equation (6.24) to be $F_r > 0.071$. In this instance, forced convection accounts for all of the mass transfer from the surface and equation (6.34) may be used to calculate the total flux from the surface. For a plate of given height, there exists a minimum upward velocity, namely U_0, required to prevent separation from occurring. This can be given in terms of the non-dimensional Froude number as $U_0 = [gx]^{\frac{1}{2}} F_r$. Once this minimum velocity is

Table 6.1: Point of Boundary Layer Separation for Various Velocities

U_∞(cm/s)	0.1	0.25	0.5	1	2.5	5	10
Sep. Point(cm)	0.002	0.0127	0.0509	0.2037	1.273	5.093	20.372

exceeded, the mass transfer due to the upward velocity will approach the solution of Lévêque[1] for horizontal flat plate flow, for which the flux from the surface is given by Schlichting[20] as

$$\text{Flux / Unit Width} = 0.677\frac{U_\infty^{\frac{1}{2}} D^{\frac{2}{3}} C_s x^{\frac{1}{2}}}{\nu^{\frac{1}{6}}}. \tag{6.35}$$

Figure (6.3) shows the relationship between the non-dimensional velocity, $\frac{U_\infty}{U_0}$, and the flux per unit width from the surface of a soluble material as a proportion of the corresponding horizontal flow case.

Chapter 7

Mass Transfer from the Upper Curved Surface of a Horizontally Aligned Cylinder: Natural Convection

Figure (7.1) shows the top curved surface of a horizontally aligned cylinder of radius a, where the y-axis extends radially from the surface and x measures distance along the surface. The gravitational force acting on a dissolved particle is therefore given as $g_0 = g\sin\theta$, where $g = 9.81\text{m/s}^2$. As a first approximation, the surface is treated as an incline for which the gravitational effect is taken to be $g_0 = g\left[\frac{x}{a}\right]$. Using this solution as a basic approximation, a perturbation

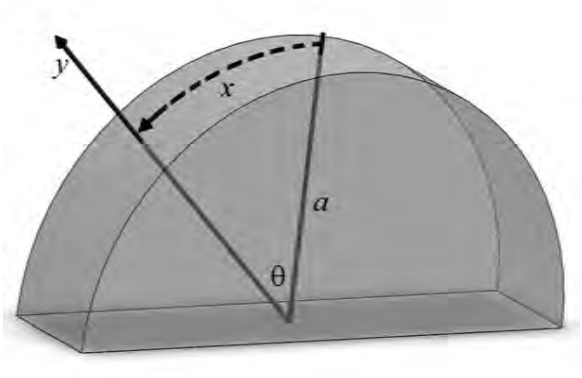

Figure 7.1: Top Curved Surface

term is then added to give a second approximation to the problem where the gravitational effect is given by the first two terms of the Taylor series expansion of $\sin\left(\frac{x}{a}\right)$.

7.1 Mass Transfer from the Upper Curved Surface of a Horizontally Aligned Cylinder: Natural Convection

First Approximation

The boundary layer equations are

$$\frac{\partial^2 u}{\partial y^2} + \frac{g_0 c}{\rho\nu} = 0 \tag{7.1}$$

$$u\frac{\partial c}{\partial x} + v\frac{\partial c}{\partial y} = D\frac{\partial^2 c}{\partial y^2} \tag{7.2}$$

$$\frac{\partial u}{\partial x} + \frac{\partial v}{\partial y} = 0, \tag{7.3}$$

where x measures distance along the curved surface, y is the radial distance from the surface, u and v are the components of velocity in the x and y directions respectively, c is the concentration of dissolved particles, D is the coefficient of diffusion of the soluble material, ν is the kinematic viscosity, ρ is the density and g_0 is the effect due to gravity. Introducing a stream function of the form $u = \frac{\partial\psi}{\partial y}$, from the continuity equation we obtain $v = -\frac{\partial\psi}{\partial x}$. Also, introducing $c = CC_s$, where C_s is the concentration saturation, $\gamma = \frac{gC_s}{\rho\nu a}$ and $g_0 = g\left[\frac{x}{a}\right]$, equations (7.1) and (7.2) may be written as

$$\frac{\partial^3\psi}{\partial y^3} + \gamma x C = 0 \tag{7.4}$$

and

$$\frac{\partial \psi}{\partial y}\frac{\partial C}{\partial x} - \frac{\partial \psi}{\partial x}\frac{\partial C}{\partial y} = D\frac{\partial^2 C}{\partial y^2}. \tag{7.5}$$

As with the case of the vertical flat surface a similarity solution is sought, where the stream function is of the form

$$\psi \approx x^m f_0(\eta), \tag{7.6}$$

where

$$\eta \approx y x^{-n} \tag{7.7}$$

and

$$C \approx h_0(\eta). \tag{7.8}$$

This leads to the following derivatives

$$\begin{aligned}
\tfrac{\partial \psi}{\partial y} &= x^{m-n} f_0'(\eta) \\
\tfrac{\partial^2 \psi}{\partial y^2} &= x^{m-2n} f_0''(\eta) \\
\tfrac{\partial^3 \psi}{\partial y^3} &= x^{m-3n} f_0'''(\eta) \\
\tfrac{\partial \psi}{\partial x} &= m x^{m-1} f_0(\eta) - n\eta x^{m-1} f_0'(\eta) \\
\tfrac{\partial C}{\partial y} &= x^{-n} h_0'(\eta) \\
\tfrac{\partial^2 C}{\partial y^2} &= x^{-2n} h_0''(\eta) \\
\tfrac{\partial C}{\partial x} &= -n\eta x^{-1} h_0'(\eta).
\end{aligned}$$

Substituting these into equations (7.4) and (7.5) gives

$$f_0'''(\eta) + \gamma x^{1+3n-m} h_0(\eta) = 0 \tag{7.9}$$

$$D h_0''(\eta) + m x^{2n+m-1} f_0(\eta) h_0'(\eta) = 0. \tag{7.10}$$

Now, in order for similarity to be achieved it must be possible to eliminate any dependence on the length x. In order to eliminate x from equations (7.9) and (7.10) it is required that

$$m = 1 \quad \text{and} \quad n = 0.$$

This leads to a stream function of the form

$$\psi = x f_0(\eta), \tag{7.11}$$

where

$$\eta = y. \tag{7.12}$$

As in the previous chapters it is beneficial to take a more generalised form of the stream function and similarity variable, namely

$$\psi = kx f_0(\eta) \tag{7.13}$$

and

$$\eta = jy, \tag{7.14}$$

where j and k are arbitrary constants. Substituting this stream function, along with the relevant derivatives, into equations (7.4) and (7.5) gives

$$f_0'''(\eta) + \frac{\gamma}{j^3 k} h_0(\eta) = 0 \tag{7.15}$$

$$h_0''(\eta) + \frac{k}{jD} f_0(\eta) h_0'(\eta) = 0. \tag{7.16}$$

Equations (7.15) and (7.16) may be simplified by taking $j^3 k = \gamma$ and $\frac{k}{jD} = 3$, where $j = \left[\frac{gC_s}{3D\rho\nu a}\right]^{\frac{1}{4}}$ and $k = 4D\left[\frac{gC_s}{3D\rho\nu a}\right]^{\frac{1}{4}}$. This leads to the stream function

$$\psi = 4D\left[\frac{gC_s x^4}{3D\rho\nu a}\right]^{\frac{1}{4}} f_0(\eta), \tag{7.17}$$

where

$$\eta = y\left[\frac{gC_s}{3D\rho\nu a}\right]^{\frac{1}{4}}. \tag{7.18}$$

The differential equations to be solved are

$$f_0'''(\eta) + h_0(\eta) = 0 \tag{7.19}$$

$$h_0''(\eta) + 3f_0(\eta)h_0'(\eta) = 0. \tag{7.20}$$

Equations (7.19) and (7.20) are identical to those solved in chapter five. The results are given as

$$\begin{aligned} f_0''(0) &\approx 0.825 \\ h_0'(0) &\approx -0.711 \\ f_0'(\infty) &\approx 0.511 \quad . \end{aligned}$$

The resulting flux per unit area is given by

$$\begin{aligned} \text{Flux / Unit Area} &= -D\left[\frac{\partial c}{\partial y}\right]_{y=0} \\ &= -DC_s\left[jh_0'(0)\right]. \end{aligned} \tag{7.21}$$

From equation (7.21), the total flux per unit width is given by

$$\begin{aligned} \text{Flux / Unit Width} &= -DC_s\int_0^x \left[jh_0'(0)\right]dx \\ &= -h_0'(0)DC_s\left[\frac{gC_s}{3D\rho\nu a}\right]^{\frac{1}{4}}x. \end{aligned} \tag{7.22}$$

Second Approximation

In this section a perturbation term is introduced to the gravity term to give

$$g_0 = g\left[\frac{x}{a} - \frac{x^3}{6a^3}\right]. \tag{7.23}$$

The stream function and concentration profile from the first approximation are given as

$$\psi = kxf_0(\eta) \tag{7.24}$$

and

$$C = h_0(\eta) \tag{7.25}$$

Now introducing a perturbation term leads to

$$\psi = kx\left[f_0(\eta) - \epsilon f_1(\eta)\right] \tag{7.26}$$

and

$$C = h_0(\eta) - \epsilon h_1(\eta). \tag{7.27}$$

where the perturbation parameter is given by $\epsilon = \frac{x^2}{6a^2}$. As with the first approximation the similarity variable, η, and the arbitrary constants, j and k, are given as $\eta = jy$, $j = \left[\frac{gC_s}{3D\rho\nu a}\right]^{\frac{1}{4}}$ and $k = 4D\left[\frac{gC_s}{3D\rho\nu a}\right]^{\frac{1}{4}}$. The various derivatives of the stream function and the non-dimensional concentration are found to be

$$\frac{\partial\psi}{\partial y} = jkxf_0'(\eta) - \tfrac{1}{6}jk\tfrac{x^3}{a^2}f_1'(\eta)$$

$$\frac{\partial^2\psi}{\partial y^2} = j^2kxf_0''(\eta) - \tfrac{1}{6}j^2k\tfrac{x^3}{a^2}f_1''(\eta)$$

$$\frac{\partial^3\psi}{\partial y^3} = j^3kxf_0'''(\eta) - \tfrac{1}{6}j^3k\tfrac{x^3}{a^2}f_1'''(\eta)$$

$$\frac{\partial\psi}{\partial x} = kf_0(\eta) - \tfrac{3}{6}k\tfrac{x^2}{a^2}f_1(\eta)$$

$$\frac{\partial C}{\partial x} = -\tfrac{2}{6}\tfrac{x}{a^2}h_1(\eta)$$

$$\frac{\partial C}{\partial y} = jh_0'(\eta) - \tfrac{1}{6}j\tfrac{x^2}{a^2}h_1'(\eta)$$

$$\frac{\partial C^2}{\partial y^2} = j^2h_0''(\eta) - \tfrac{1}{6}j^2\tfrac{x^2}{a^2}h_1''(\eta).$$

From equations (7.1) and (7.2) the boundary layer equations are

$$\frac{\partial^2 u}{\partial y^2} + \frac{g_0 c}{\rho \nu} = 0 \tag{7.28}$$

$$u\frac{\partial c}{\partial x} + v\frac{\partial c}{\partial y} = D\frac{\partial^2 c}{\partial y^2}, \tag{7.29}$$

which may be written in terms of the stream function as

$$\frac{\partial^3 \psi}{\partial y^3} + \gamma\left[x - \frac{x^3}{6a^2}\right] C = 0 \tag{7.30}$$

$$\frac{\partial \psi}{\partial y}\frac{\partial C}{\partial x} - \frac{\partial \psi}{\partial x}\frac{\partial C}{\partial y} = D\frac{\partial^2 C}{\partial y^2}, \tag{7.31}$$

where $\gamma = \frac{gC_s}{\rho\nu a}$. Inserting the stream function and the non-dimensional concentration, along with the relevant derivatives, into equations (7.30) and (7.31) and then equating coefficients of x leads to the following set of differential equations:

$$f_0'''(\eta) + h_0(\eta) = 0 \tag{7.32}$$

$$h_0''(\eta) + 3f_0(\eta)h_0'(\eta) = 0 \tag{7.33}$$

$$f_1'''(\eta) + h_1(\eta) + h_0(\eta) = 0 \tag{7.34}$$

$$h_1''(\eta) - 6f_0'(\eta)h_1(\eta) + 3f_0(\eta)h_1'(\eta) + 9f_1(\eta)h_0'(\eta) = 0. \tag{7.35}$$

Equations (7.32) $\rightarrow$ (7.35) are solved subject to the boundary conditions:

$$\begin{array}{lllll}
\eta = 0: & f_0(\eta) = 0 & f_0'(\eta) = 0 & & f_0''(\eta) = 0.825 \\
& f_1(\eta) = 0 & f_1'(\eta) = 0 & & \\
& h_0(\eta) = 1 & h_0'(\eta) = -0.711 & & h_1(\eta) = 0 \\
\eta \rightarrow \infty: & f_0(\eta) \rightarrow \infty & f_0'(\eta) \rightarrow \text{constant} & & f_0''(\eta) = 0 \\
& f_1(\eta) \rightarrow \infty & f_1'(\eta) \rightarrow \text{constant} & & f_1''(\eta) = 0 \\
& h_0(\eta) = 0 & h_0'(\eta) = 0 & & \\
& h_1(\eta) = 0 & h_1'(\eta) = 0\ . & &
\end{array}$$

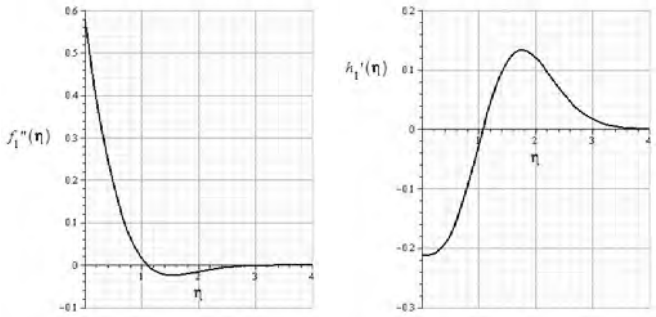

The results obtained are

$$\begin{aligned} f_1''(0) &\approx 0.577 \\ h_1'(0) &\approx -0.213 \quad . \end{aligned} \tag{7.36}$$

The resulting flux per unit area is given by

$$\begin{aligned} \text{Flux / Unit Area} &= -D\left[\frac{\partial c}{\partial y}\right]_{y=0} \\ &= -jDC_s\left[h_0'(0) - \frac{1}{6}\frac{x^2}{a^2}h_1'(0)\right]. \end{aligned} \tag{7.37}$$

From equation (7.37), the total flux per unit width is given by

$$\begin{aligned} \text{Flux / Unit Width} &= -jDC_s\int_0^x\left[h_0'(0) - \frac{1}{6}\frac{x^2}{a^2}h_1'(0)\right]dx \\ &= -DC_sx\left[\frac{gC_s}{3D\rho\nu a}\right]^{\frac{1}{4}}\left[h_0'(0) - \frac{1}{18}\frac{x^2}{a^2}h_1'(0)\right]. \end{aligned} \tag{7.38}$$

7.2 Discussion

Solid dosage forms are often manufactured to be cylindrical in shape. The analysis of drug dissolution rates from the curved surface of such compacts is not as straightforward as that for the flat surface. This chapter has analysed the mass

transfer rates from the upper curved surface of a horizontally aligned cylinder due to natural convection, for which the effect of gravity is no longer constant and is instead approximated as $g_0 = g\left[\frac{x}{a} - \frac{x^3}{6a^3}\right]$. As a first approximation the effect of gravity was taken to be that acting on a sloped surface, where $g_0 = \frac{x}{a}$, with the perturbation parameter $\epsilon = \frac{x^2}{6a^2}$ then introduced to produce a second approximation. Figure (7.2) compares the first approximation with the second and shows a modest decrease in the overall mass transfer from the surface. From equation (7.38) this decrease may be calculated to be about 4% for the entire upper surface. This suggests that the curved surface may be adequately approximated by a sloping flat plate.

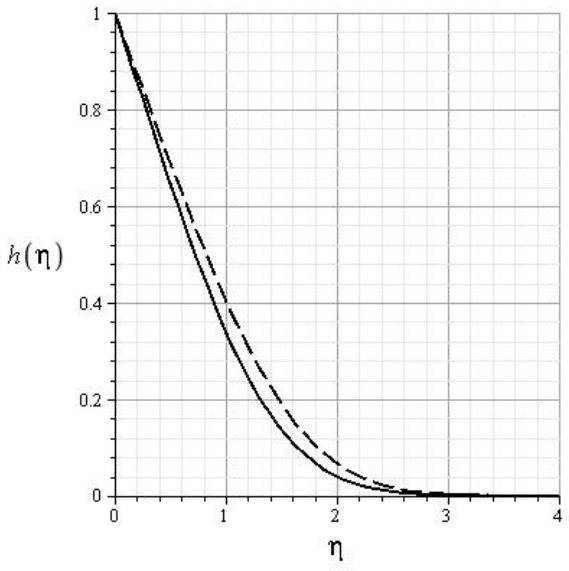

Figure 7.2: Non-Dimensional Concentration: 1st Approx. (dashed) vs 2nd Approx. (solid)

Chapter 8

Mass Transfer from the Lower Curved Surface of a Horizontally Aligned Cylinder: Forced Convection

Figure (8.1) shows the lower curved surface of a horizontally aligned cylinder of radius a, where the y-axis extends radially from the surface and x measures distance along the surface. This chapter examines the mass transfer from this surface for forced convection due to a constant upward flow. For the case of a constant upward flow the surface is treated as a horizontal plate. This leads to a stagnation point flow for which an expression for the shear stress is found in terms of the horizontal distance, x. This expression for the shear stress is then

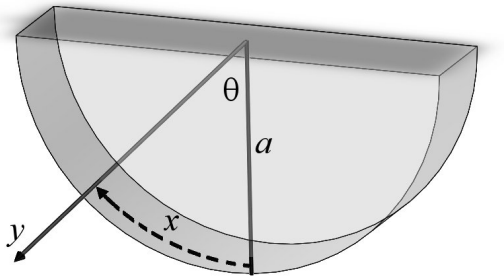

Figure 8.1: Lower Curved Surface

inserted into the Lévêque[1] solution, as discussed in chapter two, in order to find the point of boundary layer separation.

8.1 Mass Transfer from the Lower Curved Surface of a Horizontally Aligned Cylinder: Forced Convection

The case of flow around a circular cylinder has been studied in detail by many authors. The differential equations to be solved are taken from Schlichting[20] as

$$f_0'(\eta)f_0'(\eta) - f_0(\eta)f_0''(\eta) = 1 + f_0'''(\eta) \tag{8.1}$$

$$4f_0'(\eta)f_1'(\eta) - 3f_0''(\eta)f_1(\eta) - f_0(\eta)f_1''(\eta) = 1 + f_1'''(\eta), \tag{8.2}$$

where the stream function is given by

$$\psi = \sqrt{\frac{\nu}{U_1}}\left[U_1 x f_0(\eta) - 4U_3 x^3 f_1(\eta)\right] \tag{8.3}$$

and the similarity variable is

$$\eta = \frac{y}{a}\sqrt{\frac{2U_\infty a}{\nu}}, \tag{8.4}$$

where $U_1 = \frac{2U_\infty}{a}$ and $U_3 = \frac{2U_\infty}{6a^3}$. The velocity distribution is therefore given by

$$u = 2U_\infty\left[\frac{x}{a}f_0'(\eta) - \frac{4x^3}{6a^3}f_1'(\eta)\right] \tag{8.5}$$

and the shear stress at the surface is given as

$$\tau_0 = \mu\sqrt{\frac{8U_\infty^3}{\nu a}}\left[\frac{x}{a}f_0''(0) - \frac{4x^3}{6a^3}f_1''(0)\right]. \tag{8.6}$$

Equations (8.1) and (8.2) are solved subject to the boundary conditions:

$$
\begin{aligned}
\eta = 0: \quad & f_0(\eta) = 0 \qquad f_0'(\eta) = 0 \\
& f_1(\eta) = 0 \qquad f_1'(\eta) = 0 \\
\eta \to \infty: \quad & f_0(\eta) \to \infty \quad f_0'(\eta) \to 1 \\
& f_1(\eta) \to \infty \quad f_1'(\eta) \to \tfrac{1}{4} \ .
\end{aligned}
$$

The results obtained are

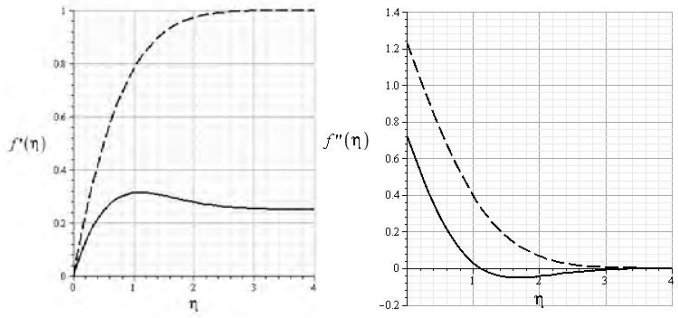

Figure 8.2: Graphical Results for $f'(\eta)$ and $f''(\eta)$

$$
\begin{aligned}
f_0''(0) &\approx 1.2326 \\
f_1''(0) &\approx 0.7244 \quad .
\end{aligned}
\tag{8.7}
$$

Point of Boundary Layer Separation

To estimate the point of boundary layer separation the first term in the expression for the shear stress is taken as

$$\tau_0 = \mu \sqrt{\frac{8U_\infty^3}{\nu a}} \frac{x}{a} f_0''(0). \tag{8.8}$$

For convenience this is written as

$$\tau_0 = \mu \lambda_1 x, \tag{8.9}$$

where $\lambda_1 = \sqrt{\frac{8U_\infty^3}{\nu a}}\left[\frac{f_0''(0)}{a}\right]$. Now from the solution of Lévêque[1] (see chapter two), we have

$$C = \frac{3}{\Gamma\left(\frac{1}{3}\right)} \int_\eta^\infty e^{-\eta^3} d\eta, \tag{8.10}$$

where

$$\eta = \frac{y\sqrt{\frac{\tau_0}{\mu}}}{\left[9D\int_0^x \sqrt{\frac{\tau_0}{\mu}}dx\right]^{\frac{1}{3}}}. \tag{8.11}$$

The weight of dissolved particles at any point along the surface is given by

$$p_D = gC_s \int_0^\infty C dy. \tag{8.12}$$

Substituting equations (8.10) and (8.11) into (8.12) gives

$$p_D = \sqrt[3]{9} g C_s D^{\frac{1}{3}} \left[\frac{\Gamma\left(\frac{2}{3}\right)}{\Gamma\left(\frac{1}{3}\right)}\right] \left[\frac{\left[\int_0^x \sqrt{\lambda_1 x}dx\right]^{\frac{1}{3}}}{\sqrt{\lambda_1 x}}\right]. \tag{8.13}$$

Performing the integration above and substituting in the values $\Gamma\left(\frac{2}{3}\right) \approx 1.3541$, $\Gamma\left(\frac{1}{3}\right) \approx 2.6789$ and $\lambda_1 = \sqrt{\frac{8U_\infty^3}{\nu a}}\left[\frac{f_0''(0)}{a}\right]$, equation (8.13) may be written as

$$p_D = 0.6057 \left[\frac{g C_s D^{\frac{1}{3}} a^{\frac{1}{2}} \nu^{\frac{1}{6}}}{U_\infty^{\frac{1}{2}}}\right]. \tag{8.14}$$

Now, the pressure distribution about a circular cylinder is given by Schlichting[20] as

$$p = p_0 - \frac{1}{2}\rho u^2, \tag{8.15}$$

where p_0 is the stagnation point pressure, given as $p_0 = \frac{1}{2}\rho {U_\infty}^2$ and $u = 2U_\infty \sin\theta$. Separation of the boundary layer will occur at the point when the pressure is equal to the weight of dissolved particles. Equating (8.14) and (8.15) gives

$$2\rho U_\infty^2 \sin^2\theta - \frac{1}{2}\rho U_\infty + 0.6057 \left[\frac{g C_s D^{\frac{1}{3}} a^{\frac{1}{2}} \nu^{\frac{1}{6}}}{U_\infty^{\frac{1}{2}}}\right] = 0. \tag{8.16}$$

Now, making the substitution $\sin^2\theta \approx \left[\frac{x}{a} - \frac{x^3}{6a^3}\right]^2$ and rearranging gives

$$x^4 - 3a^2x^2 + \frac{3a^4}{4} - 0.9084\left[\frac{gC_sD^{\frac{1}{3}}a^{\frac{9}{2}}\nu^{\frac{1}{6}}}{\rho U_\infty^{\frac{5}{2}}}\right] = 0. \tag{8.17}$$

Equation (8.17) is solved by reducing it to a quadratic to obtain

$$x_{sep} = \sqrt{\frac{3a^2 \pm \sqrt{6a^4 + 3.634\left[\frac{gC_sD^{\frac{1}{3}}a^{\frac{9}{2}}\nu^{\frac{1}{6}}}{\rho U_\infty^{\frac{5}{2}}}\right]}}{2}}. \tag{8.18}$$

Flux from the Surface

An expression for the flux from the surface in terms of the shear stress , τ_0, is provided in chapter six. This is given as

$$\text{Flux / Unit Area} = D^{\frac{2}{3}}C_s\frac{\sqrt[3]{3}}{\Gamma\left(\frac{1}{3}\right)}\left[\frac{\sqrt{\frac{\tau_0}{\mu}}}{\left[\int_0^x\sqrt{\frac{\tau_0}{\mu}}dx\right]^{\frac{1}{3}}}\right]. \tag{8.19}$$

For small values of x_{sep} the first approximation for the shear stress may be taken as

$$\tau_0 = \mu\lambda_1 x. \tag{8.20}$$

Substituting equation (8.20) into (8.19) gives

$$\text{Flux / Unit Area} = D^{\frac{2}{3}}C_s\frac{\sqrt[3]{3}}{\Gamma\left(\frac{1}{3}\right)}\lambda_1^{\frac{1}{3}}\left[\frac{x^{\frac{1}{2}}}{\left[\int_0^x x^{\frac{1}{2}}dx\right]^{\frac{1}{3}}}\right]. \tag{8.21}$$

Performing the integration in equation (8.21) and simplifying gives

$$\text{Flux / Unit Area} = D^{\frac{2}{3}}C_s\frac{\sqrt[3]{\frac{9}{2}}}{\Gamma\left(\frac{1}{3}\right)}\lambda_1^{\frac{1}{3}}. \tag{8.22}$$

Finally integrating across the length and substituting in for λ_1 gives the total flux per unit width as

$$\text{Flux / Unit Width} = 0.9345\frac{D^{\frac{2}{3}}C_sU_\infty^{\frac{1}{2}}x}{a^{\frac{1}{2}}\nu^{\frac{1}{6}}}. \tag{8.23}$$

A Note on Natural Convection from the Lower Curved Surface

In the case of mass transfer we may neglect the effect of natural convection on the lower curved surface of a horizontally aligned cylinder. If for a moment we consider that a natural convection flow is present on the lower surface, the mass of soluble material dissolved will have a force acting on it due to gravity, say F_g. This force may be divided into two components; a tangential force (F_1) and a radial force (F_2). The only other force acting on this mass would be that of the shear stress at the surface, F_τ. This is illustrated in figure (8.3) and it is clear to see that this would result in an imbalance of forces. Hence, no natural convection flow can develop on the lower curved surface.

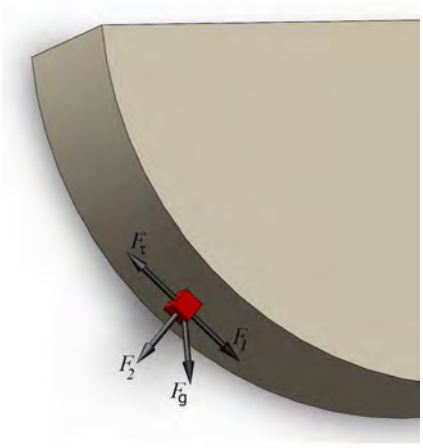

Figure 8.3: Imbalance of Forces

8.2 Discussion

This chapter has analysed the mass transfer rates from the lower curved surface of a horizontally aligned cylinder due to forced convection. For the case of forced convection due to a constant upward flow the shear stress, τ_0, is taken from Schlichting[20] as the first approximation to flow about a circular cylinder. This is then inserted into the expression derived in chapter six, which gives the concentration of dissolved particles in terms of τ_0. On calculation of the concentration of dissolved particles, the weight of these particles is then equated with the pressure distribution about a circular cylinder, taken from Schlichting[20]. Boundary layer separation occurs at the point at which the weight of these particles overcome the pressure. For moderate velocities the boundary layer is found to separate at small values of x, which indicates, except for cases of very large upward velocities, the mass transfer rate will be negligible.

Chapter 9

Natural Convection Flow on a Vertical Flat Plate: A Pohlhausen Method

This chapter investigates the decelerating effect on a natural convection flow regime caused by the introduction of a surface that lies perpendicular to the direction of flow. Chapter two of this thesis explored the case of mass transfer from a vertical flat surface due to natural convection, based on work by Kuiken[2]. In this chapter, a Pohlhausen method is developed which models the exact solution of Kuiken[2]. This Pohlhausen method is then altered to model the introduction of a surface perpendicular to the direction of flow. The results are then compared with those of the unimpeded case.

9.1 Pohlhausen Approximation to Natural Convection Flow on a Vertical Flat Plate

In chapter five the maximum downward velocity due to natural convection was shown to be

$$U_{max} = jkx^{\frac{1}{2}} f'(\eta), \tag{9.1}$$

where $j = \left[\frac{gC_s}{4D\rho\nu}\right]^{\frac{1}{4}}$ and $k = 4D\left[\frac{gC_s}{4D\rho\nu}\right]^{\frac{1}{4}}$. This gives

$$U_{max} = 4D\left[\frac{gC_s}{4D\rho\nu}\right]^{\frac{1}{2}} x^{\frac{1}{2}} f'(\eta). \tag{9.2}$$

The Pohlhausen method was first used to model natural convection flow by Squire[18]. In his work, Squire[18] used the following polynomial distributions for the velocity and concentration:

$$u = 5.17\nu\left[S_c + \frac{20}{21}\right]^{-\frac{1}{2}}\left[\frac{gC_s}{\rho\nu^2}\right]^{\frac{1}{2}} x^{\frac{1}{2}}\left[\frac{y}{\delta}\right]\left[1-\frac{y}{\delta}\right]^2 \tag{9.3}$$

$$c = C_s\left[1-\frac{y}{\delta}\right]^2. \tag{9.4}$$

Now, for large Schmidt numbers, the velocity profile of Squire[18] may be written as

$$u = [2.585]\,[4D]\left[\frac{gC_s}{4D\rho\nu}\right]^{\frac{1}{2}} x^{\frac{1}{2}}\left[\frac{y}{\delta}\right]\left[1-\frac{y}{\delta}\right]^2 \tag{9.5}$$

or

$$u = 5.17U_{max}\left[\frac{y}{\delta}\right]\left[1-\frac{y}{\delta}\right]^2. \tag{9.6}$$

In the work of Squire[18] it is assumed that the momentum and concentration boundary layer thicknesses are equal, and that the maximum velocity is achieved at $y = \frac{\delta}{3}$. From observation of figures (5.3) and (5.4) from chapter five it can be seen that the edge of the concentration boundary layer occurs at $\eta \approx 3$ and that the maximum velocity is achieved at $\eta \approx 2.2$. That is to say that the maximum velocity is achieved at $y = \frac{11}{15}\delta_c$. Amending the velocity profile taken from Squire[18] accordingly gives

$$u = 3.375Ax^{\frac{1}{2}}\left[\frac{5y}{11\delta_c}\right]\left[1-\frac{5y}{11\delta_c}\right]^2, \tag{9.7}$$

where $A = 4D\left[\frac{gC_s}{4D\rho\nu}\right]^{\frac{1}{2}}$. The concentration profile is taken to be

$$c = C_s\left[1-\frac{y}{\delta_c}\right]^2. \tag{9.8}$$

The concentration integral equation is

$$\frac{d}{dx}\int_0^{\delta_c} uc\,dy = -D\left[\frac{\partial c}{\partial y}\right]_{y=0}. \tag{9.9}$$

Substituting equations (9.7) and (9.8) into equation (9.9) gives

$$\frac{d}{dx}\left\{x^{\frac{1}{2}}\int_0^{\delta_c}\left[\frac{5y}{11\delta_c}\right]\left[1-\frac{5y}{11\delta_c}\right]^2\left[1-\frac{y}{\delta_c}\right]^2 dy\right\} = \frac{2D}{3.375A\delta_c}. \tag{9.10}$$

Performing the integration in equation (9.10) and rearranging gives

$$\frac{d}{dx}\left\{x^{\frac{1}{2}}\delta_c\right\} = \frac{23.085D}{A\delta_c}, \tag{9.11}$$

which may in turn be simplified to give the ordinary differential equation

$$2\delta_c\frac{d\delta_c}{dx} + \frac{1}{x}\delta_c^2 = \frac{46.17D}{Ax^{\frac{1}{2}}}. \tag{9.12}$$

Equation (9.12) is solved by means of an integrating factor to yield

$$\delta_c = \left[\frac{30.78D}{A}\right]^{\frac{1}{2}} x^{\frac{1}{4}}. \tag{9.13}$$

The flux per unit area is given by

$$\begin{aligned}\text{Flux / Unit Area} &= -D\left[\tfrac{\partial c}{\partial y}\right]_{y=0}\\ &= 2DC_s\left[\tfrac{A}{30.78D}\right]^{\frac{1}{2}} x^{-\frac{1}{4}}.\end{aligned} \tag{9.14}$$

Integrating equation (9.14) with respect to x, the flux per unit width is found to be

$$\text{Flux / Unit Width } = \frac{8}{3}DC_s\left[\frac{A}{30.78D}\right]^{\frac{1}{2}} x^{\frac{3}{4}}. \tag{9.15}$$

The total flux from the surface is therefore given as

$$\text{Total Flux } = 0.9613DC_s\left[\frac{gC_s}{4D\rho\nu}\right]^{\frac{1}{4}} x^{\frac{3}{4}}W. \tag{9.16}$$

Comparing equation (9.16) with the exact solution for mass transfer from a vertical flat surface, given as

$$\text{Total Flux } = 0.948 D C_s \left[\frac{g C_s}{4 D \rho \nu}\right]^{\frac{1}{4}} x^{\frac{3}{4}} W, \tag{9.17}$$

we find that the Pohlhausen method approximates the exact solution to within 2%.

9.2 Pohlhausen Approximation to Natural Convection Flow on a Vertical Flat Plate Approaching a Perpendicular Surface

In this section the velocity profile of the previous section is amended to model the introduction of a perpendicular surface. Schlichting[20] reports on a family of solutions presented by Howarth[15] and Tani[16] in which the velocity profiles are of the form

$$U(x) = U_\infty - a x^n. \tag{9.18}$$

In the instance where $n = 1$ and $a = \frac{U_\infty}{L}$ the velocity profile may be used to represent forced flow along a flat plate which abuts onto another surface placed at right angles. Applying this method to the Pohlhausen approximation for natural convection presented in the previous section leads to the following velocity and concentration profiles

$$u = 3.375 A x^{\frac{1}{2}} \left[\frac{5y}{11\delta_c}\right] \left[1 - \frac{5y}{11\delta_c}\right]^2 \left[1 - \frac{x}{L}\right] \tag{9.19}$$

and

$$c = C_s \left[1 - \frac{y}{\delta_c}\right]^2, \tag{9.20}$$

where L is the distance from the leading edge at which the flow meets the perpendicular surface. The concentration integral equation is

$$\frac{d}{dx}\int_0^{\delta_c} ucdy = -D\left[\frac{\partial c}{\partial y}\right]_{y=0}. \tag{9.21}$$

Substituting equations (9.19) and (9.20) into equation (9.21) leads to

$$\frac{d}{dx}\left\{x^{\frac{1}{2}}\left[1-\frac{x}{L}\right]\delta_c\right\} = \frac{23.085D}{A\delta_c}, \tag{9.22}$$

which may in turn be simplified to give the ordinary differential equation

$$\frac{d\delta_c}{dx} = \frac{23.085D}{A\delta_c x^{\frac{1}{2}}}\left[\frac{L}{L-x}\right] - \frac{\delta_c}{2x} + \frac{\delta_c}{[L-x]}. \tag{9.23}$$

Equation (9.23) is applied to a vertical flat plate of length 1cm and solved numerically for values of $L = 0.1, 0.2, 0.4, 0.6, 0.8, 1.0$. The effect on the boundary layer thickness is shown in figure (9.1). The flux per unit area is given by

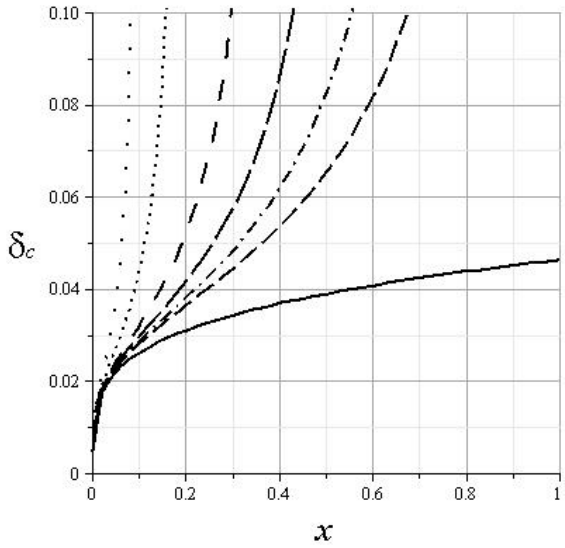

Figure 9.1: Effect on Boundary Layer Thickness due to Perpendicular Surface

$$\begin{aligned}\text{Flux / Unit Area} &= -D\left[\tfrac{\partial c}{\partial y}\right]_{y=0} \\ &= 2DC_s\left[\ \tfrac{1}{\delta_c}\ \right].\end{aligned} \tag{9.24}$$

Therefore the flux per unit width is

$$\text{Flux / Unit Width } = 2DC_s \int_0^x \frac{1}{\delta_c} dx. \tag{9.25}$$

The effects on the total flux from a vertical flat surface composed of benzoic acid dissolving in water, for which $C_s = 4.564 \times 10^{-3}\text{g/cm}^3$, $D = 1.236 \times 10^{-5}\text{cm}^2/\text{s}$ and $\nu = 0.7 \times 10^{-2}\text{cm}^2/\text{s}$, are shown in table (9.1) and visually presented in figure (9.2).

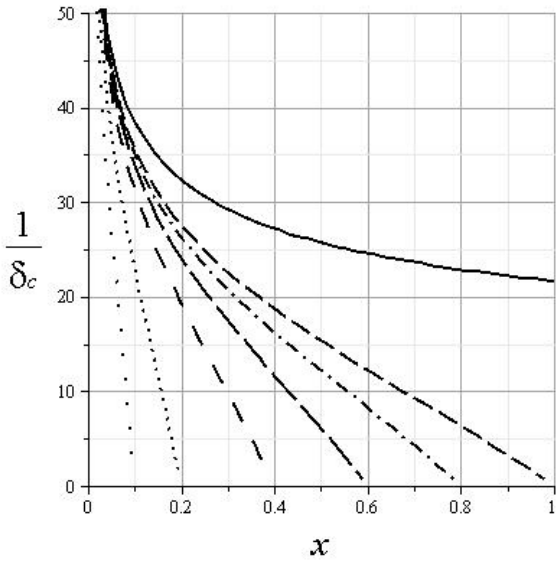

Figure 9.2: Effect on Flux due to Perpendicular Surface

Table 9.1: Flux from Surface of a Vertical Flat Plate

Surface Length (cm)	Unimpeded Flow(g/s)	Impeded Flow(g/s)
1.0	3.207×10^{-6}	1.996×10^{-6}
0.8	2.712×10^{-6}	1.683×10^{-6}
0.6	2.186×10^{-6}	1.341×10^{-6}
0.4	1.613×10^{-6}	0.979×10^{-6}
0.2	0.959×10^{-6}	0.569×10^{-6}
0.1	0.570×10^{-6}	0.324×10^{-6}

9.3 Pohlhausen Approximation to Natural Convection Flow Developing at a Stagnation Point

In this section the velocity profile of Squire[18] is again amended, this time to model the introduction of a perpendicular surface at the top of a vertical flat plate. The velocity and concentration profiles are

$$u = 3.375Ax^{\frac{1}{2}}\left[\frac{5y}{11\delta_c}\right]\left[1-\frac{5y}{11\delta_c}\right]^2\left[\frac{x}{x_{max}}\right] \tag{9.26}$$

and

$$c = C_s\left[1-\frac{y}{\delta_c}\right]^2, \tag{9.27}$$

where x_{max} is the length of the vertical surface. The concentration integral equation is

$$\frac{d}{dx}\int_0^{\delta_c} ucdy = -D\left[\frac{\partial c}{\partial y}\right]_{y=0}. \tag{9.28}$$

Substituting equations (9.26) and (9.27) into equation (9.28) leads to

$$\frac{d}{dx}\left\{x^{\frac{1}{2}}\left[\frac{x}{x_{max}}\right]\delta_c\right\} = \frac{23.085D}{A\delta_c}, \tag{9.29}$$

which may in turn be simplified to give the ordinary differential equation

$$2\delta\frac{d\delta_c}{dx} + 3\frac{\delta^2}{x} = \frac{56.17Dx_{max}}{A\delta_c x^{\frac{3}{2}}}. \tag{9.30}$$

Equation (9.30) is solved by means of an integrating factor to give

$$\delta_c = \left[\frac{22.468Dx_{max}}{A}\right]^{\frac{1}{2}} x^{-\frac{1}{4}}. \tag{9.31}$$

The flux per unit area is given by:

$$\begin{aligned}\text{Flux / Unit Area} &= -D\left[\tfrac{\partial c}{\partial y}\right]_{y=0}\\ &= 2DC_s\left[\tfrac{A}{22.468Dx_{max}}\right]^{\frac{1}{2}} x^{\frac{1}{4}}.\end{aligned} \tag{9.32}$$

Integrating equation (9.32) with respect to x, the flux per unit width is found to be

$$\text{Flux / Unit Width } = \frac{8}{5} DC_s \left[\frac{A}{22.468 D x_{max}}\right]^{\frac{1}{2}} x^{\frac{5}{4}}. \tag{9.33}$$

The total flux from the surface is therefore given as

$$\text{Total Flux } = 0.6751 DC_s \left[\frac{gC_s}{4D\rho\nu}\right]^{\frac{1}{4}} x^{\frac{3}{4}} \left[\frac{x}{x_{max}}\right]^{\frac{1}{2}} W. \tag{9.34}$$

The boundary layer thickness is shown in figure (9.3) alongside the case of an unimpeded natural convection flow along a vertical flat surface composed of benzoic acid of height 1cm dissolving in water.

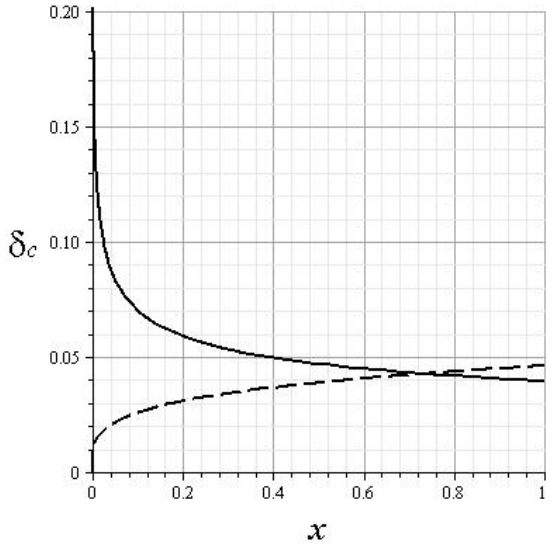

Figure 9.3: Natural Convection Flow Developing at a Stagnation Point (solid) against Pure Natural Convection (dashed)

9.4 Discussion

In this chapter a Pohlhausen method has been developed for natural convection flow on a vertical flat surface. This was achieved by taking the velocity profile

used by Squire[18], for Schmidt numbers close to unity, and amending it to model the case for large Schmidt numbers. The results for the Pohlhausen method are extremely accurate and are within 2% of the exact solution. Using this Pohlhausen method as a starting point the velocity profile was again amended to model the introduction of a surface that was perpendicular to the direction of flow. The solution was obtained numerically for a 1cm surface composed of benzoic acid dissolving in water. The introduction of this perpendicular surface accounted for almost a 40% decrease in the mass transfer rate when compared with that of the unimpeded natural convection case.

Finally, the velocity profile used by Squire[18] was amended to model natural convection flow developing at a stagnation point. In this instance an analytical solution was obtained and the overall percentage decrease in mass transfer was found to be about 29% . Overall it is clear to see from the results that the introduction of a surface that lies perpendicular to the direction of flow, whether at the leading edge or further down the vertical plate, leads to a significant decrease in the mass transfer rates from the surface.

Chapter 10

Dissolution Rates from the Surface of a Compact in the USP Flow Through Apparatus

In this chapter, the dissolution rate from the surface of a compact in the USP Flow Through Apparatus is analysed. The apparatus may be assembled using either a large 22.6mm diameter flow through cell or a smaller 12mm cell (see figure (1.3)). The pump delivers a flow with a sinusoidal profile, with typical volumetric flow rates of between 4 and 16mL/min, although higher flow rates are achievable. For the purpose of estimating the dissolution rate from the surface, a time averaged constant upward flow is taken in place of this sinusoidal profile, for the period over which the pump is active.

Experimental results for the dissolution rates from the surface of a compact have been produced by D'Arcy[8]. In these experiments a compact of 8.5mm in diameter was used in the smaller flow through cell and a compact of 13mm in diameter used for the larger cell, both with an approximate height of 3mm. In order to apply the methods of the previous chapters to the surface of the compact, the surface is divided into strips of 1mm for the larger compact and 0.5mm for the smaller compact. This is illustrated in figure (10.1). Again the following values for the concentration saturation, coefficient of diffusion and kinematic viscosity are taken as; $C_s = 4.564 \times 10^{-3}\text{g/cm}^3$, $D = 1.236 \times 10^{-5}\text{cm}^2/\text{s}$ and $\nu =$

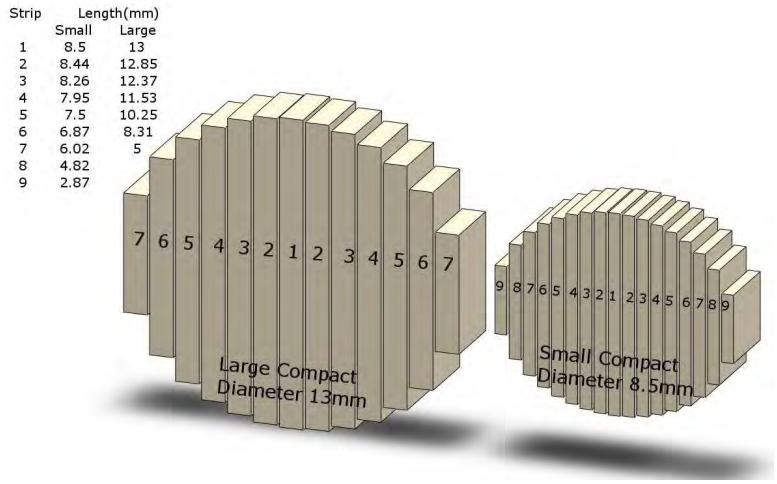

Figure 10.1: Surface Strips for Large and Small Compacts

$0.7 \times 10^{-2}\text{cm}^2/\text{s}$, which correspond to benzoic acid dissolving in water. Wherever available, the results are compared with those of experiment, as reported by D'Arcy[8].

10.1 Dissolution Rates in the USP Flow Through Apparatus: Pure Natural Convection

For the case of natural convection only, the flux per unit width for each strip is taken from equation (2.75) to be

$$\text{Flux / Unit Width} = 0.948 D C_s \left[\frac{g C_s}{4 D \rho \nu}\right]^{\frac{1}{4}} x^{\frac{3}{4}}, \tag{10.1}$$

where x is the length of the strip. The maximum downward velocity due to natural convection for each individual strip is calculated as

$$U_{max} = \left[\frac{gC_s x}{\rho S_c}\right]^{\frac{1}{2}}. \tag{10.2}$$

The maximum downward velocities for both the large and small compacts are shown in table (10.1). Equation (10.1) is applied to the flat surface of both the

Table 10.1: Maximum Downward Velocity due to Natural Convection

Strip Number	Large Cell Velocities(cm/s)	Small Cell Velocities(cm/s)
1	0.101	0.082
2	0.101	0.082
3	0.099	0.081
4	0.096	0.079
5	0.090	0.077
6	0.081	0.074
7	0.063	0.069
8	N/A	0.062
9	N/A	0.048

large and small compacts, the results of which are shown in table (10.2).

Table 10.2: Vertical Flat Surface: Dissolution Rates due to Natural Convection

Compact Diameter (mm)	Predicted Rate of Dissolution(g/s)
8.5	1.996×10^{-6}
13	4.166×10^{-6}

For the case of the upper curved surface the flux per unit width is taken from equation (7.38) as

$$\text{Flux / Unit Width } = DC_s x \left[\frac{gC_s}{3D\rho\nu a}\right]^{\frac{1}{4}} \left[0.711 - 0.0118\frac{x^2}{a^2}\right]. \tag{10.3}$$

For the lower curved surface the effect of natural convection is negligible, as discussed in chapter eight. The predicted dissolution rates from the curved surface of a compact are shown in table (10.3).

Table 10.3: Total Curved Surface: Dissolution Rates due to Natural Convection

Compact Diameter (mm)	Predicted Rate of Dissolution(g/s)
8.5	1.229×10^{-6}
13	1.691×10^{-6}

10.2 Dissolution Rates in the USP Flow Through Apparatus: Small Upward Velocities

This section analyses the dissolution rates from the vertical flat surface of a compact for small upward velocities. A small upward velocity may be classified as one that is less than 15% of the maximum downward velocity due to natural convection, as shown in table (10.1). For velocities of this magnitude the upward flow will not penetrate the concentration boundary layer formed due to natural convection and will instead have the effect of a slow moving counterflow. As such the flux per unit width is taken from equation (5.57) to be

$$\text{Flux / Unit Width} = 0.948DC_s \left[\frac{gC_s}{4D\rho\nu}\right]^{\frac{1}{4}} x^{\frac{3}{4}} \left[1 - 0.76\left[\frac{U_0^2\rho S_c}{gC_s x}\right]^{\frac{1}{2}}\right], \qquad (10.4)$$

where U_0 is the velocity of the counterflow. Such small upward velocities exist in the large flow through cell at volumetric flow rates less than 6mL/min and in the small cell for velocities less than 2mL/min. Equation (10.4) is applied to the

surface of a compact for several small velocities and table (10.4) compares the results with that of natural convection.

Table 10.4: Flat Vertical Surface:Dissolution Rates for Small Upward Velocities

Volumetric Flow Rate (mL/min)	Predicted Rate of Dissolution(g/s)
Large Cell	
0	4.166×10^{-6}
2	3.981×10^{-6}
4	3.795×10^{-6}
6	3.609×10^{-6}
Small Cell	
0	1.996×10^{-6}
0.5	1.898×10^{-6}
1	1.800×10^{-6}

10.3 Dissolution Rates in the USP Flow Through Apparatus: Large Upward Velocities

In chapter six of this thesis, mass transfer from a vertical flat plate due to a constant upward flow was investigated. It was shown that for small velocities the boundary layer formed due to this upward flow would separate due to the weight of dissolved particles. However, for sufficiently large upward velocities boundary layer separation will not occur across the height of the surface and the solution will approach that of horizontal flat plate flow. The criterion to prevent separation occurring is $F_r > 0.071$, where F_r is the non-dimensional Froude number. The required upward velocity may be calculated using

$$U_0 = [gx]^{\frac{1}{2}} F_r. \tag{10.5}$$

For the small and large compacts in the USP Flow Through Apparatus, this translates to volumetric flow rates of 215 and 945mL/min respectively. Such velocities are highly unlikely in the large cell; however, in the smaller cell these velocities may be achievable. The flux per unit width is given by equation (6.34), which is

$$\text{Flux / Unit Width} = 0.2625 \left[\frac{DC_s\rho U_\infty^3 \tilde{X}}{g}\right]^{\frac{1}{2}} \left[1.33 - 0.314\tilde{X} - 0.095\tilde{X}^2 + ...\right]^{\frac{2}{3}}, \tag{10.6}$$

where $\tilde{X} = 9\left[\frac{\Gamma\left(\frac{2}{3}\right)}{\Gamma\left(\frac{1}{3}\right)}\right]\left[\frac{gC_s x}{\rho U_0^2}\right]\left[\frac{1}{S_c}\right]^{\frac{1}{3}}$. Table (10.5) shows the predicted average dissolution rates from the vertical flat surface of a compact at several large flow rates.

Table 10.5: Flat Vertical Surface: Dissolution Rates for Large Upward Velocities

Volumetric Flow Rate (mL/min)	Predicted Rate of Dissolution(g/s)
Small Cell	
250	3.510×10^{-6}
300	4.499×10^{-6}
400	6.082×10^{-6}
500	8.103×10^{-6}

10.4 Dissolution Rates in the USP Flow Through Apparatus: Intermediate Velocities

The most interesting cases are those which involve intermediate velocities. In such instances the upward flow will penetrate the natural convection boundary layer; however, it will also separate under the weight of dissolved particles at

some distance, say x_{sep}. This means that the rate of drug dissolution below this point may be calculated using the modified Blasius flow of chapter six, for which the flux is given as

$$\text{Flux / Unit Width} = 0.2625 \left[\frac{DC_s \rho U_\infty^3 \tilde{X}}{g}\right]^{\frac{1}{2}} \left[1.33 - 0.314\tilde{X} - 0.095\tilde{X}^2 + ...\right]^{\frac{2}{3}}. \tag{10.7}$$

Above the separation point the flow will be that of natural convection. However,

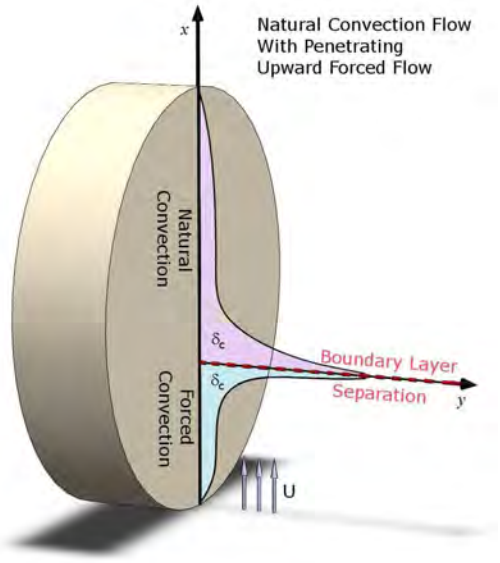

Figure 10.2: Natural Convection Flow with Penetrating Upward Forced Flow

this natural convection flow must also separate at the same height along the surface as the modified Blasius flow and will therefore behave like that of natural convection on a vertical flat plate approaching a perpendicular surface. This is illustrated in figure (10.2). This type of flow is examined in chapter nine of this thesis and the flux per unit width is taken from equation (9.25), given by

$$\text{Flux / Unit Width } = 2DC_s \int_0^x \frac{1}{\delta_c} dx. \tag{10.8}$$

where δ_c must be found by means of numerically solving the ordinary differential equation:

$$\frac{d\delta_c}{dx} = \frac{23.085D}{A\delta_c x^{\frac{1}{2}}}\left[\frac{L}{L-x}\right] - \frac{\delta_c}{2x} + \frac{\delta_c}{[L-x]}, \tag{10.9}$$

where $L = x - x_{sep}$. Table (10.6) shows the results for several intermediate velocities in both the small and large flow through cells.

Table 10.6: Predicted Dissolution Rates for Intermediate Upward Velocities

Volumetric Flow Rate (mL/min)	Predicted Dissolution Rate (g/s)	Predicted Dissolution Rate (g/s)
	Small Cell	Large Cell
4	1.617×10^{-6}	N/A
8	1.620×10^{-6}	3.393×10^{-6}
16	1.629×10^{-6}	3.394×10^{-6}
32	1.667×10^{-6}	3.399×10^{-6}
43	1.706×10^{-6}	3.408×10^{-6}
50	1.737×10^{-6}	3.408×10^{-6}
100	2.060×10^{-6}	3.416×10^{-6}
200	N/A	3.632×10^{-6}
300	N/A	3.911×10^{-6}

10.5 Discussion

This chapter has applied the methods of the previous chapters to the surface of a compact in the USP Flow Through Apparatus. Table (10.7) compares a selection of predicted dissolution rates with those of experiment in the large flow through cell as reported by D'Arcy[7,8]. The predicted results exhibit some similarities to those of experiment in the sense that no significant increase in the mass transfer rate from the surface is recorded with increased volumetric flow rate. However, all the predicted dissolution rates appear to be much larger than the reported experimental dissolution rates.

Table 10.7: Predicted Dissolution Rates versus Experimental Results

Volumetric Flow Rate (mL/min)	Predicted Dissolution Rate (g/s)	Experimental Dissolution Rate (g/s)
0	4.166×10^{-6}	2.720×10^{-6} *
8	3.393×10^{-6}	2.078×10^{-6}
16	3.394×10^{-6}	2.101×10^{-6}
43	3.404×10^{-6}	2.255×10^{-6}

Initially, especially for the case of natural convection alone, this result would seem to be somewhat disappointing since the model is well documented historically. However, D'Arcy[7] states that for the natural convection case the experiment is performed in a jar with the compact fixed to the inside of the lid. Such a system may be better modeled by the case of a natural convection flow developing from a stagnation point, as analysed in chapter nine. If we apply this model to the surface of a compact the predicted rate of dissolution is 2.958×10^{-6}. This result is within 9% of the experimental result, which itself has a tolerance of about $\pm 3\%$. Taking this information into account it is likely that the lid of the jar has a significant deceleration effect on the flow. The predicted results for volumetric flow rates of 8, 16 and 43mL/min would also seem to be overestimates when compared with those of experiment. These experiments were performed in the large flow through cell in which the compact is suspended about half way along the height of the cell. It would therefore not seem that any additional boundary was present that would account for this decreased mass transfer rate, as may be the case in the jar system. However, on further investigation it would appear that the holder which keeps the compact in place may be responsible for deflecting the upward flow (see figure (1.4)). Also, as the metal used to construct the holder is 0.5mm in diameter it is possible that this impedes the natural con-

*Natural Convection Result: Experiment not performed in Flow Through Cell.

vection flow, as this diameter is of the same order of magnitude as the maximum concentration boundary layer thickness of such a flow. If this is the case, a better model for this system would be that of natural convection flow approaching a perpendicular surface, as discussed in chapter nine. Applying this model to the surface of a compact for volumetric flow rates of 8, 16 and 43mL/min gives the results shown in table (10.8). These results are extremely close to the recorded

Table 10.8: Predicted Dissolution Rates versus Experimental Results

Volumetric Flow Rate (mL/min)	Predicted Dissolution Rate (g/s)	Experimental Dissolution Rate (g/s)
8	2.103×10^{-6}	2.078×10^{-6}
16	2.104×10^{-6}	2.101×10^{-6}
43	2.110×10^{-6}	2.255×10^{-6}

experimental values of D'Arcy[8]. However further experimental data is required to verify that the tablet holder has such an effect on the mass transfer rates from the surface of the compact.

Chapter 11

Conclusions and Future Work

11.1 The USP Paddle Apparatus

Boundary layer theory may be used to successfully model the process of drug dissolution in the USP Paddle Apparatus. The model consists of a concentration boundary layer which has thickness an order of magnitude less than that of the momentum boundary layer. For this reason the concentration boundary layer only occupies the region of the momentum boundary layer across which the velocity profile is linear.

For the case of off-centre compacts the flow across the top planar surface may be described as mass transfer from a horizontal flat plate for large Schmidt numbers, for which an exact solution exists due to the work of Lévêque[1]. Applying this exact solution to the top planar surface of a compact in positions 1 and 2 produced results for the rate of dissolution that are within 1% and 10% of the experimental results of D'Arcy[6]. The variation in error from position 1 and 2 may arise due to the fact that the streamlines of the flow are curved. The curvilinear nature of the streamlines becomes less important as the compact is moved away from the centre of the vessel, leading to a more accurate result in position 2. Also, the hemispherical base of the vessel causes the compact in position 2 to be tilted more to the vertical which leads to less variation in velocities from one side of the compact to the other.

It is also shown in chapter three that a Pohlhausen method can be used to

model the flow across the top planar surface. The results of the Pohlhausen method are extremely accurate when compared with those of the exact solution. The development of this approximate method proved invaluable as it is possible to apply it to a compact in the central position for which the exact solution was not valid. This is achieved by constructing a suitable velocity profile from CFD simulation data provided by D'Arcy[25]. Using this technique for both a 3mm and 8.5mm tall compact in the central position produced mixed results. The results for the 3mm tall compact had an error of about 1% in relation to experimental data while the error for the 8.5mm tall compact was about 25%. There is no obvious reason for the large error in estimating the dissolution rate from the surface of the taller compact; however given that the Pohlhausen method is largely dependent on the accuracy of the velocity profile used, this may be an area worth investigating further.

The dependence that the Pohlhausen method has on the accuracy of the velocity profile used is further highlighted in chapter four. When applied to the curved side surface of a compact in the central position, the results for the 3mm and 8.5mm tall compacts have errors of 35% and 1.3% respectively. The main factor in these varying results was the CFD data available for both compacts. For the 8.5mm compact, data was available for points along the surface at increments of 0.5mm. In contrast, data was only available for three points along the surface of the smaller compact. Finally, this Pohlhausen method was applied to the curved side surface of a compact in position two. On obtaining the streamlines about the surface it was clear that although for much of the surface the direction of the flow was obvious, many parts of the surface did not exhibit clear flow regimes. The error when compared with the experimental results of D'Arcy[6] was 18%.

In conclusion it is shown in chapters three and four that boundary layer theory may be successfully applied to the process of drug dissolution in the USP Paddle Apparatus. In the cases where the Pohlhausen method is used it is clear that the overall accuracy of the results depends largely on the constructed velocity profile.

11.2 The USP Flow Through Apparatus

The second part of this thesis concentrates on the USP Flow Through Apparatus. As the process of drug dissolution in the flow through apparatus is dependent on a vertical flow, the analysis is complicated by the introduction of buoyancy effects. Chapters five to nine analyse a number of general cases for buoyancy driven flows on both flat and curved surfaces. Later, in chapter ten, these general cases are applied to the process of drug dissolution from the surface of a compact in the USP Flow Through Apparatus. Many authors, including D'Arcy[8] and Beyssac[11], have reported a decrease, or stagnation, in dissolution rates for increased flow rates. The assumption made by these authors is that forced convection is the dominant mass transfer mechanism within the flow through apparatus. Chapters five and six of this thesis challenge that assumption and instead consider natural convection as the dominant mass transfer mechanism, with the upward flow having a decelerating effect on this flow at times when the pump is active.

Typical volumetric flow rates in the USP Flow through apparatus are between 4 and 16mL, however higher flow rates are achievable. These typical volumetric flow rates result in extremely low upward velocities. Chapter five of this thesis has shown that for such small velocities the upward flow will behave as that of a slow moving counterflow. This counterflow will have a decelerating effect on the natural convection flow and in chapter five it is shown that for a counterflow

velocity equivalent to 10% of the maximum downward velocity due to natural convection, a decrease in the mass transfer rate of 7.6% is obtained.

Chapter six of this thesis analyses drug dissolution rates from the surface of a vertical flat plate due to large upward velocities. Now, a typical compact is about 1cm in diameter. For a vertical plate of height 1cm it is shown that an upward velocity of about 2.5cm/s would be required in order to prevent the upward flow from separating from the surface across the height of the plate. In the large flow through cell it would take a volumetric flow rate of above 900mL/min to achieve such upward velocities. This is outside the standard operational norms of the apparatus, however the analysis is important to show just how large a flow rate would be required before forced convection dominated.

The most interesting cases are those which involve intermediate velocities. In such circumstances it is shown that the upward flow will penetrate the natural convection boundary layer. However, this upward flow also separates from the surface due to the weight of dissolved particles. This leads to a region below the separation point across which forced convection dominates and a region above, across which a decelerated natural convection flow regime exists. This decelerated natural convection flow is examined in chapter nine by means of a Pohlhausen method. This involves the introduction of a surface that lies perpendicular to the direction of flow. The introduction of this surface results in a reduction of about 38% in the mass transfer rate from the surface, Also in chapter nine, the case of a natural convection flow developing at a stagnation point is examined, which leads to a decrease in dissolution rates of about 29%.

At first when the predicted dissolution rates from the vertical flat surface are compared with those of experiment, as reported by D'Arcy[8], it would seem that

there is a large over-estimation. However, when the possible effect of the tablet holder is taken into account the predicted results fall within 3% of those from experiment. For the case of natural convection only, the experiments were not performed in the flow through cell. Instead, the experiments were conducted in a jar with the compact fixed to the underside of the lid. When the effect of the lid is taken into account the predicted dissolution rates have an error of about 9% when compared with those of experiment.

Chapters seven and eight deal with the curved side surface of a compact in the flow through cell. Due to the geometry of the problem it is clear that the top curved surface of the compact is shielded from the upward flow. For this reason the flow along the surface is one of natural convection only. In the case of the lower curved surface it is shown in chapter eight that a natural convection flow is not possible along this surface. Also in order for the upward flow to have any significant effect on this surface would require large velocities which are not normally present at the typical flow rates used in the apparatus. For these reasons it is assumed that the lower curved surface is a relatively static region with little or no mass transfer. There is at present no experimental data to either support or refute this conclusion.

11.3 Recommendations for Future Work

In recent years much experimental research has concentrated on the USP Flow Through Apparatus instead of the Paddle Apparatus. A number of authors cite reasons for this and outline the advantages that the flow through apparatus has over its predecessor. Stevens[13] reports that the flow through cell controls the placement of the compact better and that the hydrodynamics of the system are

more clearly defined, which is certainly true when we examine the case of an off-centre compact in the paddle apparatus. The flow through cell can also be used in an open configuration, which according to Singh[12], allows sink conditions to be maintained. This better models the operation of the gastro-intestinal tract. Finally, the flow through cell allows for a change in dissolution media throughout an experiment. This better mimics in-vivo conditions as a compact passes through different regions of the gastro-intestinal tract[13].

With regards to the USP Flow Through Apparatus, many of the the advantages outlined do hold true. The position of the compact is better controlled by the tablet holder and the hydrodynamics of the system would seem to be more clearly defined than in the Paddle Apparatus. However, the assumption that the dominant mass transfer mechanism is that of forced convection has been challenged in this thesis. Due to the small velocities generated within the cell it is more likely that natural convection provides the mechanism for dissolution and that the upward velocities have a deceleration effect on this downward flow during the periods in which the pump is active. Also, the effects of the tablet holder are often neglected. CFD simulations performed often do not include the tablet holder; however, from images provided by D'Arcy[25] it is clear that the tablet holder could possibly have an effect on both the upward flow and the buoyancy driven flow (see figure (1.4)).

The aim of much, if not all, of the experimental and simulation work conducted for both apparatuses is to better understand the hydrodynamics of the systems and how this translates to dissolution rates from the surface of a compact. Listed below are a number of recommendations for future work which may help to achieve these goals and also improve upon the design of each apparatus.

The USP Paddle Apparatus

- Design of a tablet holder for the Paddle Apparatus. This would solve the problem of compact movement along the bottom surface. The holder could also be designed to suspend the compact above the bottom surface of the vessel where the hydrodynamics of the system can be complicated by the geometry of the apparatus.

- Perform CFD simulations that specifically concentrate on velocities at very small distances from the surface of the compact. It has been shown in this thesis that the concentration boundary layer occupies only a thin region within the momentum layer. For this reason, it is the velocities close to the surface of the compact that are most important. Analysing these velocities in more detail may be achieved by designing a finer mesh close to the surface; however, any advantages would have to be weighed against computational expense.

- Redesign the impeller in the Paddle Apparatus. In the work of McCarthy[17] it is noted that directly below the impeller is a region of low velocities. Off-setting the position of the impeller in relation to the centre of the vessel may alleviate this problem. Also, this may allow the Paddle Apparatus to better mimic the churning motion experienced within the human stomach, as any such movements must be generated by the walls of the organ.

The USP Flow Through Apparatus

- Suspend the compact at a distance from the lid in the jar system used by D'Arcy[7] to simulate the case of free convection. If experiments were

performed using this alternate set-up it would either confirm or deny the effect of the lid that is proposed in chapter ten of this thesis.

- Redesign the tablet holder for the USP flow through apparatus. If the tablet holder was redesigned so as to only clamp the curved side surface of a compact, the dissolution rate from the vertical flat surface of the compact could be analysed. The results could then be compared with those predicted in chapter ten of this thesis, to either confirm or deny the effect of the current holder.

- Reconfigure the system so that the pulse produced by the pump is in a downward direction. If we consider that the dominant mass transfer mechanism is that of natural convection, the main direction of flow is vertically downward. The fact that the pulsing force is in direct opposition to this leads to a complication in the analysis of the apparatus. Reconfiguring the apparatus so that the pulse is in the same direction as that of the natural convection flow would lead to a simpler analysis of the problem. Also, as the apparatus is designed to mimic the gastro-intestinal tract, a pulsing downward flow should not invalidate this model as much of the gastro-intestinal canal is orientated in this direction.

Bibliography

[1] M.A. Lévêque, *Les lois de la transmission de chaleur par convection*, Ann Mines **13** (1928), 201–239.

[2] H.M. Kuiken, *An asymptotic solution for large Prandtl number free convection*, Journal of Engineering Mathematics **2** (1968), 355–371.

[3] H. Blasius, *Grenzshichten in Flüssigkeiten mit kleiner Reibung*, Z. Math. Phys. **56** (1908), 1–37.

[4] K. Pohlhausen, *Zur naherrungsweisen Integration der Differentialgleichung der laminaren Grenzschicht*, ZAMM **1** (1921), 252-256.

[5] L.J. Crane, *Flow Past a Stretching Plate*, Zeitschrift fur Angewandte Mathematik und Physik (ZAMP) **21** (1970), 645-647.

[6] D.M. D'Arcy, A.M. Healy and O.I. Corrigan, *Hydrodynamic Simulation of Asymmetrically Positioned Tablets in the Paddle Apparatus: Impact on the Dissolution Rates and Variability*, Journal of Pharmacy and Pharmacology **57** (2005), 1243-1250.

[7] D.M. D'Arcy, B. Liu, G. Bradley, A.M. Healy and O.I. Corrigan, *Hydrodynamic and Species Transfer Simulations in the USP 4 Dissolution Apparatus: Considerations for Dissolution in a Low Velocity Pulsing Flow*, Pharmaceutical Research **27** (2010), 246–258.

[8] D.M. D'Arcy, B. Liu, T. Persoons and O.I. Corrigan, *Hydrodynamic Complexity Induced by the Pulsing Flow Field in the USP Dissolution Apparatus 4*, Dissolution Technologies (2011), 6–13.

[9] A.M. Healy, L.G McCarthy, K.M. Gallagher and O.I. Corrigan, *Sensitivity of Dissolution Rate to Location in the Paddle Dissolution Apparatus*, Journal of Pharmacy and Pharmacology **54** (2002), 441–444.

[10] G. Bai and P.M. Armenante, *Hydrodynamic, Mass Transfer and Dissolution Effects Induced by Tablet Location during Dissolution Testing*, Journal of Pharmaceutical Sciences **98** (2009), 1511–1531.

[11] E. Beyssac and J. Lavigne, *Dissolution Study of Active Pharmaceutical Ingredients Using the Flow Through Apparatus USP 4*, Dissolution Technologies, (2005), 23–25.

[12] I. Singh and H.Y. Aboul-Enein, *Advantages of USP Apparatus IV (Flow-through Cell Apparatus) in Dissolution Studies*, Journal of the Iranian Chemical Society **3** (2006), 220–222.

[13] L.E. Stevens, P.J. Missel and A.L. Weiner, *Controlled Flow-Through Dissolution Methodology: A High Performance System* , Pharmaceutical Development and Technology **13** (2008), 135–153.

[14] A. Dokoumetzidis and P. Macheros, *A Century of Dissolution Research: From Noyes and Whitney to the Biopharmaceutics Classification System* , International Journal of Pharmaceutics **321** (2006), 1–11.

[15] L. Howarth, *On the Solution of the Laminar Boundary Layer Equations* , Proc. Roy. Soc. London A **164** (1938), 547–579.

[16] I. Tani , *On the Solution of the Laminar Boundary Layer Equations* , J. Phys. Soc. Japan **4** (1949), 149–154.

[17] L.G McCarthy, C. Kosiol, A.M. Healy, G. Bradley, J.C. Sexton and O.I. Corrigan, *Simulating the Hydrodynamic Conditions in the United States Pharmacopeia Paddle Dissolution Apparatus*, AAPS PharmSciTech **4(2)** (2003), 1–16.

[18] H.B. Squire, *'Modern Developments in Fluid Dynamics' in S.Goldstein*, Oxford University Press New York, 1938.

[19] I.G. Currie, *Fundamental Mechanics of Fluids*, 3rd Edition, CRC Press, 2003.

[20] H. Schlichting, *Boundary Layer Theory*, 7th Edition, McGraw-Hill, 1979.

[21] Y. Jaluria, *HMT: Natural Convection Heat and Mass Transfer*, 1st Edition, Pergamon Press, 1980.

[22] D.J. Acheson, *Elementary Fluid Dynamics*, 1st Edition, Clarendon Press, 1990.

[23] J. Jeans, *An Introduction to the Kinetic Theory of Gases*, Cambridge Press, 1967.

[24] G.K. Batchelor, *An Introduction to Fluid Dynamics* , Cambridge University Press, 1967.

[25] D.M D'Arcy, Private Correspondence